

DISSERTATION

**Functional Consequences
of Old World Hantavirus Infection
in Human Renal Cells**

by

Stefan Hägele

2017

DISSERTATION

**submitted to the
Combined Faculties for the Natural Sciences and for Mathematics
of the Ruperto-Carola University of Heidelberg, Germany
for the degree of
Doctor of Natural Sciences**

presented by

**M.Sc. Stefan Hägele
born in Schwetzingen**

Oral-examination:

**Functional Consequences
of Old World Hantavirus Infection
in Human Renal Cells**

**Referees: Prof. Dr. Stephan Frings
Prof. Dr. Martin Zeier**

Abstract

Viral infections of the kidney, with severe clinical pictures, represent an ongoing threat. The hemorrhagic fever with renal syndrome (HFRS) is caused by several species of pathogenic Old World hantaviruses and is clinically characterized by cellular permeability disorders, leading to acute kidney injury. Previously, it was shown that podocytes and tubular epithelial cells, which play a key role in renal function, are permissive for hantaviruses and further, that the infection was causing a disruption of cell-to-cell contacts correlating with the disease severity. Up until today, the renal-specific pathogenesis mechanisms of hantavirus infections, leading to the cellular leakage, are not well understood. In this study, functional and morphological consequences of hantavirus infection are examined in human renal cells and compared to African green monkey Vero E6 cells, which are commonly used to study hantaviruses.

Analysis of podocytes and tubular epithelium in human renal biopsies of hantavirus-infected patients revealed distinct morphological changes known to be involved in functional disorders of various kidney diseases. To investigate how hantaviruses cause cellular disorders, the effects were further examined using *in vitro* experiments. Infections of podocytes and tubular epithelial cells with either Hantaan (HTNV) or Puumala virus (PUUV) caused cytoskeletal rearrangements in combination with an impairment of adhesion and motility capacity. The nucleocapsid (N) protein was associated with the actin cytoskeleton and, in addition to that, the integrity of filamentous (F-) actin was crucial for viral release. Furthermore, the transfection of podocytes revealed that the expression of N protein alone was sufficient to impair cellular functions. Soluble factors contributing to the cellular disturbances were neither detected in the supernatant of *in vitro* infected podocytes nor in the serum of hantavirus-infected patients, indicating direct effects of infection on renal cells. According to the severity of the clinical picture, the *in vitro* effects of hantaviral infections and N protein expression were more pronounced for HTNV than for PUUV. In contrast, the hantavirus infections were clearly different in Vero E6 cells and no functional consequences and actin involvement were observed, demonstrating the importance of choosing relevant cell culture models.

These results demonstrate that hantavirus-induced morphological and functional injuries are species- and cell type-specific. The association of N protein with actin and its involvement in the viral release might play a role in the underlying mechanism, leading to functional impairment and cell-to-cell contact disruption. Moreover, the N protein is identified to be a pathogenicity factor of Old World hantaviruses. Conclusively, these findings might contribute to the understanding of the pathogenesis mechanisms leading to the clinical picture of hantavirus-induced acute renal failure.

Zusammenfassung

Virale Infektionen der Niere, mit schweren Krankheitsverläufen, stellen eine ernstzunehmende Bedrohung dar. Das hämorrhagische Fieber mit renalem Syndrom (HFRS) wird von verschiedenen pathogenen Altwelt-Hantaviren verursacht und ist durch Störungen der Zellpermeabilität gekennzeichnet, welche zu einem akuten Nierenversagen führen. Es konnte gezeigt werden, dass Podozyten und Tubulus-Epithelzellen, welche eine Schlüsselrolle in der Nierenfunktion einnehmen, permissiv für Hantaviren sind und dass die Infektion zu einem Zusammenbruch der Zell-Zell Kontakte führt. Bis heute ist der spezifische Pathomechanismus von Hantaviren nicht komplett aufgeklärt. In dieser Studie werden die funktionalen und morphologischen Konsequenzen der Hantavirusinfektion untersucht und mit Vero E6 Zellen aus der afrikanischen grünen Meerkatze verglichen, welche üblicherweise zur Untersuchung von Hantaviren benutzt werden.

Auswertungen diverser Nierenbiopsien von Hantavirus-infizierten Patienten, mit Fokus auf Podozyten und das Tubulus-Epithel, zeigten morphologische Veränderungen, welche dafür bekannt sind, verschiedenen Nierenerkrankungen auszulösen. Die verursachten Zellschädigungen durch Hantaviren wurden in *in vitro* Experimenten weiter untersucht. Die Infektion von Podozyten und Tubulus-Epithelzellen mit Hantaan (HTNV) oder Puumala Virus (PUUV) führten zu einer Veränderung des Zytoskeletts, sowie zu einer Verminderung der Adhäsion und Beweglichkeit der Zellen. Das Nukleokapsid- (N-) Protein war entlang des Aktin-Zytoskeletts lokalisiert und die Integrität von filamentösem (F-) Aktin war von großer Bedeutung für die Freisetzung von neuen Viruspartikeln. Die alleinige Expression von N-Protein verursachte Zellschädigungen in transfizierten Podozyten. Lösliche Faktoren, welche zu den funktionalen Beeinträchtigungen führen können, waren weder in Überständen von infizierten Podozyten noch in Patientenserum zu finden, weshalb auf direkte Effekte der Infektion auf die Zellen geschlossen werden kann. Die *in vitro* Beobachtungen der Infektion und der N-Protein Expression stimmten mit dem Krankheitsbild überein, bei dem HTNV einen schwereren Verlauf als PUUV aufweist. Funktionale Konsequenzen und eine Beteiligung des Aktin-Zytoskeletts waren in Hantavirus-infizierten Vero E6 Zellen nicht zu finden. Diese Beobachtung zeigt, dass die Wahl eines relevanten Zellkulturmodells für die Untersuchung von Hantaviren von Bedeutung ist.

Die Ergebnisse beweisen, dass morphologische und funktionale Zellschädigungen durch Hantaviren sowohl speziens-, als auch zellspezifisch sind. Die Lokalisierung von N-Proteinen an F-Aktin und die Freisetzung von neuen Viruspartikeln sind möglicherweise an dem Mechanismus, der zu funktionaler Beeinträchtigung sowie zum Zusammenbruch der Zell-Zell Kontakte führt, beteiligt. Diese Studie identifiziert außerdem die N-Proteine von Altwelt-Hantaviren als Pathogenitätsfaktor. Zusammenfassend tragen diese Erkenntnisse dazu bei, den Pathomechanismus von Hantaviren, welcher zu einem akuten Nierenversagen führt, zu verstehen.

I. Table of contents

Abstract

Zusammenfassung

| | | |
|------------|---|-----------|
| I. | Table of contents | i |
| II. | List of abbreviations | iv |
| III. | List of figures | vi |
| IV. | List of tables..... | vii |
| 1. | Introduction..... | 1 |
| 1.1 | Virus-induced kidney diseases..... | 1 |
| 1.2 | Hantaviruses | 1 |
| 1.2.1 | Epidemiology of hantaviruses | 1 |
| 1.2.2 | Clinical picture of hantaviruses | 2 |
| 1.2.3 | Virology of hantaviruses..... | 4 |
| 1.2.3.1 | Virion and genome structure | 4 |
| 1.2.3.2 | Hantaviral replication cycle | 5 |
| 1.3 | Pathogenesis of Old World hantaviruses | 6 |
| 1.3.1 | Target cells..... | 6 |
| 1.3.1.1 | The kidney as major target for Old World hantaviruses | 7 |
| 1.3.1.2 | Impairment of kidney function during hantaviral disease | 9 |
| 1.3.2 | Mechanism of pathogenesis | 9 |
| 1.4 | Aims and perspectives | 12 |
| 2. | Material & Methods..... | 13 |
| 2.1 | Material | 13 |
| 2.1.1 | Chemicals..... | 13 |
| 2.1.2 | Buffers and solutions..... | 14 |
| 2.1.3 | Plasmids..... | 15 |
| 2.1.4 | Antibodies..... | 15 |
| 2.1.5 | Cell culture media and supplements..... | 15 |
| 2.1.6 | Cells | 16 |
| 2.1.7 | Viruses | 16 |

| | | |
|------------|--|-----------|
| 2.1.8 | Software | 16 |
| 2.2 | Methods..... | 17 |
| 2.2.1 | Cell culture..... | 17 |
| 2.2.1.1 | Cell lines..... | 17 |
| 2.2.1.2 | Primary cells | 17 |
| 2.2.2 | Human serum and tissue samples..... | 17 |
| 2.2.3 | Virus propagation and infection..... | 18 |
| 2.2.4 | Immunofluorescence..... | 18 |
| 2.2.5 | Analysis of amount of infection, N protein pattern and N protein expression level | 19 |
| 2.2.6 | Viability Assay | 19 |
| 2.2.7 | Effects of cytoskeletal drugs on N protein localization and hantaviral release | 20 |
| 2.2.8 | In-Cell Western assay | 20 |
| 2.2.9 | Quantification of cellular actin forms..... | 20 |
| 2.2.10 | Western blot analysis | 21 |
| 2.2.11 | Adhesion assay | 21 |
| 2.2.12 | UV irradiation and depletion of viral particles containing supernatants..... | 22 |
| 2.2.13 | Migration assay | 22 |
| 2.2.14 | Plasmid preparation | 22 |
| 2.2.15 | Transfection of podocytes..... | 23 |
| 2.2.16 | Live cell imaging..... | 23 |
| 2.2.17 | Statistical analysis..... | 23 |
| 3. | Results..... | 24 |
| 3.1 | Analysis of hantaviral infection in glomerular structures..... | 24 |
| 3.1.1 | Glomerular alterations in kidney biopsy specimens of hantavirus patients | 24 |
| 3.1.2 | <i>In vitro</i> effects of hantavirus infection on podocytes | 25 |
| 3.1.2.1 | Localization of hantaviral N protein in podocytes..... | 25 |
| 3.1.2.2 | Effects of cytoskeletal polymerization inhibitors on N protein in podocytes | 27 |
| 3.1.2.3 | Effects of cytoskeletal polymerization inhibitors on viral release of podocytes..... | 29 |
| 3.1.2.4 | Hantaviral effects on actin cytoskeletal organization | 30 |

| | | |
|------------|---|-----------|
| 3.1.2.5 | Functional consequences of hantavirus infection in podocytes | 30 |
| 3.1.3 | <i>In vitro</i> effects of hantavirus infection on Vero E6 cells..... | 32 |
| 3.1.3.1 | Localization of hantaviral N protein in Vero E6 cells..... | 32 |
| 3.1.3.2 | Effects of cytoskeletal polymerization inhibitors on viral release of Vero E6 cells... | 33 |
| 3.1.3.3 | Hantaviral effects on the actin cytoskeletal organization of Vero E6 cells | 35 |
| 3.1.3.4 | Functional consequences of hantavirus infection in Vero E6 cells | 36 |
| 3.1.4 | Effects of hantaviruses on primary human podocytes..... | 38 |
| 3.1.4.1 | Localization of hantaviral N protein in primary podocytes | 38 |
| 3.1.4.2 | Functional consequences of hantavirus-infected primary podocytes | 38 |
| 3.2 | Analysis of hantaviral infection in renal tubules..... | 40 |
| 3.2.1 | Tubular alterations in kidney biopsy specimens of patients with hantavirus disease .. | 40 |
| 3.2.2 | Effects of hantaviruses on human renal epithelial primary cells (HREPC) | 41 |
| 3.2.2.1 | Localization of hantaviral N protein in HREPC..... | 41 |
| 3.2.2.2 | Functional consequences of hantavirus-infected HREPC..... | 43 |
| 3.3 | Analysis of underlying hantaviral mechanisms with regards to functional consequences | 44 |
| 3.3.1 | Soluble factors in supernatant of infected podocytes | 44 |
| 3.3.2 | Soluble factors in human sera | 45 |
| 3.3.3 | Effects of recombinantly-expressed hantavirus N proteins | 47 |
| 3.3.3.1 | Localization of recombinant N protein in human podocytes..... | 47 |
| 3.3.3.2 | Effects of recombinant N protein on podocyte migration | 48 |
| 4. | Discussion..... | 51 |
| 4.1 | Human renal cells as relevant cell culture models to study hantavirus disease | 51 |
| 4.2 | Old World hantaviruses cause morphological and functional changes in kidney biopsies | 54 |
| 4.3 | Determinants of hantavirus virulence | 56 |
| 4.4 | Hantaviral N protein as virulence factor | 58 |
| 5. | References..... | 61 |
| 6. | Acknowledgment..... | 68 |

II. List of abbreviations

| | |
|---------------|---|
| BHK-21 | Baby hamster kidney cell-21 |
| BKV | BK virus |
| BVK168 cell | Bank vole kidney 168 cell |
| CB | Cell body |
| CMV | Cytomegalovirus |
| CRP | C-reactive protein |
| Ctrl | Control |
| Cyto D | Cytochalasin D |
| DAF | Decay-accelerating factor |
| DMSO | Dimethyl sulfoxide |
| Dpi | Days post infection |
| Dpo | Days post onset |
| ELM | Eukaryotic linear motif (ELM) |
| ERGIC | ER-Golgi intermediate compartment |
| F-actin | Filamentous actin |
| FCS | Fetal calf serum |
| FP | Foot process |
| G-actin | Globular actin |
| GBM | Glomerular basement membrane |
| GFB | Glomerular filtration barrier |
| GFP | Green fluorescent protein |
| GSD | Glomerular slit diaphragm |
| HCPS | Hantavirus cardiopulmonary syndrome |
| HCV | Hepatitis C virus |
| HEK293T cell | Human embryonic kidney 293T cell |
| HFRS | Hemorrhagic fever with renal syndrome |
| HIV | Human immunodeficiency virus |
| HIVAN | HIV-associated nephropathy |
| HREPC | Human renal epithelial primary cell |
| HUVEC | Human umbilical vein endothelial cell |
| ICW | In-Cell Western |
| IF | Immunofluorescence |
| IFN- γ | Interferon gamma |
| IL | Interleukin |
| ISG | Interferon-stimulated gene |
| LDH | Lactate dehydrogenase |
| MOI | Multiplicity of infection |
| MP | Major process |
| MxA | Myxovirus resistance protein A |
| N protein | Nucleocapsid protein |
| NE | Nephropathia epidemica |
| NOC | Nocodazole |
| ORF | Open reading frame |
| P | Pellet |
| PDZ | Abbreviation of <u>p</u> ost synaptic density protein, <u>D</u> rosophila disc large tumor suppressor, <u>z</u> onula occludens-1 |
| RdRP | RNA-dependent RNA polymerase |
| Rec | Recovery |
| RNP | Ribonucleoprotein |
| SD | Standard deviation |
| SEM | Scanning electron microscopy |

| | |
|---------------|---|
| SN | Supernatant |
| TEM | Transmission electron microscopy |
| TNF- α | Tumor necrosis factor alpha |
| Treat | Treatment |
| UPAR | Urokinase-type plasminogen activator receptor |
| VEGF | Vascular endothelial growth factor |
| VHF | Viral hemorrhagic fever |
| WB | Western blot |
| ZO-1 | Zonula occludens-1 |

Viruses belonging to the family of *hantaviridae*

| | |
|------|-------------------------|
| ANDV | Andes virus |
| BCCV | Black Creek Canal virus |
| DOBV | Dobrava-Belgrade virus |
| HTNV | Hantaan virus |
| NY-1 | New York-1 virus |
| PUUV | Puumala virus |
| SNV | Sin Nombre virus |

III. List of figures

| | |
|--|----|
| Figure 1 Annual numbers of reported cases of hantavirus disease in Germany since 2001 | 2 |
| Figure 2 Schematic structure of kidney, nephron and glomerulus..... | 7 |
| Figure 3 Podocyte structure | 9 |
| Figure 4 Electron microscopy of human glomeruli | 25 |
| Figure 5 Localization of HTNV and PUUV N protein in podocytes | 26 |
| Figure 6 Cell viability of podocytes after treatment with inhibitors of cytoskeletal polymerization ... | 27 |
| Figure 7 Localization of N proteins in podocytes after modulation of the cytoskeleton | 28 |
| Figure 8 Viral release assay of HTNV- and PUUV-infected podocytes..... | 29 |
| Figure 9 Cytoskeletal organization in HTNV- and PUUV-infected podocytes | 31 |
| Figure 10 Adhesion and migration capacity of HTNV- and PUUV-infected podocytes..... | 32 |
| Figure 11 Localization of HTNV and PUUV N protein in Vero E6 cells | 34 |
| Figure 12 Viral release assay of HTNV- and PUUV-infected Vero E6 cells | 35 |
| Figure 13 Cytoskeletal organization in HTNV- and PUUV-infected Vero E6 cells | 36 |
| Figure 14 Adhesion and migration capacity of HTNV- and PUUV-infected Vero E6 cells..... | 37 |
| Figure 15 Localization of HTNV and PUUV N protein in primary podocytes | 39 |
| Figure 16 Migration capacity of PUUV-infected primary podocytes | 40 |
| Figure 17 Electron microscopy of human renal tubules | 42 |
| Figure 18 Localization of HTNV and PUUV N protein in HREPC..... | 43 |
| Figure 19 Adhesion and migration capacity of HTNV- and PUUV-infected HREPC..... | 44 |
| Figure 20 Migration of podocytes inoculated with cell-free viral supernatants..... | 46 |
| Figure 21 Migration capacity of podocytes after inoculation with sera of PUUV-infected patients.... | 47 |
| Figure 22 Localization of recombinantly-expressed HTNV and PUUV N protein in podocytes. | 48 |
| Figure 23 Effect of HTNV and PUUV infection or N protein expression on podocyte migration..... | 50 |

IV. List of tables

| | |
|---|----|
| Table 1 Selection of pathogenic Old World hantaviruses with associated case fatality rates. | 4 |
| Table 2 Characteristics, peak, and nadir levels of laboratory parameters obtained from three patients with acute PUUV hantavirus disease used for electron microscopy analysis of glomeruli. | 24 |
| Table 3 Characteristics, peak, and nadir levels of laboratory parameters obtained from three patients with acute PUUV hantavirus disease used for electron microscopy analysis of renal tubules..... | 41 |
| Table 4 Characteristics, peak, and nadir levels of laboratory parameters obtained from three patients with acute PUUV hantavirus disease used for migration assays | 46 |

1. Introduction

1.1 Virus-induced kidney diseases

In recent times, the amount of patients with severe kidney disease continuously increased and is displaying a public health problem [1]. Inflammations of the human kidney and the adjacent urinary tract are among the most common infectious diseases in humans. Viral infections are representing important causative agents for renal injury and failure. Viruses affecting renal function are often associated with immunocompromised or immunosuppressed hosts. During kidney transplantations, the reactivation of the cytomegalovirus (CMV) or the BK-virus (BKV) represents a hazard leading to complications and in the worst case to a loss of renal grafts [2, 3]. Renal dysfunction and injuries are also described in the course of the clinical picture in chronic viral infections, such as the hepatitis C virus (HCV) or the human immunodeficiency virus (HIV) [4, 5]. In contrast, viral hemorrhagic fever (VHF) caused by Hantaviruses, Dengue virus or Ebola virus is associated with acute kidney injuries [6, 7]. Due to the emerging number of cases and outbreaks worldwide displaying severe clinical pictures and fatality within the last decades, VHF-causing hantaviruses gained an increased interest of viral renal research.

1.2 Hantaviruses

1.2.1 Epidemiology of hantaviruses

Hantaviruses, belonging to the order of *bunyavirales*, are a zoonotic viral disease and maintain as a persistent infection of rodents. Since outbreaks during the Korean War (1950-53) and the isolation of the causative agent, named Hantaan virus (HTNV) in 1976, more than 41 pathogenic and non-pathogenic species have been found worldwide with the exception of Australia [8, 9]. Each hantavirus is associated with a single species of wild rodents, which serves as its natural reservoir and thereby determines the geographical distribution. The hosts are lifelong, chronically, and asymptotically infected and excrete infectious hantaviral particles by urine, feces, and saliva [10, 11]. Transmission of hantaviruses to humans occurs predominately by inhalation of contaminated aerosolized rodent excretes. Person-to-person transmission was only sporadically reported for Andes virus (ANDV) in Argentina [12, 13]. Humans are exposed to an increasing risk of infection during leisure time or professional activities in the natural habitat of host species [14]. Individual risk factors such as certain gene polymorphisms or smoking were also reported [15-17]. The incidence of disease is described to be greater for males and young adults and in contrast is rare in children and the

elderly [18]. Behavioral differences of males may account for the observation that more men are affected. Nevertheless, possible gender-specific factors determining the severity of hantavirus disease are controversially discussed [19-21].

The first cases in Europe and Germany were described in 1980 and 1986, respectively [22, 23]. Since 2001, a hantavirus infection is notifiable in Germany and the Robert Koch Institute classifies hantaviruses to the highest priority group of pathogens [24]. In 2016, the European Centre for Disease Prevention and Control reported that hantaviruses are widely endemic across Europe [25]. Two pathogenic hantaviruses, causing the majority of clinical infections, are found along with their natural hosts: Puumala virus (PUUV), transmitted by bank voles (*Myodes glareolus*), throughout most of Europe with the exception of Mediterranean countries, and Dobrava-Belgrade virus (DOBV) spread by the yellow-necked mouse (*Apodemus flavicollis*) in Eastern and Central Europe. The majority of cases were reported in Finland, Sweden, Germany, Croatia, and France. Numbers of hantavirus cases in Germany undergo fluctuations and are associated with climatic changes and environmental parameters affecting the rodent population (Fig.1) [26].

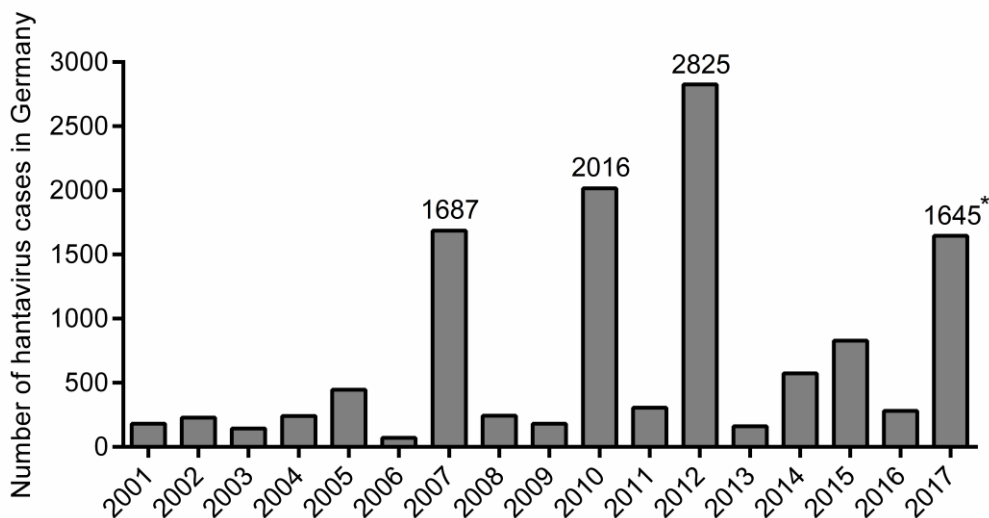


Figure 1 Annual numbers of reported cases of hantavirus disease in Germany since 2001. The asterisk (*) indicates cases in 2017 until 12/09/2017 (Source: SurvStat of Robert Koch Institute [27]).

1.2.2 Clinical picture of hantaviruses

Spillover of hantaviruses to humans has the potential to cause two types of acute disease. Old World hantaviruses in Europe and Asia cause hemorrhagic fever with renal syndrome (HFRS) with about

150,000 to 200,000 annually reported cases [28]. In addition, about 200 cases are described each year for hantavirus in the New World inducing hantavirus cardiopulmonary syndrome (HCPS) [29].

The incubation time upon exposure to HFRS-causing hantaviruses such as HTNV or DOBV usually ranges from two to three weeks. The following febrile phase is characterized by a sudden onset of unspecific flu-like symptoms such as high fever, cephalgia, myalgia, accompanied by myopia, gastrointestinal symptoms, nausea, vomiting, abdominal and flank pain. Hemorrhages can occur and display as injection of the conjunctiva, petechial rash or even as gastrointestinal hemorrhage. In the hypotensive phase, patients suffer from vascular leakage potentially leading to shock, tachycardia and hypoxemia. Characteristically for hantavirus disease is the occurrence of leukocytosis, elevated levels of lactate dehydrogenase (LDH), and C-reactive protein (CRP). The subsequent oliguric phase is the most critical stage and is responsible for over 50% of hantavirus-related deaths. The systemic disease starts to primarily manifest in the kidney and is associated with the onset of renal failure and loss of blood proteins, called proteinuria. Laboratory findings include the decrease of serum albumin and an increase of serum creatinine levels. The renal filtration starts to improve in the following polyuric phase and recovers in the convalescent phase. PUUV infections in Europe generally cause a mild form of HFRS, called nephropathia epidemica (NE), and severe symptoms like hemorrhages and shocks are rare [30, 31].

New World hantavirus-induced HCPS shares similarities with the clinical picture of HFRS, with the exception that capillary leakage mainly manifests in the lung. The disease is usually more severe and patients suffer from initial symptoms like shortness of breath, which are rapidly developing into an acute respiratory failure. The mortality rate of HCPS is high and varies between 25% and 40% [32]. The reason for the different organ manifestations, however, is unclear. Clinical findings revealed that a distinction between HFRS and HCPS is not always possible since renal and lung involvement has been reported for both diseases [33, 34].

Nevertheless, the kidney involvement with massive proteinuria is a hallmark of Old World hantavirus infection. The severity is determined by the hantavirus species that causes the disease and differs enormously (Tab. 1). Dialysis is required for about 40% of HTNV-, 16-48% of DOBV-, and 5% of PUUV-infected patients [28, 35]. In addition, the case-fatality rate ranges from up to 15% for HTNV, up to 12% for DOBV and less than 0.4% for PUUV infections [31, 36-39]. Interestingly, even highly related genotypes of DOBV vary in their virulence to humans (Tab. 1) [40]. The mechanisms behind the different severities of the disease are unknown.

At present, only hantavirus-induced symptoms can be medicated to keep the severity under control since no specific hantaviral therapy or effective vaccines are available [41]. An early treatment of

hantavirus-infected patients with the nucleoside analog ribavirin is discussed controversially and differs in the efficacy and safety depending on the virus species [42, 43].

Table 1 Selection of pathogenic Old World hantaviruses with associated case fatality rates.

| Virus species | Distribution | Disease | Case fatality | Source |
|-------------------------------|--------------------------|-----------------|---------------|--------|
| Puumala virus (PUUV) | Central, Northern Europe | HFRS (NE), mild | 0.4% | [36] |
| Hantaan virus (HTNV) | Asia | HFRS, severe | 5-15% | [31] |
| Dobrava-Belgrade virus (DOBV) | | | | |
| ▪ Dobrava (DOBV-Af) | Balkans | HFRS, severe | 10-12% | [37] |
| ▪ Sochi (DOBV-Ap) | Crimea | HFRS, moderate | 6% | [38] |
| ▪ Kurkino (DOBV-Aa) | Central, Eastern Europe | HFRS, mild | <1% | [39] |

1.2.3 Virology of hantaviruses

1.2.3.1 Virion and genome structure

Despite specific endemic distribution and differences in the severity of the clinical picture, hantaviruses share a common virion structure and high genome homology (Fig. 1). The virion is enveloped and possesses a trisegmented negative-sense, single-stranded RNA genome of about 12,000 nucleotides. Each segment consists of one open reading frame (ORF) and the small (S), medium (M) and large (L) segment encode for the nucleocapsid (N) protein, a polyprotein, which is cotranslationally cleaved into the glycoproteins Gn and Gc, and the RNA-dependent RNA polymerase (RdRP), respectively [44]. However, an overlapping ORF in the S segment exists in several hantavirus species encoding for a functional nonstructural protein counteracting interferon- β activation [45]. The two glycoproteins Gn and Gc are organized in spike-like complexes and embedded into the viral envelope. The segments of the genome are encapsulated by N proteins forming the ribonucleoprotein (RNP) complexes and are enclosed inside the viral membrane.

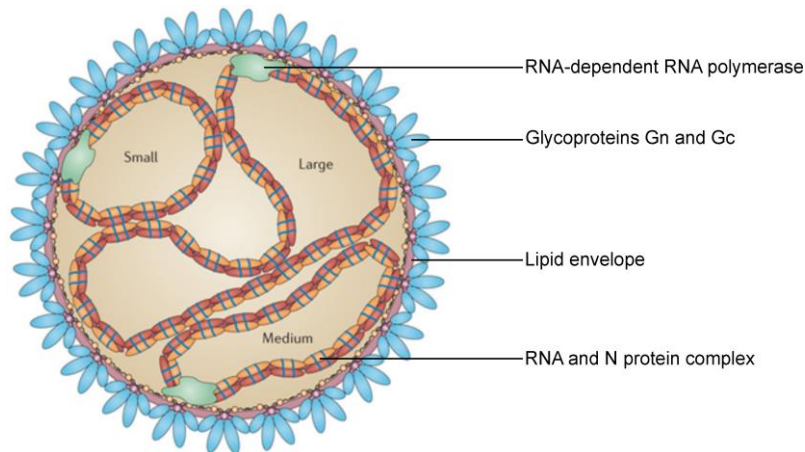


Figure 1 Schematic structure of the hantaviral particle. Hantaviruses consist of a trisegmented negative-sense, single-stranded RNA genome. The segments small, medium, and large are encapsulated in a complex with the N protein and the RNA-dependent RNA polymerase. The lipid envelope is coated by glycoproteins arranged in spikes (Image adapted from Vaheri *et al.* [46]).

1.2.3.2 Hantaviral replication cycle

Virus entry into host cells is mediated by attachment to cellular receptors. For pathogenic hantaviruses, integrin $\alpha_v\beta_3$ has been described as main entry receptor and, in addition, decay-accelerating factor (DAF/CD55) and gC1qR act as critical cofactors [47-49]. Followed by different pathways of endocytosis, the RNPs are released to the cytoplasm from late endosomes by pH-mediated fusion of viral and endosomal membranes [50-53]. The site of viral replication and/or transcription is suggested to be located at processing bodies and at endoplasmic reticulum-Golgi intermediate compartment (ERGIC) [50, 54]. Hantaviruses use different assembly sites and egress pathways and it seems that Old World hantaviruses bud at the ER, Golgi complex and plasma membrane, while New World hantaviruses bud exclusively at the plasma membrane [55-58].

Hijacking of intracellular pathways is an overall requirement for an efficient transport of viral RNA and proteins to sites of replication, assembly, and release. In several studies, the role of the cytoskeleton was analyzed during hantavirus infection. African green monkey Vero E6 cells and baby hamster kidney-21 (BHK-21) cells were used and revealed a different utilization of host cytoskeleton components and partially contradictory results. Early studies by Ravkov *et al.* on the morphogenesis of New World Black Creek Canal virus (BCCV) in Vero E6 cells revealed a filamentous pattern of N protein, which was associated with F-actin and the disruption of actin resulted in a decreased release of infectious particles [59]. Moreover, the transfection of BHK-21 cells with BCCV and PUUV N protein-encoding plasmids also revealed a filamentous pattern indicating an actin localization [60]. In subsequent publications, Ramanathan *et al.* showed that hantavirus species differ in their

localizations and dependency of cytoskeletal components in Vero E6 cells [50, 51]. While the entry was enabled by F-actin and microtubules for all hantaviruses, New World hantaviruses depend on actin for late events and Old World hantaviruses require intact microtubules during assembly and release. Interestingly, neither effects of F-actin disruption nor a filamentous pattern of BCCV, as seen by Ravkov *et al.*, were detected in the studies of Ramanathan *et al.*, although Vero E6 cells were used in both studies. Discrepancies in the experimental conditions might contribute to the contradictory results such as differences in the multiplicity of infection (MOI) for viral infection or choosing of varying points of time for the observation. Moreover, Vero E6 cells are interferon-deficient and do not secrete interferons like normal mammalian cells, which might influence the viral replication cycle.

1.3 Pathogenesis of Old World hantaviruses

1.3.1 Target cells

The exact pathogenicity factor, responsible for the different organ manifestation and clinical symptoms of hantavirus species, has not been elucidated. The use of a relevant cell culture model or organism is mandatory for the study of the pathogenesis since Vero E6 cells already show no reliable results in the viral replication cycle.

Up until today, no appropriate animal infection model has been found that completely recapitulates severe human HFRS. Therefore, research is hampered to study multifaceted processes in an organism. Experimental inoculation of adult or suckling small laboratory animals such as mice, rats and hamsters with various hantaviruses resulted in an asymptomatic and persistent infection or in lethal neurological symptoms, which are uncharacteristic for HFRS, respectively [61]. Cynomolgus macaques (*Macaca fascicularis*) infected with PUUV developed a mild form of HFRS, which is similar to NE in humans [62-64]. The clinical picture of macaques displayed hantavirus-characteristic symptoms and deteriorated clinical parameters such as proteinuria and elevated levels of creatinine and CRP. Since no small animal model for hantavirus infection exists and the macaque model is limited, *in vitro* cell culture and human biopsy or blood samples are commonly used to study the pathogenesis of hantavirus disease.

Humans demonstrate a wide range of target cells for Old World hantavirus infection. Analysis of *in vitro* infections showed that different endothelial and epithelial cell lines and primary cells of kidney, lung and liver, as well as immune cells, are permissive for hantaviruses [65-68]. This wide range of tropism might explain the different symptoms during the clinical picture. Analysis of biopsies and

autopsies of humans and monkeys revealed that viral antigen, particles, and RNA can be found in different organs such as kidney, liver and spleen [62, 65, 69-71]. Moreover, extrarenal involvement during disease was reported and hantaviral antigens have been found in the intestine and hypophysis of human tissue samples and might be involved in the development of abdominal pain, headache, fatigue, and central nervous system complications [72-74]. The reason for the different organ manifestations during the clinical course of disease is not completely understood. Nevertheless, the kidney and its function are predominantly affected by Old World hantaviruses in humans and macaques leading to proteinuria and renal failure.

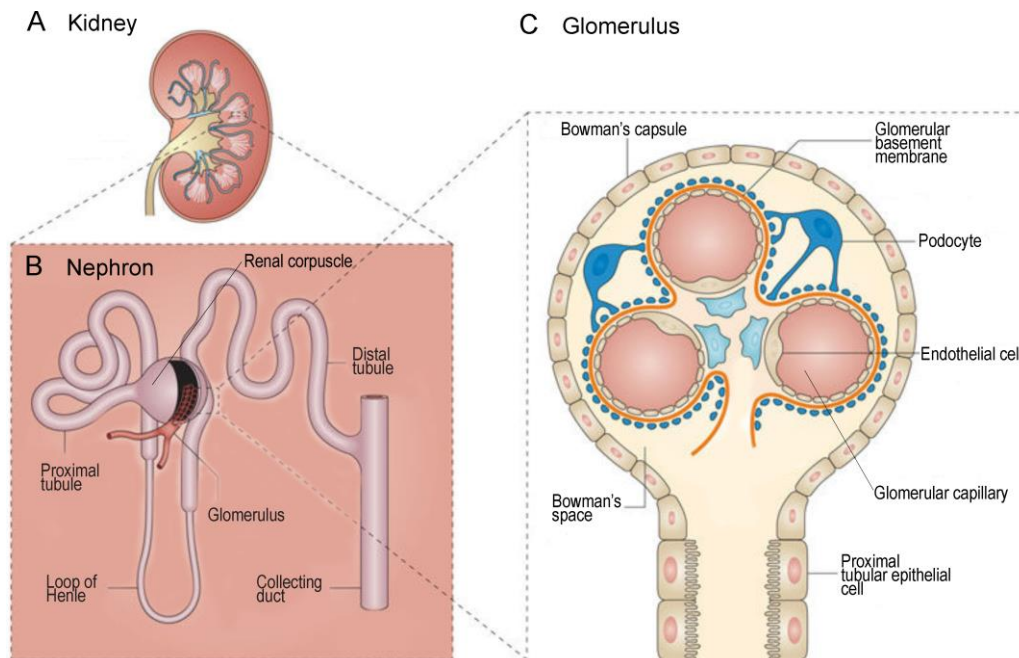


Figure 2 Schematic structure of kidney, nephron and glomerulus. (A and B) Nephrons are the functional renal subunits of the kidney and are divided into the renal corpuscle and the adjacent renal tubule. (C) Within the renal corpuscle, the blood is filtrated at the capillaries of the glomerulus by the filtration barrier consisting of endothelial cells, glomerular basement membrane and podocytes. The filtrate is further processed by reabsorption of essential molecules in renal tubules and finally excreted in form of urine (Image adapted from Kurts *et al.* [75]).

1.3.1.1 The kidney as major target for Old World hantaviruses

The analysis of kidney biopsy specimens of hantavirus-infected patients further revealed that viral antigen can be found in cells of the glomerular and tubular apparatus [65]. Both structures are located in the nephron, the smallest renal subunit, and are essential for blood filtration and urine processing (Fig. 2A and B). Analysis of *in vitro* infection studies with human renal cells showed that

primary glomerular endothelial cells and podocytes, as well as primary tubular epithelial cells, are permissive to Old World hantavirus infection and release of infectious particles [65].

The glomerulus is a network of blood capillaries located at the renal corpuscle at the start of each nephron and functions as the blood filtration unit of the kidney. The glomerular filtration barrier (GFB) consists of three layers (fenestrated endothelial cells, glomerular basement membrane (GBM) and podocytes) and is impermeable for large proteins and blood cells, but allows the passage of small molecules (Fig. 2C) [76].

During filtration, podocytes play a key role and form the basic backbone of the GFB. Podocytes consist of a complex structure. Proceeding from the cell body, major processes arise and split into multiple foot processes (FP) (Fig. 2C and 3A). The FPs of neighboring podocytes form a tight interdigitating network wrapping the outer surface of the glomerular capillaries and are interconnected by multiprotein complexes of the glomerular slit diaphragm (GSD) [77, 78]. Crucial for proper podocyte function and the integrity of FPs are highly-ordered actin filament bundles [79]. In recent years, the view of podocytes as a static molecular sieve has been changed into a highly regulated dynamic structure. Rapid reorganization of the actin-based cytoskeleton of FPs allows podocytes to migrate along the GBM in order to react to different environmental conditions such as hydrostatic stress. Proteins regulating the actin cytoskeleton are therefore of critical importance to maintain podocyte function [80]. Interference with signaling pathways controlling the actin cytoskeleton during kidney disease leads to changes of the actin organization and a deteriorated motility capacity of podocytes. It was shown that hypo- and hypermotility of podocytes can result into a loss of proper interdigitating FPs, which is called effacement (Fig. 3B). Effacement is characterized by disruption of the GSD, resulting in disorders of filtration function and proteinuria [81-85].

After passing the GFB, the filtrate is consisting of metabolites for excretion, as well as, water and essential molecules such as small proteins, electrolytes, amino acids, or glucose which are reabsorbed by the renal tubules into the peritubular capillaries by intracellular and transcellular pathways (Fig. 2C) [86-88]. The tubular epithelium maintains a barrier between urinary lumen and the interstitial tissue and their ability to migrate along the underlining basement membrane is of crucial importance for reaction to environmental conditions and wound closing [89]. Afterwards, the processed filtrate is passed on to the collecting duct and finally excretes the human body in form of urine.

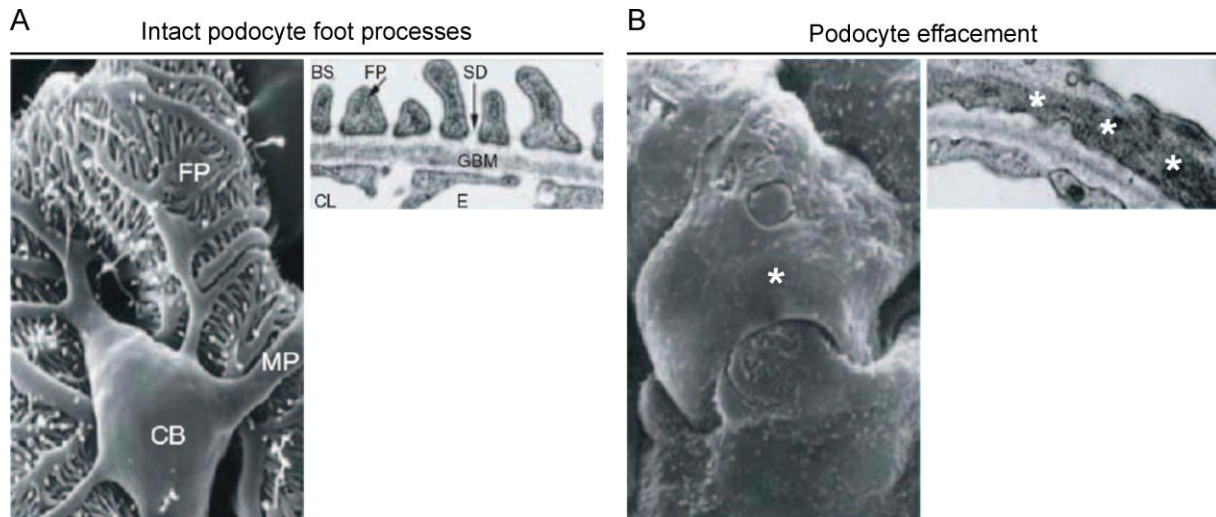


Figure 3 Podocyte structure. (A) Healthy podocyte. Left: Scanning electron microscopy (SEM) from Bowman's space view. Podocyte consists of a cell body (CB) that is branched into major processes (MP) and foot processes (FP). Right: Transmission electron microscopy (TEM) of the glomerular filtration barrier. BS: Bowman's space; CL: capillary lumen; SD: glomerular slit diaphragm; GBM: glomerular basement membrane; E: endothelial cell. (B) Podocyte during disease. SEM (left) and TEM (right) show foot process effacement characterized by a loss of cell shape and interdigitating FP (*) (Image adapted from Mundel *et al.* [81]).

1.3.1.2 Impairment of kidney function during hantaviral disease

Histopathological examination of renal tissue of hantavirus-infected humans and macaque infection models reveals acute tubulointerstitial nephritis with infiltrates of immune cells and minor changes of the glomeruli [62, 90-92]. However, by using electron microscopy analysis, an effacement of podocyte FPs is detectable in renal biopsy specimens of hantavirus patients [91]. One hallmark of HFRS is a renal permeability dysfunction and proteinuria is found in up to 94% of patients [30, 93]. By measurement of the urinary excretion of hantavirus patients, both high- and low-molecular weight proteins are found in the urine [94, 95]. Normally, the glomerular filtration barrier is impermeable for large proteins and crossed small proteins are completely reabsorbed by the tubular epithelial cells. Therefore, the non-selective proteinuria indicates glomerular filtration disorders, as well as, an impaired tubular reabsorption capacity during hantavirus disease [85].

1.3.2 Mechanism of pathogenesis

Hantavirus disease is characterized by leakage of endothelial and epithelial cells, which explains many of the underlying symptoms such as hypotension, hemorrhages, and proteinuria. The pathogenesis of the glomerular and tubular disorders leading to non-selective proteinuria is not completely understood. Research studies of the hantaviral mechanisms in cell culture and renal

biopsies suggest that multifaceted mechanisms of immunopathological and direct viral effects play a role during hantaviral disease.

In hantavirus-infected patients, high counts of activated cytotoxic and T helper lymphocytes were measured in human blood samples with renal infiltrations of immune cells [92, 96]. Since no obvious histomorphological cytopathic effects were detected during infection, it is assumed that the release of inflammatory cytokines contributes to the barrier breakdown of endothelial and epithelial cells.

An intact cell permeability barrier depends on the integrity of cell-to-cell contacts mediated by tight and adherens junctions and consist of transmembrane and cytosolic proteins interconnected by the cellular cytoskeleton [97]. The GSD of podocytes, a specific variant of adherens and tight junctions, and the tight junctions of tubular epithelial cells are important for filtration and reabsorption processes, respectively [98, 99]. The barrier function is highly regulated by intracellular pathways and extracellular soluble factors [100]. Elevated cytokines levels, which are known to interfere with the maintenance of cellular permeability such as interleukin-6 (IL-6), IL-10 and tumor necrosis factor- α (TNF- α) were measured in blood samples of hantavirus-infected patients [101]. Additionally, hantaviruses are able to infect dendritic cells, enhance the production of proinflammatory cytokines and might directly trigger the release of molecules inducing cellular leakage [67]. Several studies examined the role of soluble factors, which are involved in the regulation of cellular permeability. They detected elevated levels of vascular epithelial growth factor (VEGF), urokinase plasminogen activator receptor (uPAR), and dysregulation of angiopoietins, which correlate with disease severity [102-104].

However, the detection of cytokines in peripheral blood does not explain the organ-specific effects of hantavirus infections. Analysis of the underlying direct molecular effects revealed that hantaviruses interfere with the susceptibility to extracellular stimuli and integrity of cell-to-cell contacts. *In vitro* infection of human umbilical vein endothelial cell (HUVEC) monolayers demonstrated that HTNV induces a prolonged permeability by sensitizing the cellular response to TNF- α and VEGF [104, 105]. Moreover, VEGF treatment of HTNV-infected HUVEC but not of uninfected control cells reduced the mRNA and protein levels of cell-to-cell contact proteins [104]. A study with human renal cells revealed that the barrier function was disturbed by the infection of HTNV in primary human renal epithelial cells alone [65]. Biopsy specimens of renal tubules of infected patients demonstrated that cellular hantaviral antigen expression correlates with a breakdown and deteriorated localization of the tight junction protein zonula occludens-1 (ZO-1) [65]. ZO-1 is a cytosolic protein and links transmembranous tight junction proteins with the actin cytoskeleton [106]. Uninfected neighboring tubules showed no breakdown of ZO-1 indicating a direct link between viral replication and cellular changes [65]. Moreover, a weaker ZO-1 expression was also detected in hantavirus-infected

glomerular structures and correlates with disease severity. Cell culture experiments of human glomerular endothelial cells, podocytes and tubular epithelial cells infected with HTNV or PUUV revealed a breakdown of cell-to-cell contacts as indicated by a decreased expression of ZO-1 and its relocalization from the cell borders to perinuclear regions.

The mechanisms resulting in direct effects are not completely understood. Expression of hantaviral N protein executes a plethora of functions. During infection, N proteins play an important role in various steps during the viral replication cycle such as encapsulation and replication of RNA [107, 108]. Besides virus-related functions, the N protein has properties in interfering and modulation of host signaling pathways and cell structure [59, 109-111]. The N protein of New World ANDV is involved in the regulation of the innate immune system, as well as, in the enhanced permeability of microvascular endothelial cells [112, 113]. It remains to be examined whether N proteins of Old World hantavirus also contribute to the pathogenesis in renal cells.

1.4 Aims and perspectives

Pathogenic Old World hantaviruses mainly affect the kidney function and cause an enhanced permeability and massive proteinuria leading to acute renal failure. This research aims to investigate cellular changes by Old World hantaviruses using human renal cells as a relevant *in vitro* cell culture model since most of the previous studies in hantaviral biology and pathogenesis were performed in HUVEC and interferon-deficient monkey Vero E6 cells, which differ significantly from renal target cells. This project will focus on glomerular podocytes and tubular epithelial cells, which are both crucial for kidney function and are affected by hantaviruses *in vitro* and *in vivo*.

The above mentioned aim will be accomplished by fulfilling the following research objectives:

- Study of morphological changes of cells in renal biopsies by electron microscopy and by *in vitro* cell culture experiments.
- Analysis of subcellular localization of hantaviral N protein.
- Evaluation of the role of cytoskeletal components in hantaviral release.
- Investigation of functional consequences of hantavirus infection in renal cells.
- Examination of soluble factors in cell culture supernatants and human sera contributing to cellular renal dysfunction.
- Analysis of the role of N protein in virus-mediated effects on renal function.

This research project should provide new insights into the hantaviral pathogenesis of acute renal failure and may be of use in the identification of determinants regarding disease severity.

2. Material & Methods

2.1 Material

2.1.1 Chemicals

| Chemicals | Supplier (Location) |
|--|----------------------------------|
| Albumin fraction V (BSA) | Carl Roth (Karlsruhe, Germany) |
| Ammonium chloride (NH ₄ Cl) | Carl Roth (Karlsruhe, Germany) |
| Ammonium persulfate (APS) | Carl Roth (Karlsruhe, Germany) |
| Ampicillin sodium salt | Carl Roth (Karlsruhe, Germany) |
| Bromphenol blue | Serva (Heidelberg, Germany) |
| Cytochalasin D (Cyto D) | Merck (Darmstadt, Germany) |
| Dimethyl sulfoxide (DMSO) | VWR (Radnor, USA) |
| Disodium phosphate (Na ₂ HPO ₄) | AppliChem (Darmstadt, Germany) |
| Distillated water | Braun (Melsungen, Germany) |
| DRAQ5 | BioStatus (Shepshed, UK) |
| Endotoxin-free water | Promega (Fitchburg, USA) |
| Fish gelatin | Sigma-Aldrich (St. Louis, USA) |
| Glycine | AppliChem (Darmstadt, Germany) |
| Kanamycin sulfate | Carl Roth (Karlsruhe, Germany) |
| Mercaptoethanol | Merck (Darmstadt, Germany) |
| Methanol | Sigma-Aldrich (St. Louis, USA) |
| Milk powder | Carl Roth (Karlsruhe, Germany) |
| Monopotassium phosphate (KH ₂ PO ₄) | Merck (Darmstadt, Germany) |
| Mounting medium | Linaris (Wertheim, Germany) |
| N',N',N',N'-tetramethylethylenediamine (TEMED) | Carl Roth (Karlsruhe, Germany) |
| Nocodazole (NOC) | Merck (Darmstadt, Germany) |
| Paraformaldehyde (PFA) | Sigma-Aldrich (St. Louis, USA) |
| Rotiphorese Gel 30 | Carl Roth (Karlsruhe, Germany) |
| Roti-Transform | Carl Roth (Karlsruhe, Germany) |
| Sapphire700 | LI-COR Bioscience (Lincoln, USA) |
| Sodium chloride (NaCl) | Sigma-Aldrich (St. Louis, USA) |
| Sodium dodecyl sulfate (SDS) | Serva (Heidelberg, Germany) |
| Trishydroxymethylaminomethan (Tris) | Carl Roth (Karlsruhe, Germany) |
| Triton X-100 | Sigma-Aldrich (St. Louis, USA) |
| Tween 20 | Carl Roth (Karlsruhe, Germany) |

2.1.2 Buffers and solutions

| Name | Amount | Chemical |
|--|---|---|
| APS solution | 10% (w/v) in ddH ₂ O | APS |
| Blocking solution | 2% (v/v) 2% (w/v) 0.2% (w/v) in 1xPBS | FCS BSA Fish gelatin |
| Cell lysis buffer (6x) | 390 mM 6% (w/v) 10% (v/v) 10% (v/v) 0.5% (w/v) in ddH ₂ O | Tris pH 6.8 SDS Mercaptoethanol Glycerol Bromphenol blue |
| Fixation buffer | 3% (w/v) in 1xPBS | PFA |
| Milk blocking solution | 5% (w/v) in 1xPBS | Milk powder |
| PBS (10x) pH 7.2 | 1200 mM 180 mM 250 mM 25 mM in ddH ₂ O | NaCl Na ₂ HPO ₄ KH ₂ PO ₄ Tris |
| PBST washing buffer | 0.05% (v/v) in 1xPBS | Tween 20 |
| Permeabilization buffer | 0.2% (v/v) in 1xPBS | Triton X-100 |
| Quenching buffer | 50 mM 20 mM in 1xPBS | NH ₄ Cl Glycine |
| SDS blotting buffer | 25 mM 192 mM 20% (v/v) 0.05% (w/v) in ddH ₂ O | Tris Glycine Methanol SDS |
| SDS running buffer (10x) | 250 mM 1920 mM 0.5% (w/v) in ddH ₂ O | Tris Glycine SDS |
| Tris buffer pH 6.8 (for stacking gel) | 1000 mM in ddH ₂ O | Tris |
| Tris buffer pH 8.8 (for separation gel) | 1500 mM in ddH ₂ O | Tris |

2.1.3 Plasmids

| Vector | Encoded protein | Supplier, Location |
|---------|-----------------|---|
| pCR3.1 | PUUV N protein | Cloned in Section of Nephrology (Heidelberg, Germany) [114] |
| pCR3.1 | HTNV N protein | Cloned in Section of Nephrology (Heidelberg, Germany) [114] |
| pmaxGFP | maxGFP | Lonza (Basel, Germany) |

2.1.4 Antibodies

| Primary antibodies | | | | | | |
|--------------------|-------|---------|-----------|--------|-------|----------------------------------|
| Type | Clone | Species | Dilutions | | | Supplier, Localization |
| | | | IF | WB | ICW | |
| HTNV-N | B5D9 | mouse | 1:100 | - | 1:100 | Progen (Heidelberg, Germany) |
| HTNV-N | - | rabbit | - | 1:1000 | - | Nephrology (Heidelberg, Germany) |
| PUUV-N | A1C5 | mouse | 1:100 | - | 1:100 | Progen (Heidelberg, Germany) |
| PUUV-N | - | rabbit | - | 1:1000 | - | Nephrology (Heidelberg, Germany) |
| Actin | - | rabbit | - | 1:200 | - | Cytoskeleton Inc. (Acoma, USA) |
| Tubulin alpha | DM1A | mouse | 1:100 | 1:1000 | - | Sigma-Aldrich (St. Louis, USA) |
| Synaptopodin | - | goat | 1:20 | - | - | Santa Cruz (Dallas, USA) |

| Secondary antibodies | | | | | | |
|----------------------|------------|---------|-----------|----------|-------|----------------------------------|
| Type | Conjugate | Species | Dilutions | | | Supplier, Localization |
| | | | IF | WB | ICW | |
| anti-goat IgG | Cy3 | donkey | 1:1000 | - | - | Jackson Immuno (Newmarket, UK) |
| anti-mouse IgG | Cy3 | donkey | 1:1000 | - | - | Jackson Immuno (Newmarket, UK) |
| anti-mouse IgG | Dylight488 | donkey | 1:1000 | - | - | Jackson Immuno (Newmarket, UK) |
| anti-rabbit IgG | Cy3 | donkey | 1:1000 | - | - | Jackson Immuno (Newmarket, UK) |
| anti-mouse IgG | IRDye800 | donkey | - | 1:15,000 | 1:600 | LI-COR Bioscience (Lincoln, USA) |
| anti-rabbit IgG | IRDye680 | donkey | - | 1:15,000 | - | LI-COR Bioscience (Lincoln, USA) |

2.1.5 Cell culture media and supplements

| Description | Supplier |
|--|--|
| DetachKit for primary cells | PromoCell (Heidelberg, Germany) |
| DMEM, high glucose (4.5 g/l) | Capricorn Scientific (Ebsdorfergrund, Germany) |
| Fetal calf serum (FCS), heat-inactivated | Biochrom (Berlin, Germany) |
| Interferon-gamma (IFN- γ) | Thermo Fisher Scientific (Waltham, USA) |
| Insulin, Transferrin, Selenium | Capricorn Scientific (Ebsdorfergrund, Germany) |
| PBS without Ca ²⁺ /Mg ²⁺ | Capricorn Scientific (Ebsdorfergrund, Germany) |
| Penicillin-Streptomycin | Sigma-Aldrich (St. Louis, USA) |
| Renal Epithelial Cell Growth Medium-2 | PromoCell (Heidelberg, Germany) |
| RPMI-1640 | Capricorn Scientific (Ebsdorfergrund, Germany) |
| Trypsin-EDTA solution | Sigma-Aldrich (St. Louis, USA) |

2.1.6 Cells

| Cell | Species | Type | Origin | Supplier |
|---|-------------------------|--------------|---|---|
| Podocyte | human | cell line | kidney, derived from <i>in vivo</i> podocytes | provided by Prof. Dr. Jochen Reiser (Rush University, Medical Center, Chicago, USA) [115] |
| Vero E6 | African green monkey | cell line | Epithelium, kidney | ATCC (Manassas, USA) |
| Podocyte, primary | human | primary cell | isolated from donated human tissue | Lonza (Basel, Switzerland) |
| Human renal epithelial primary cell (HREPC) | human | primary cell | isolated from adult kidney | PromoCell (Heidelberg, Germany) |
| DH5 α | <i>Escherichia coli</i> | - | bacteria | Thermo Fisher Scientific (Waltham, USA) |

2.1.7 Viruses

| Virus | Strain | Origin |
|----------------------|---------|---|
| Hantaan virus (HTNV) | 76-118 | Isolated from striped field mouse (<i>Apodemus agrarius</i>) in South Korea in 1978 [8] |
| Puumala virus (PUUV) | Vranica | Isolated from bank vole (<i>Myodes glareolus</i>) in Bosnia-Herzegovina in 1986 [116] |

2.1.8 Software

| Software | Version | Supplier, Localization |
|--------------------------|---------------|---|
| EndNote | x7 | Clarivate Analytics (New York, USA) |
| GraphPad Prism | 6.01 | GraphPad Software (La Jolla, USA) |
| Image J | 1.51n | National Institutes of Health (Bethesda, USA) |
| Chemotaxis tool | 1.01 | Ibidi (Martinsried, Germany) |
| Manual tracking tool | 2005/06/15 | Fabrice Cordelires (Orsay, France) |
| Image Studio | v3 | LI-COR Bioscience (Lincoln, USA) |
| Office Professional 2010 | 14.07184.5000 | Microsoft (Redmond, USA) |
| Photoshop | CS6 | Adobe Systems (San José, USA) |

2.2 Methods

2.2.1 Cell culture

2.2.1.1 Cell lines

The podocyte cell line, derived from normal human podocytes, was conditionally transformed with a temperature-sensitive SV40 large T antigen [115]. For proliferation, cells were cultured in RPMI medium supplemented with 10% FCS, 1% penicillin/streptomycin, 1% ITS, and 5000 U IFN- γ at 33°C and 5% CO₂. After transfer to 37°C for 14 days in RPMI medium without IFN- γ , podocytes undergo growth arrest and express markers of differentiation. Expression of the podocyte-specific marker protein synaptopodin was routinely controlled. Experiments were performed with non-proliferating and differentiated podocytes. Vero E6 cells were cultivated in DMEM supplemented with 10% FCS and 1% penicillin/streptomycin at 37°C and 5% CO₂. At a confluence of 70-80%, both cell lines were sub-cultivated or seeded for experiments. Therefore, culture medium was discarded and cells were washed with PBS. Adherent cells were enzymatically detached by incubation for two minutes in Trypsin-EDTA solution at 37°C. Cells were centrifuged at 1000 g for three minutes, resuspended in fresh medium, counted and seeded for experiments or sub-cultivation. Podocytes and Vero E6 cells were seeded at a density of 5,000 cells/cm² and 10,000 cells/cm², respectively.

2.2.1.2 Primary cells

Primary podocytes were maintained in RPMI medium supplemented with 10% FCS and 1% ITS. HREPCs were cultured in renal epithelial cell growth medium-2. Primary cells were only used for experiments from passages two to six. Cells were sub-cultivated and seeded for experiments at a confluence of 70-80% by using the DetachKit for primary cells according to the manufacturer's protocol for detachment. Primary podocytes and HREPCs were centrifuged at 200 g for three minutes, resuspended in fresh medium, counted and seeded at a density of 5,000 cells/cm² and 15,000 cells/cm², respectively.

2.2.2 Human serum and tissue samples

Patients with serologically-confirmed acute hantavirus infection and healthy volunteers were included in this study. Clinical data were collected through a review of medical charts from the Section of Nephrology (University of Heidelberg, Germany). This study was approved by the Ethics Committee of the University of Heidelberg and it adhered to the Declaration of Helsinki. Written

informed consent was obtained from all participants. Human serum samples of three healthy volunteers were donated and, in addition, samples of three hantavirus-infected patients were obtained during clinical routine. Samples were collected in S-Monovettes (Sarstedt, Nümbrecht, Germany) with clotting activators and centrifuged at 2000 g for seven minutes to remove erythrocytes and clotting factors. Sera were aliquoted and stored at -80°C. Before usage in cell culture experiments, samples were heated at 56°C for 30 minutes. Specimens of renal biopsies of three patients with serologically-confirmed PUUV infection and specimens of a healthy kidney from living donor were fixed in glutaraldehyde and embedded in Epon-Araldite after post-fixation with osmium tetroxide. Fixed specimens were cut in ultra-thin sections of <100 nm and loaded on electron microscopy grids. Prepared samples were analyzed by transmission electron microscopy (JEM-1400, Jeol, Freising, Germany). Sample preparation and electron microscopy analysis were performed at the Institute of Pathology (University of Heidelberg, Germany).

2.2.3 Virus propagation and infection

HTNV and PUUV were propagated on Vero E6 cells. For the production of viral stocks, cells were infected with a multiplicity of infection (MOI) of 1 for three hours followed by a medium exchange. After 5 days, cell culture supernatants were collected, centrifuged to remove cell debris, aliquoted and stored at -80°C. The amount of infectious particles in the respective stocks was analyzed by titration assay on Vero E6 cells in triplicates. Therefore, cells were inoculated with 1, 5, 10 and 50 µl of collected virus-containing supernatants and the amount of infectious particles was determined by measuring the infected cells two days post infection (dpi) by immunofluorescence.

For infection during experiments, culture medium was reduced to 50% and cells were inoculated with respective viral stocks. Virus inoculum of HTNV or PUUV at a MOI of 1 was added to the cells. After three hours, medium was exchanged to remove unbound virus and cells were incubated in fresh medium for the indicated points of time. Experiments with PUUV and HTNV were performed under biosafety level 2 and 3 (University of Heidelberg, Germany) conditions, respectively.

2.2.4 Immunofluorescence

Cells grown on cover slips from *in vitro* experiments were fixed with fixation solution for ten minutes. Cells were further incubated with quenching buffer for four minutes and, after PBS washing, with permeabilization solution for two minutes. Cells were stained in a humidified chamber with primary antibodies and after washing with fluorescently-labeled secondary antibodies for one hour each.

Antibody concentrations were diluted in blocking solution (see chapter 2.1.4 for dilutions). Hoechst 33342 (3.2 μ M, Thermo Fisher Scientific, Waltham, USA) for cell nuclei and Alexa Fluor-488 phalloidin (6.6 μ M Thermo Fisher Scientific, Waltham, USA) for F-actin staining were incubated together with secondary antibodies. After staining, cells were washed with PBS and deionized water and afterwards mounted head-down on microscope glass slides by covering in mounting media. Fluorescence microscopy analysis was performed with the Observer D1 with an Axiocam 506 mono camera (Carl Zeiss, Jena, Germany). The TE-2000 microscope with a Hamamatsu EMCCD camera (Nikon, Tokyo, Japan) was used for confocal analysis.

2.2.5 Analysis of amount of infection, N protein pattern and N protein expression level

The amount of infected cells was determined via fluorescence microscopy by staining cells for nuclei and hantaviral N protein. Per approach, ten randomly-selected fields at a magnification of x100 were recorded. Cells showing N protein expression were determined as positive for infection. Uninfected and infected cells were counted and the amount of infected cells was defined in percent.

A total of 100 randomly-selected infected cells were analyzed for the cellular localization of N protein by fluorescence microscopy. N protein expression was distinguished by a punctuate and a filamentous-like distribution. Cells were positive for a filamentous pattern by detecting at least one N protein fiber-like structure.

The expression level of N proteins was determined by analysis of 100 randomly-selected transfected cells that were stained for N proteins. The fluorescence levels were calculated with ImageJ as total corrected cell fluorescence (TCCF) of N protein (TCCF = integrated density – (area of selected cell \times mean background fluorescence)) [117, 118].

2.2.6 Viability assay

The number of viable cells was determined by quantification of the ATP amount according to the manufacturer's protocol of the CellTiter-Glo Luminescent Cell Viability Assay (Promega, Fitchburg, USA). In brief, cells were grown in opaque-walled 96-well plates (Greiner Bio-One, Kremsmünster, Austria), inoculated with hantaviruses as described above and lysed with a luciferase-containing buffer at indicated points of time. Thereby, the intracellular amount of ATP is directly proportional to the number of cells. The luminescent signal of the luciferase reaction was recorded by the Glomax

microplate reader (Promega, Fitchburg, USA). Viability of infected cells was assessed in quadruplicates and compared to uninfected control cells.

2.2.7 Effects of cytoskeletal drugs on N protein localization and hantaviral release

In each experiment, cells were inoculated with hantaviruses in triplicates for six days. Cells were washed three times with medium to remove remaining viral particles and incubated with fresh medium for four hours as reference for viral release. For treatment, cells were washed and incubated with fresh medium for four hours supplemented with either DMSO solvent control or cytoskeletal depolymerization inhibitors. Podocytes were incubated with 1 μ M Cyto D and 10 μ M NOC whereas Vero E6 cells were treated with 8 μ M Cyto D and 10 μ M NOC. Again, for recovery, cells were washed and incubated with normal medium for another four hours. Supernatants were harvested after reference, treatment, and recovery phase, centrifuged at 1000 g for three minutes to remove cell debris and stored at -80°C . The amount of infectious viral particles in the supernatants was determined by In-Cell Western assay. Cells on coverslips were fixed after treatment and recovery phase and stained for hantaviral N protein and for either F-actin or tubulin.

2.2.8 In-Cell Western assay

Vero E6 cells on opaque-walled 96-well plates were inoculated with equal amounts of virus-containing supernatants in triplicates and medium was exchanged after three hours. Cells were fixed at two days post infection, quenched and permeabilized as described above for immunofluorescence. After incubation of 30 minutes in blocking solution, cells were stained with primary antibodies against N protein and respective near-infrared fluorescence-conjugated secondary antibodies for one hour each (see chapter 2.1.4 for antibody dilutions). Nuclei were stained for cell number normalization with DRAQ5/Sapphire according to the manufacturer's protocol together with secondary antibodies. After staining, cells were washed three times with PBST for ten minutes and once with deionized water. The plate was turned upside down and blotted gently on paper towels to remove remaining solution. Cells were scanned by the Odyssey Imaging System (LI-COR, Lincoln, USA) and quantification of infection was performed using the Image Studio software with the In-Cell Western module.

2.2.9 Quantification of cellular actin forms

The ratio of intracellular filamentous (F-) and globular (G-) actin was quantified according to the manufacturer's protocol of the G-actin/F-actin In Vivo Assay Kit (Cytoskeleton Inc, Denver, USA).

Briefly, uninfected or hantavirus-infected cells were lysed at six days post infection in a detergent-based buffer that maintains F- and G-actin pools. After an ultracentrifugation step at 100,000 g for one hour at 37°C, soluble G-actin is found in the supernatant, whereas insoluble F-actin was pelleted. To control an effective fractionation, uninfected control cells were treated with the actin-polymerization drug phalloidin, which resulted in the accumulation of actin in the insoluble pelletized fraction. G-actin-containing supernatants were harvested. Pellets were resuspended in the same volume in depolymerization buffer to dissociate F-actin and incubated for one hour. All samples were diluted with the supplied 5x SDS lysis buffer and analyzed by Western blot.

2.2.10 Western blot analysis

Protein samples in SDS lysis buffer were loaded on a 12% polyacrylamide gel and separated by electrophoresis at 120 V in SDS running buffer by the Mini-PROTEAN Tetra Cell System (Bio-Rad, Munich, Germany). The PageRuler Plus Prestained Protein Ladder (Thermo Fisher Scientific, Waltham, USA) was used to determine protein size. Separated proteins were blotted from the gel onto nitrocellulose membranes (GE Healthcare, Little Chalfont, UK) enclosed between Whatman papers (GE Healthcare, Little Chalfont, UK) in the Tetra Blotting Module (Bio-Rad, Munich, Germany) for one hour at 1.57 mA/cm² in blotting buffer. After transfer, membranes were incubated in milk blocking solution for 30 minutes. Proteins were stained with indicated primary antibodies and, after a triple washing step with PBST for ten minutes each, with near-infrared fluorescence-conjugated secondary antibodies for one hour each. Antibodies were diluted in milk blocking solution as described in chapter 2.1.4. After additional washing steps, membranes were scanned by the Odyssey Clx Imaging System. Multiple proteins on the same blot were distinguished by staining with different secondary antibodies which emit after excitation in either the 700 nm or 800 nm channel. Quantitative image analysis was performed by using the Image Studio software.

2.2.11 Adhesion assay

Uninfected and hantavirus-infected cells were detached at day six post infection by Trypsin-EDTA solution, centrifuged and counted as described above. A total of 1×10^4 cells of a single-cell suspension were added in quadruplicates per approach in each well of an opaque-walled 96-well plate. Cells were left to adhere in equal volumes for one hour at 37°C and subsequently washed three times with PBS and fixed with fixation solution. The amount of adhered cells was quantified by In-Cell Western assay.

2.2.12 UV irradiation and depletion of viral particles containing supernatants

Infectious viral particles in supernatants derived from hantavirus-infected podocytes were either inactivated by UV irradiation or depleted. For UV irradiation, supernatants were transferred to a culture medium plate with lid opened and placed into the Stratalinker 1800 UV-transilluminator (Agilent, Santa Clara, USA). Infectious particles were inactivated with the energy of 1.4 J/cm². For virus depletion, supernatants were loaded into centrifugal filter devices equipped with an Omega membrane 300k (Pall, New York, USA) with a molecular weight cut-off of 300 kilodalton (kDa) and centrifuged at 5,000 g until complete filtration. A portion of supernatants were diluted in 6x cell lysis buffer and analyzed for the presence of N proteins by Western blot. The presence of infectious particles was examined by inoculation of Vero E6 cells and immunofluorescence analysis of N protein.

2.2.13 Migration assay

Cells were seeded into 2-well μ -dishes (Ibidi, Martinsried, Germany) with a detachable insert defining a cell-free gap and inoculated with hantaviruses. The insert was removed at six days post infection to allow cell migration. The cell-free gap was imaged immediately after insert removal and after eight hours by JuLI Smart Fluorescence Cell Imager (Bulldog-Bio, Portsmouth, USA). In case of Vero E6 cells, the culture medium was supplemented with mitomycin C (50 μ g/ml, Sigma-Aldrich, St. Louis, USA) to exclude cell proliferation. Cell migration was determined by calculation of the covered distance between beginning and end of each experiment. To monitor the infection, cells were stained for nuclei and hantaviral N protein by immunofluorescence as described above. For the analysis of possible soluble factors in supernatants or human sera causing changes in migration, uninfected cells in 2-well μ -dishes were incubated 30 minutes prior insert removal with either supernatants of infected cells or 50% human sera in normal culture medium.

2.2.14 Plasmid preparation

Bacteria (strain DH5 α) were made competent according to the Roti-Transform protocol and used for propagation of plasmids encoding for maxGFP, HTNV N, or PUUV N protein. About 2.5×10^5 competent cells were incubated with 1 μ g of plasmid DNA for 30 minutes on ice. After a heat-shock of 42°C for 45 seconds, cells were immediately rested on ice for 15 minutes. Cells were pre-incubated in LB medium (BD, Franklin Lakes, USA) for 45 minutes at 37°C prior to cultivation in overnight approaches in LB medium containing respective antibiotics (0.287 mM ampicillin or 0.006 mM kanamycin). Plasmids from overnight cultures were harvested according to the EndoFree Plasmid

Maxi Kit protocol (Qiagen, Venlo, Netherland). Plasmid DNA was dissolved in endotoxin-free water and concentration was determined by measuring the absorbance at 260 nm in the photometer before storage at -20°C.

2.2.15 Transfection of podocytes

Podocytes were transfected by nucleofection according to the manufacturer's protocol of the Amaxa Basic Nucleofector Kit for Primary Mammalian Epithelial Cells (Lonza, Basel, Switzerland). Briefly, differentiated podocytes at 70-80% confluency were detached. A total of 1×10^6 cells were resuspended in nucleofector solution VPI-1005 and incubated with 1 μ g plasmid DNA encoding for maxGFP, HTNV N, and PUUV N protein or with empty vectors. The suspension was transferred to electrode cuvettes and transfection was performed with the T-013 program of the Nucleofector 2b device (Lonza, Basel, Switzerland). To enhance the transfection efficacy, cells in cuvettes were rested for ten minutes, followed by resuspension in pre-warmed medium and transfer to appropriate culture dishes. After eight hours cells were washed with media and subjected to live cell imaging or immunofluorescence.

2.2.16 Live cell imaging

Uninfected and infected podocytes were detached, centrifuged, and counted as described above. A total of 5×10^4 cells were seeded on μ -slide 2-wells (Ibidi, Martinsried, Germany) and left to adhere for two hours. After a triple wash with culture medium, cells were monitored every 10 minutes for eight hours by the JuLI Smart Fluorescence Cell Imager (Bulldog-Bio, Portsmouth, USA). Podocytes were tracked by the ImageJ manual tracking plugin. The covered distances of single cells were analyzed by using the chemotaxis tool plugin. The migration of podocytes on μ -slide 2-wells co-transfected with plasmids encoding for N protein and maxGFP were monitored by using the Ti-HCS microscope (Nikon, Tokyo, Japan). Images were recorded every ten minutes for eight hours. Cells expressing maxGFP were tracked and analyzed as described above for infected cells.

2.2.17 Statistical analysis

Data analysis was performed by using Prism 6.0. The Kolmogorov-Smirnov test was applied to test for normal distribution of values and, furthermore, the significance level of two groups was measured by two-tailed Student's t-test. *P* values of ≤ 0.05 were considered significant. **P* ≤ 0.05 ; ***P* ≤ 0.01 ; ****P* ≤ 0.001 ; *****P* ≤ 0.0001 ; ns: not significant.

3. Results

3.1 Analysis of hantaviral infection in glomerular structures

3.1.1 Glomerular alterations in kidney biopsy specimens of hantavirus patients

The clinical picture of an Old World hantavirus infection is characterized by an acute kidney failure with non-selective proteinuria indicating that cells of the glomerulus are affected. In order to study the underlying mechanism of disease, renal biopsies of three patients with serologically-confirmed acute hantavirus infection and of one healthy control person were analyzed by electron microscopy for changes in glomerular structures. All patients presented characteristics of hantavirus infection with an initial sudden onset of flu-like symptoms. During the clinical course, patients showed an impairment of laboratory blood parameters such as thrombocytopenia, rise in levels of serum creatinine, leucocytes, LDH, CRP and low levels of serum albumin (Tab. 2). In all three patients, electron microscopy analysis of glomeruli between day seven and 13 after onset of symptoms revealed changes of important structures, which maintain the blood-urine filtration barrier (Fig. 4). Compared to the control biopsy, the diameter of the glomerular basement membrane was mildly thickened without accumulation of immune complexes. The overlaying podocytes showed the most severe structural alterations. Cells were enlarged, vacuolated and their FPs were focally effaced.

The analysis of biopsies show that podocytes, which are crucial for the renal filtration, are affected during hantavirus disease as displayed by a loss of proper FPs. Therefore, the effects of hantavirus infection on podocytes was further examined *in vitro*.

Table 2 Characteristics, peak, and nadir levels of laboratory parameters obtained from three patients with acute PUUV hantavirus disease used for electron microscopy analysis of glomeruli.

| Characteristic | #19 | #64 | #131 | reference |
|---|-------|-------|-------|-----------|
| Age (yr) | 48 | 37 | 39 | - |
| Gender | m | m | m | - |
| Duration of hospitalization (days) | 6 | 8 | 9 | - |
| Max serum creatinine level (mg/dl) | 8.35 | 11.94 | 5.33 | 0.1-1.3 |
| Min serum albumin level (g/liter) | 32.9 | 28 | 33.3 | 30-50 |
| Max leukocyte count (G/liter) | 11.12 | 15.6 | 19.91 | 4-10 |
| Min platelet count (G/liter) | 75 | 65 | 37 | 150-440 |
| Max LDH ^a activity (U/liter) | 335 | 329 | 540 | < 248 |
| Max CRP ^b level (mg/liter) | 51.1 | 94.5 | 127.6 | < 5 |
| Point of renal biopsy (dpo ^c) | 13 | 9 | 7 | - |

^aLDH: lactate dehydrogenase, ^bCRP: C-reactive protein, ^cdpo: days post onset

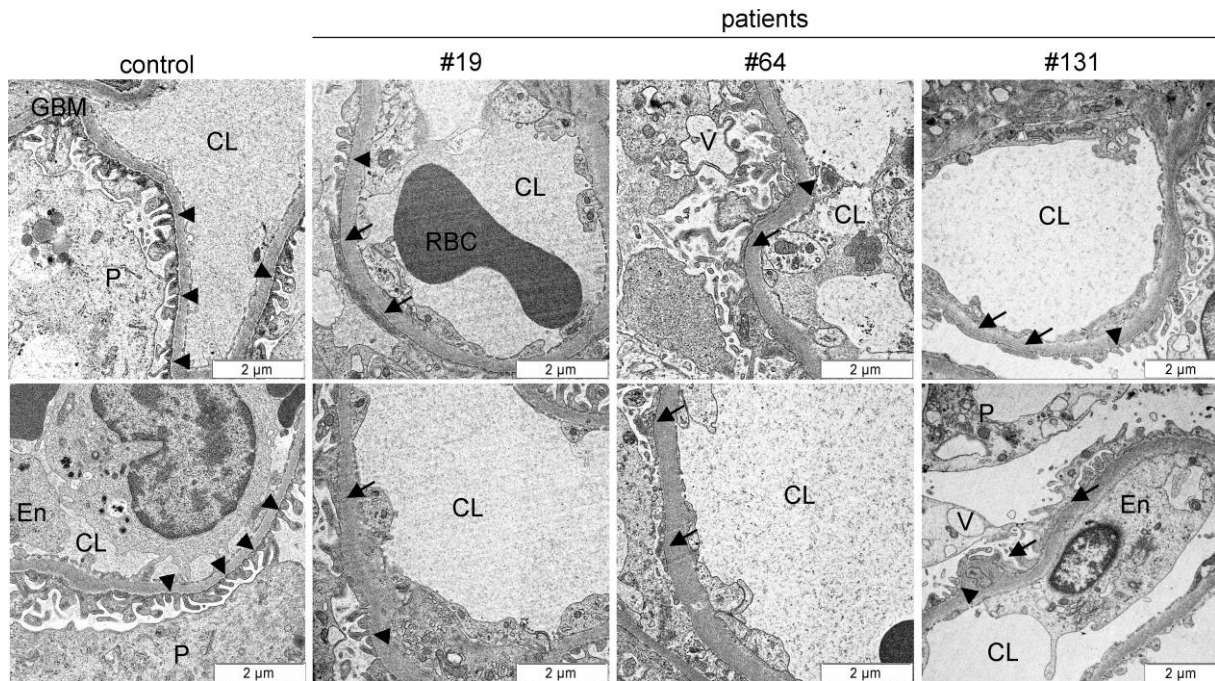


Figure 4 Electron microscopy of human glomeruli. Renal biopsy specimens of three patients with acute hantavirus disease and one of a healthy control kidney were analyzed by transmission electron microscopy. Arrowheads indicate intact foot processes of podocytes. Arrows show effacement of podocyte foot processes. CL: capillary lumen; En: endothelium; P: podocyte; GBM: glomerular basement membrane; RBC: red blood cell; V: vacuole.

3.1.2 *In vitro* effects of hantavirus infection on podocytes

3.1.2.1 Localization of hantaviral N protein in podocytes

The electron microscopy studies demonstrated that foot processes of podocytes were effaced during hantavirus disease. The integrity of proper foot processes is mainly maintained by the cytoskeleton. Therefore, a possible involvement of the cytoskeleton components actin and microtubules was analyzed in human podocytes *in vitro* (Fig. 5).

First, the localization of the hantaviral N protein was examined. Infection of podocytes with HTNV revealed that the N protein appears in a punctate and a filamentous distribution (Fig. 5A). The amount of cells showing the filamentous pattern increased during infection to a maximum of $42.03\% \pm 0.97\%$ (Fig. 5C). Moreover, confocal microscopy analysis revealed that the filamentous N protein pattern partially co-localized with F-actin as displayed by the histogram showing the fluorescence intensities of both proteins. In contrast, no co-localization was observed between HTNV N protein and microtubules (Fig. 5A). In order to investigate if this localization is exhibited by other Old World hantaviruses as well, the infection of podocytes with the less pathogenic PUUV was analyzed for the described effects (Fig. 5B and D). The amount of filamentous PUUV N protein co-localizing with F-actin considerably differed compared to HTNV and was only observed in a maximum of $7.62\% \pm 2.26\%$ of infected cells. Even the co-localization of F-actin and PUUV N protein was less distinctive

than for HTNV N protein. An association between PUUV N protein and microtubules was not detected. The infection kinetics of both virus species were comparable, indicating that the disparity in the appearance and localization of N proteins were not due to different infection rates (Fig. 5C and D).

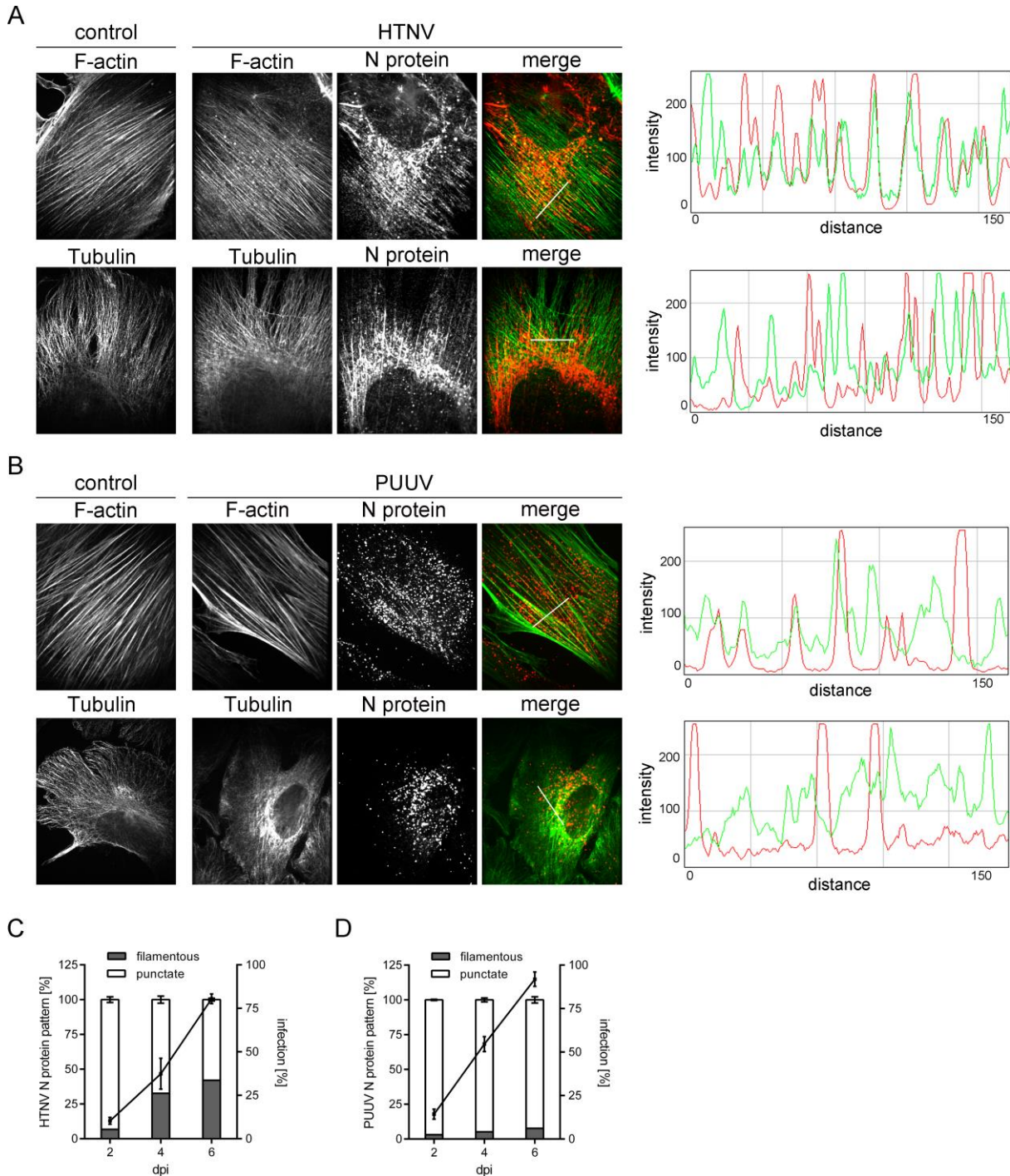


Figure 5 Localization of HTNV and PUUV N protein in podocytes. (A and B) Podocytes infected with HTNV (A) and PUUV (B) were analyzed for N protein, F-actin, and tubulin localization by confocal microscopy on day six after infection. The histogram shows the fluorescence intensity profiles of F-actin (green), tubulin (green), and N protein (red) stainings along the indicated lines. Cells were imaged at a magnification of $\times 1000$. (C and D) Podocytes were analyzed for the N protein localization pattern (left y-axis) and infection (right y-axis) of HTNV (C) and PUUV (D) at indicated points of time. Data were obtained from three independent experiments. Shown is mean \pm SD.

3.1.2.2 Effects of cytoskeletal polymerization inhibitors on N protein in podocytes

In order to examine if an intact cytoskeleton is a prerequisite for the filamentous N protein pattern, hantavirus-infected podocytes were treated with inhibitors of cytoskeleton polymerization (Fig. 6 and 7). Cytochalasin D was used for actin filament disruption and nocodazole for depolymerization of microtubules. The drug concentrations were adjusted to an adequate concentration, which efficiently inhibited the polymerization of the cytoskeleton structures without any cytopathic effect, as revealed by measurement of the cell viability after treatment (Fig. 6 and 7).

The inhibition of actin polymerization in HTNV- and PUUV-infected podocytes significantly resulted in the disappearance of almost the entire filamentous N protein pattern (Fig. 7A-D). Moreover, it seems that N proteins of both virus species were re-located into perinuclear regions (Fig. 7A and C). Interestingly, after washout of the inhibitors the N protein pattern ratio between punctate and filamentous distribution was completely restored compared to control cells. In contrast, the depolymerization of microtubules had neither an effect on the localization nor on the filamentous N protein structures.

These results indicate that an intact integrity of the actin cytoskeleton is crucial for the filamentous N protein distribution.

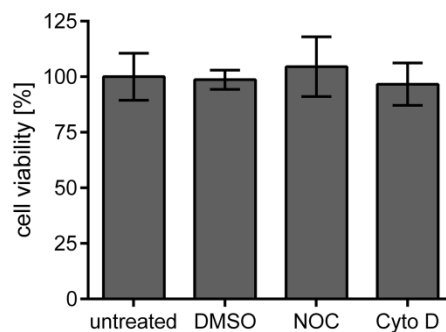


Figure 6 Cell viability of podocytes after treatment with inhibitors of cytoskeletal polymerization. Uninfected cells were treated with solvent control (DMSO), nocodazole (NOC), or cytochalasin D (CytoD) and viability was assessed. The viability of untreated cells was set to 100%. Three independent experiments were performed in triplicates. Shown is mean \pm SD.

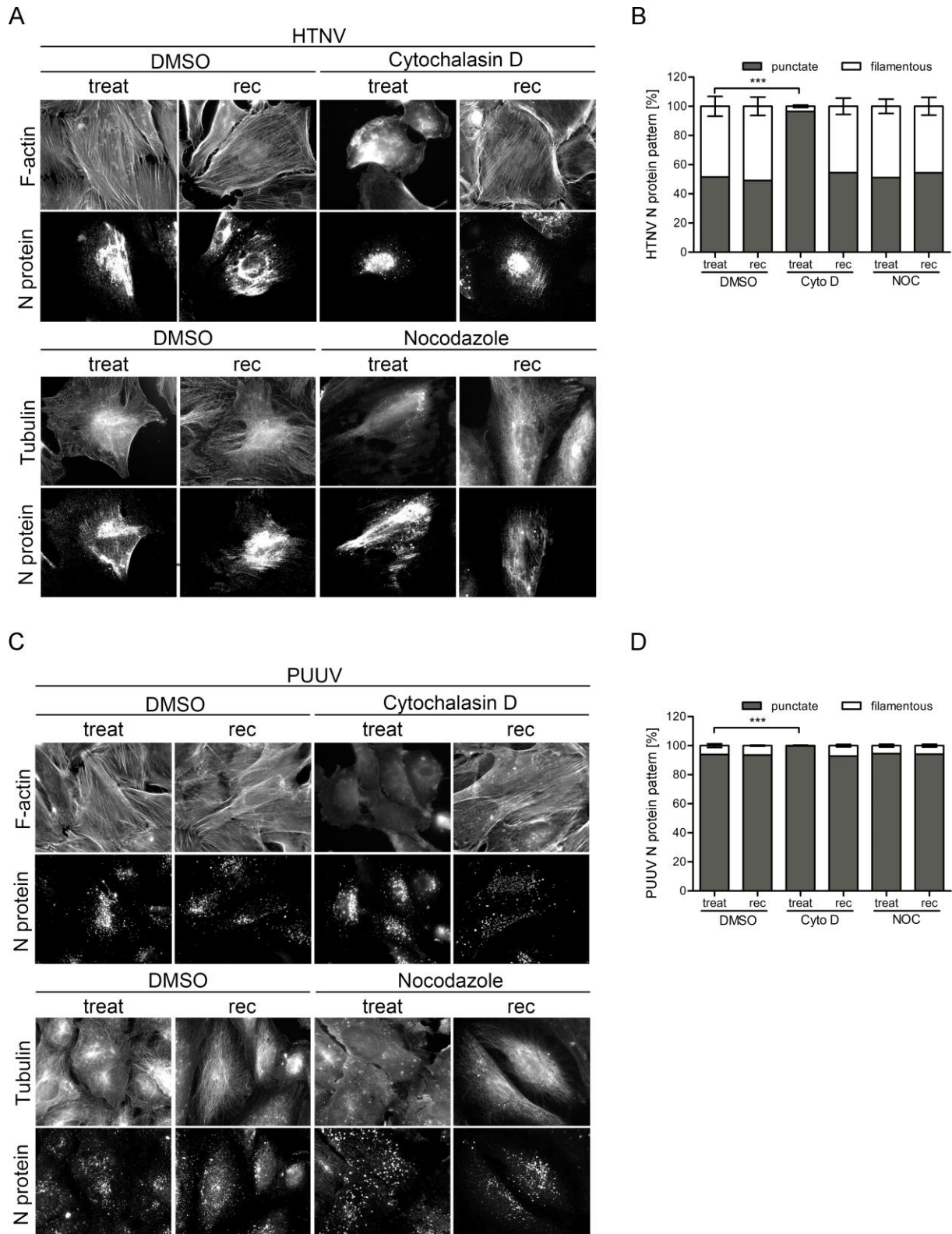


Figure 7 Localization of N proteins in podocytes after modulation of the cytoskeleton. (A and C) Podocytes were infected with HTNV (A) and PUUV (C) and treated with solvent control (DMSO), cytochalasin D (Cyto D), or nocodazole (NOC) on day six post infection. Localization of N protein, F-actin, and tubulin was analyzed after drug treatment (treat) and after recovery (rec) by fluorescence microscopy. Cells were imaged at a magnification of $\times 1000$. (B and D) The localization pattern of N protein of 100 DMSO- and drug-treated podocytes was quantified in each experiment. Three independent experiments were performed. Shown is mean \pm SD.

3.1.2.3 Effects of cytoskeletal polymerization inhibitors on viral release of podocytes

The role of cytoskeleton components was further analyzed regarding the hantaviral replication cycle. To investigate the importance of F-actin and microtubules for the release of infectious particles, hantavirus-infected podocytes were treated with cytochalasin D, nocodazole or solvent control (Fig. 8). Supernatants were harvested four hours after treatment with cytoskeleton polymerization inhibitors because this was the earliest point of time to reproducibly obtain supernatants with detectable amounts of infectious particles.

Interestingly, the disruption of the cytoskeleton components caused different consequences for both virus species (Fig. 8A). Nocodazole had a similar reducing effect on the viral release of HTNV- ($81.05\% \pm 4.73\%$ vs. $100\% \pm 11.91\%$, $P = 0.0108$) and PUUV-infected podocytes ($75.81\% \pm 6.93\%$ vs. $100\% \pm 9.15\%$, $P = 0.0003$) compared to control cells. The amount of infectious particles found in the supernatants after cytochalasin D treatment differed enormously. After F-actin disruption, the viral release of HTNV-infected cells was significantly decreased compared to untreated cells ($53.84\% \pm 8.50\%$ vs. $100\% \pm 11.91\%$, $P > 0.0001$). In contrast, depolymerization of actin had no significant effect on the release of PUUV particles ($110.13\% \pm 6.70\%$ vs. $100\% \pm 9.15\%$, $P = 0.0543$). After washout of the inhibitors, viral release of both viruses was completely restored compared to controls as determined by subsequent analysis of supernatants four hours later (Fig. 8B).

These data indicate that hantaviruses depend on microtubules for an efficient release of infectious particles. In addition, the viral release of HTNV is also dependent on an intact actin cytoskeleton. The data suggest a correlation between F-actin localization of N protein and the release of hantaviruses.

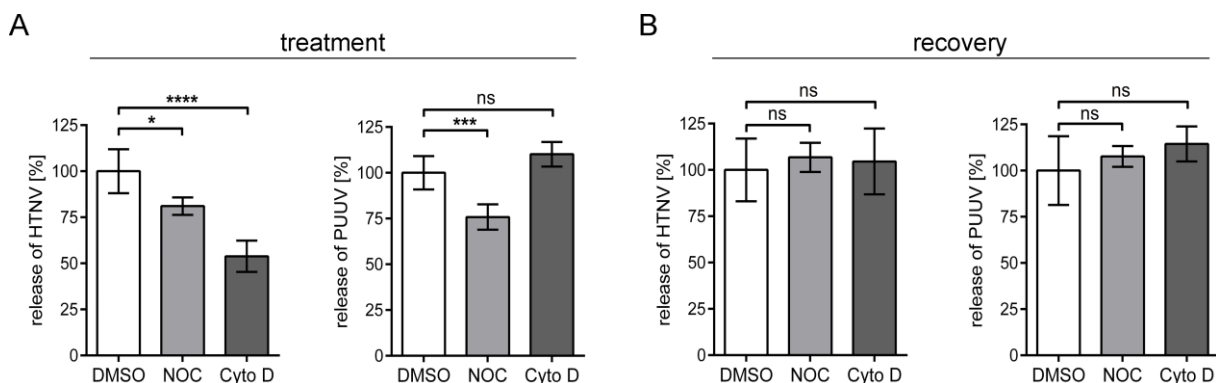


Figure 8 Viral release assay of HTNV- and PUUV-infected podocytes. Podocytes were infected with HTNV or PUUV and treated with solvent control (DMSO), cytochalasin D (Cyto D), or nocodazole (NOC) on day six post infection for four hours. (A) Supernatants of treated cells were harvested and the amount of infectious particles was quantified by In-Cell Western. Three independent experiments were performed in triplicates. The viral release of solvent control-treated cells was set to 100%. Shown is mean \pm SD. (B) Cells were washed after treatment and incubated for another four hours in fresh medium. The amount of released viral particles was quantified as described above.

3.1.2.4 Hantaviral effects on actin cytoskeletal organization of podocytes

Crucial for podocyte function and FP formation is an intact actin cytoskeleton. The results displayed above revealed FP effacement during hantavirus disease and an involvement of actin during the viral replication cycle. Therefore, changes of the actin cytoskeleton after hantavirus infection were examined by quantifying the amount of F- and G-actin in infected and uninfected podocytes (Fig. 9).

At first, any cytopathic effect after infection leading to a loss of cells was excluded by measuring the cell viability. Neither HTNV nor PUUV caused any effect on the viability of podocytes (Fig. 9A and C). Uninfected, hantavirus-infected, and phalloidin-treated podocytes were lysed and cellular fractions were analyzed for cellular actin forms (Fig. 9B and D). The F-actin enhancer phalloidin, which drives actin polymerization to more than 80%, served as positive control and demonstrated an effective pelleting of F-actin. Cellular fractionation of podocytes revealed that the amount of F-actin in the insoluble fraction of HTNV-infected cells was decreased and the F-/G- ratio was significantly changed compared to control cells (0.45 ± 0.09 vs. 1.00 ± 0.14 , $P = 0.0045$) (Fig. 9B). The cytoskeletal organization was also influenced by PUUV, but to a lower extent. Compared to control cells, the F-/G-actin ratio of PUUV-infected podocytes was reduced to 0.67 ± 0.12 vs. 1.00 ± 0.11 , $P = 0.0245$ (Fig. 9D).

These results show that an infection with hantaviruses changes the actin cytoskeleton in podocytes by decreasing the F-actin amount.

3.1.2.5 Functional consequences of hantavirus infection in podocytes

Since the hantaviral N protein is associated with F-actin and its amount is decreased after infection, it could be possible that these interactions cause consequences for podocyte function. Therefore, the migration and adhesion, which are crucial for proper podocyte function, were examined.

First, the adhesion capacity of podocytes was analyzed after infection with hantaviruses and compared to uninfected control cells (Fig. 10A and B). The infection was monitored by immunostaining for hantaviral N protein revealing that more than 90% of cells were positive for HTNV or PUUV N protein. The amount of HTNV-infected podocytes that adhered after detachment was decreased to $57.13\% \pm 16.28\%$ vs. $100\% \pm 15.7\%$, $P = 0.0304$ (Fig. 10A). The effect of PUUV was less pronounced and the adhesion ability was reduced to $70.96\% \pm 7.88\%$ vs. $100\% \pm 15.53\%$, $P = 0.0446$ (Fig. 10B).

Next, the migration capacity was analyzed by investigating podocyte motility into a cell-free gap. The area covered by podocytes was measured at the beginning and the end of each experiment (Fig. 10C

and D). The infection of HTNV and PUUV caused an impaired migration of podocytes compared to uninfected cells. The migration was reduced to $27.49\% \pm 10.69\%$ vs. $100\% \pm 9.29\%$, $P = 0.0009$ for HTNV and to $72.80\% \pm 4.89\%$ vs. $100\% \pm 11.06\%$, $P = 0.0041$ for PUUV. Immunostaining of N proteins revealed that more than 90% of podocytes were infected.

In summary, hantaviruses are capable to cause functional consequences in podocytes by reducing the adhesion and migration capacity. The effects are more pronounced for HTNV than PUUV infection.

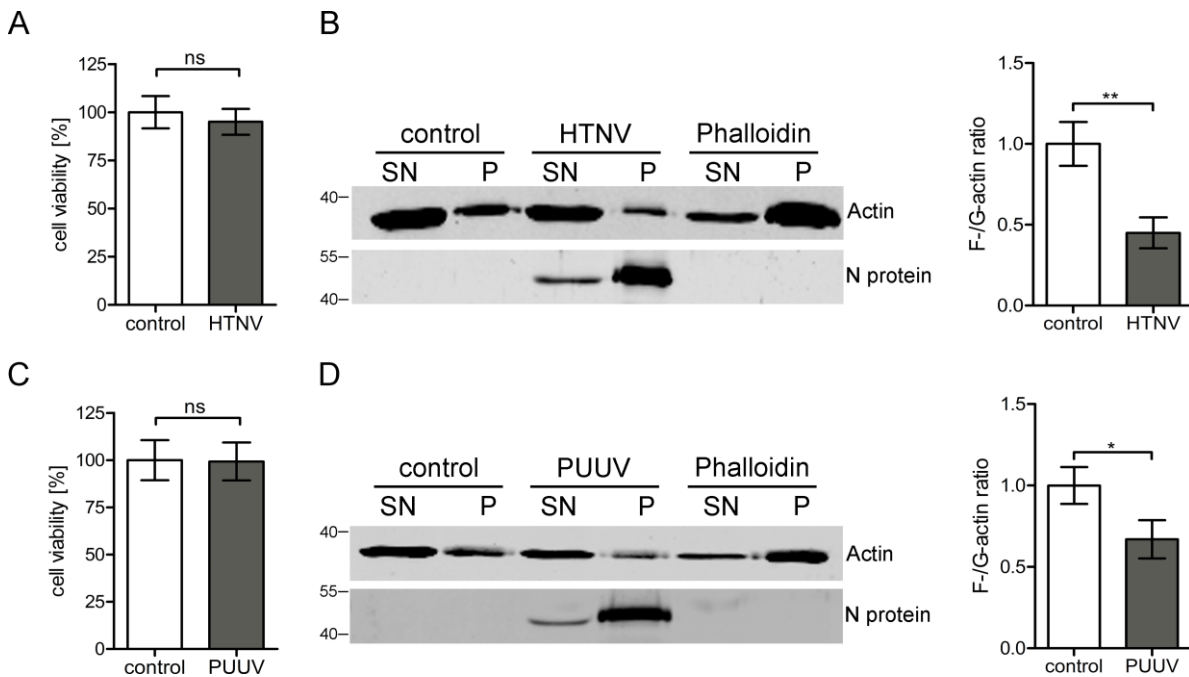


Figure 9 Cytoskeletal organization in HTNV- and PUUV-infected podocytes. (A and C) Podocytes were infected with HTNV (A) or PUUV (C) and viability was assessed on day six after infection. Control cells remained uninfected and viability was set to 100%. Three independent experiments were performed in triplicates. Shown is mean \pm SD. (B and D) Fractionated cellular lysates (SN: supernatant, P: pellet) of uninfected (control), HTNV- (B) or PUUV (D)-infected, and phalloidin-treated podocytes were analyzed for actin and N protein by Western blot on day six after infection. One representative Western blot taken out of three independent experiments is displayed. The band intensities from Western blots were quantified to measure the F-/G-actin ratio. The ratio of uninfected podocytes was set to 1. Shown is mean \pm SD.

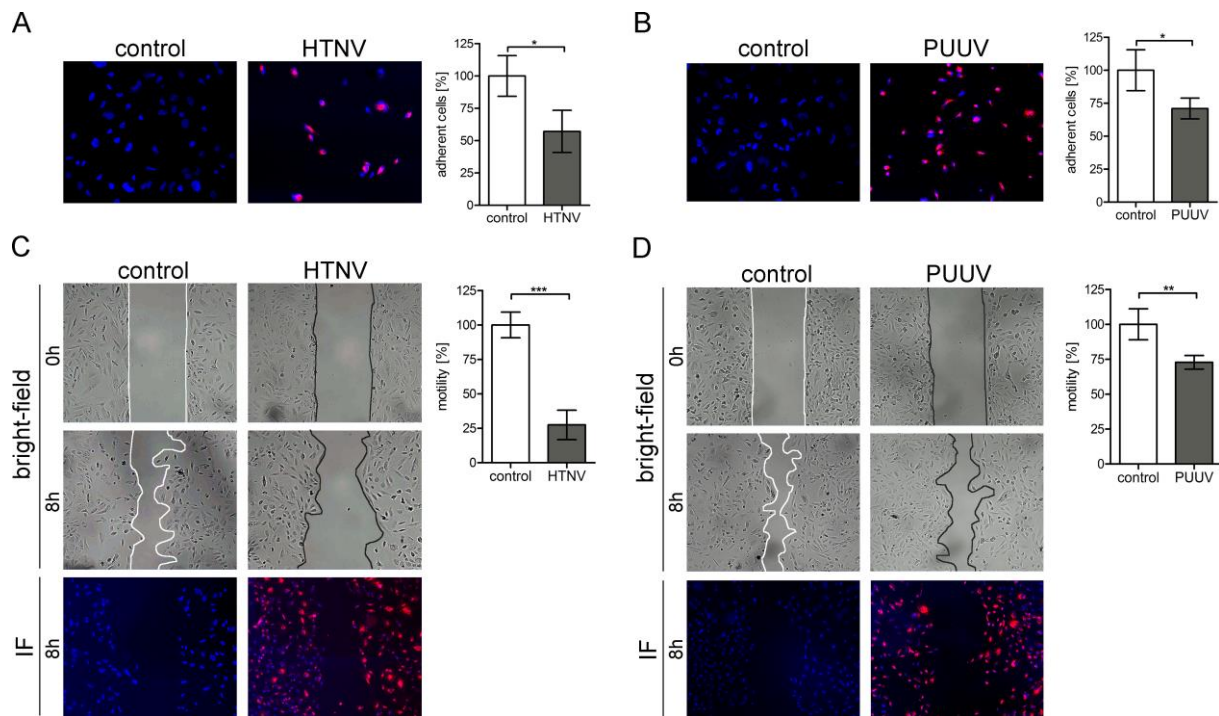


Figure 10 Adhesion and migration capacity of HTNV- and PUUV-infected podocytes. (A and B) Uninfected and HTNV-(A) or PUUV-(B) infected podocytes were detached, plated into 96-wells and numbers of attached cells were quantified after one hour by In-Cell Western. Three independent experiments were performed in quadruplicates. N protein was stained in red and cells were imaged at a magnification of $\times 200$. Adhesion of uninfected cells was set to 100%. Shown is mean \pm SD. (C and D) Confluent monolayers of podocytes were seeded into μ -plates and infected with HTNV (C) or PUUV (D). After removal of the insert and after eight hours, cell-free areas were measured and relative migration was calculated. Migration of uninfected podocytes was set to 100%. N protein was stained in red and cells were imaged at a magnification of $\times 100$. Representative images taken out of three independent experiments are displayed. Shown is mean \pm SD.

3.1.3 *In vitro* effects of hantavirus infection on Vero E6 cells

3.1.3.1 Localization of hantaviral N protein in Vero E6 cells

Vero E6 cells are renal epithelial cells from the African green monkey that are commonly used for virus propagation and most of the previous studies on hantaviruses were performed using these cells. Thus, Vero E6 cells were included in this study to analyze possible cell-specific effects after hantavirus infection (Fig. 11).

The N protein appearance in Vero E6 cells differed enormously from that found in podocytes (see Fig. 11 and Fig. 5). Vero E6 cells infected with either HTNV or PUUV showed no detectable filamentous N protein. The N protein of both virus species was strictly localized in the punctate pattern during the infection (Fig. 11A-D). Moreover, the N protein co-localization with actin, found in podocytes, was absent in hantavirus-infected Vero E6 cells. Again, no association with the microtubules was observed.

The results show that the filamentous pattern of N protein and the co-localization with actin can only be observed in human podocytes.

3.1.3.2 Effects of cytoskeletal polymerization inhibitors on viral release of Vero E6 cells

Previous studies of the hantaviral replication cycle in Vero E6 cells showed a different involvement of cytoskeletal components depending on the virus species used. Despite the fact that no co-localization was found, Vero E6 cells were examined on whether or not the release of viruses is dependent on the actin cytoskeleton.

Cytochalasin D and nocodazole inhibited efficiently the polymerization of actin and microtubules in Vero E6 cells, respectively (Fig. 12A). After treatment, both depolymerization inhibitors had no influence on the cell viability, indicating that possible effects were not caused by cell death (Fig. 12B).

The disruption of the cytoskeleton components in HTNV-infected Vero E6 cells showed different results as seen for HTNV-infected podocytes (Fig. 12C and Fig. 8A). Compared to untreated cells, the depolymerization of microtubules caused a massive decrease of released HTNV particles to $9.86\% \pm 6.04\%$ vs. $100\% \pm 12.36\%$, $P < 0.0001$. In contrast to podocytes, a deteriorated actin cytoskeleton had no effect on the viral release in HTNV-infected Vero E6 cells. The effects on PUUV-infected Vero E6 cells were similar to that and the disruption of microtubules decreased the release of infectious particles compared to controls to $17.73\% \pm 5.09\%$ vs. $100\% \pm 15.01\%$, $P < 0.0001$, while actin depolymerization had no consequences (Fig. 12C). As already shown in podocytes, the effect on the viral release was reversible after washout of the respective polymerization inhibitors in Vero E6 cells (Fig. 12D).

These data indicate that microtubules play a more important role in the release of hantavirus in Vero E6 cells than in podocytes. Moreover, the integrity of F-actin is only observed for HTNV localization and viral release in podocytes.

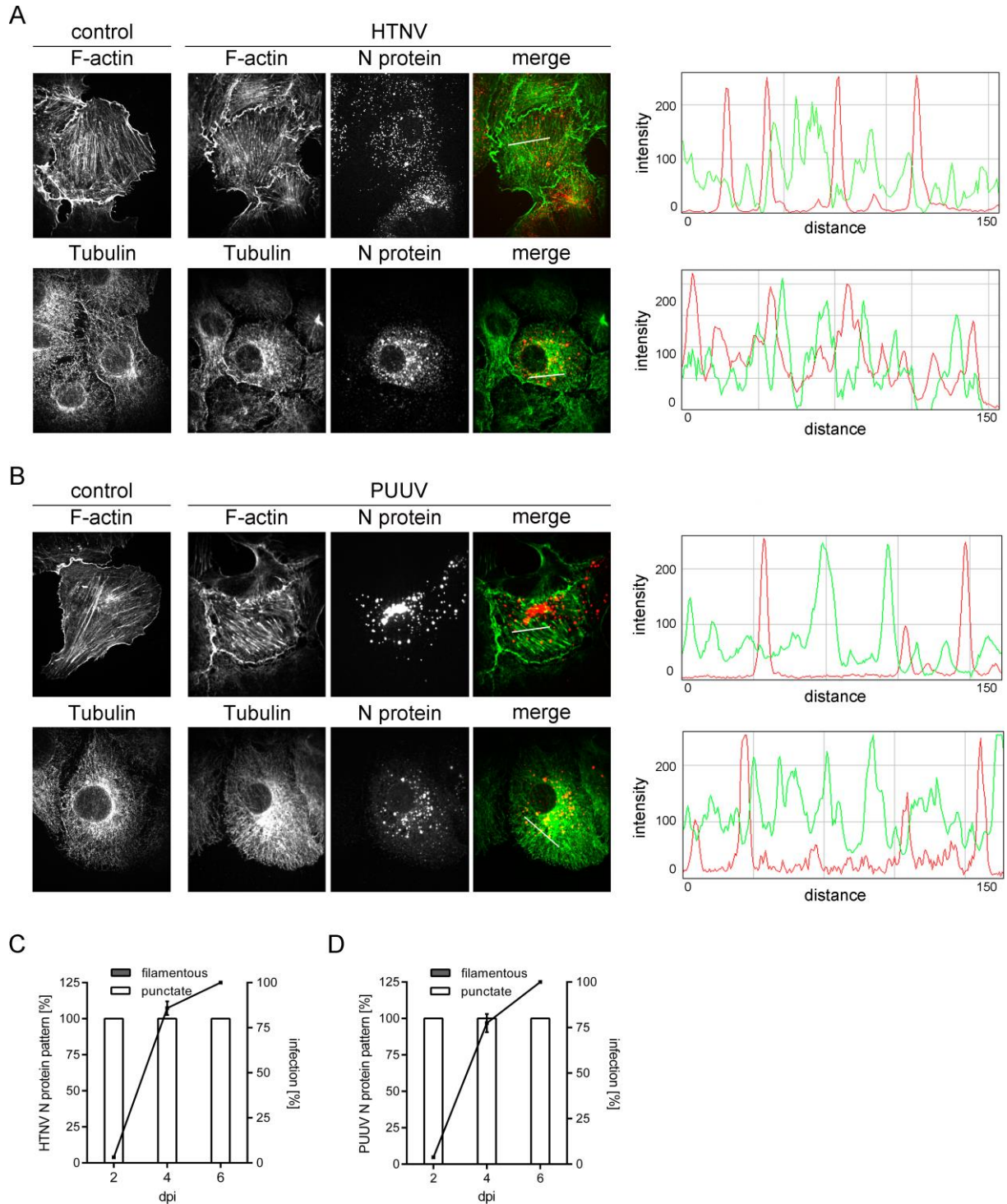


Figure 11 Localization of HTNV and PUUV N protein in Vero E6 cells. Vero E6 cells infected with HTNV (A) and PUUV (B) were analyzed for N protein, F-actin, and tubulin localization by confocal microscopy on day six after infection. The histogram shows the fluorescence intensity profiles of F-actin (green), tubulin (green), and N protein (red) stainings along the indicated lines. Cells were imaged at a magnification of $\times 1000$. (C and D) Vero E6 cells were analyzed for the N protein localization pattern (left y-axis) and infection (right y-axis) of HTNV (C) and PUUV (D) at indicated points of time. Data were obtained from three independent experiments. Shown is mean \pm SD.

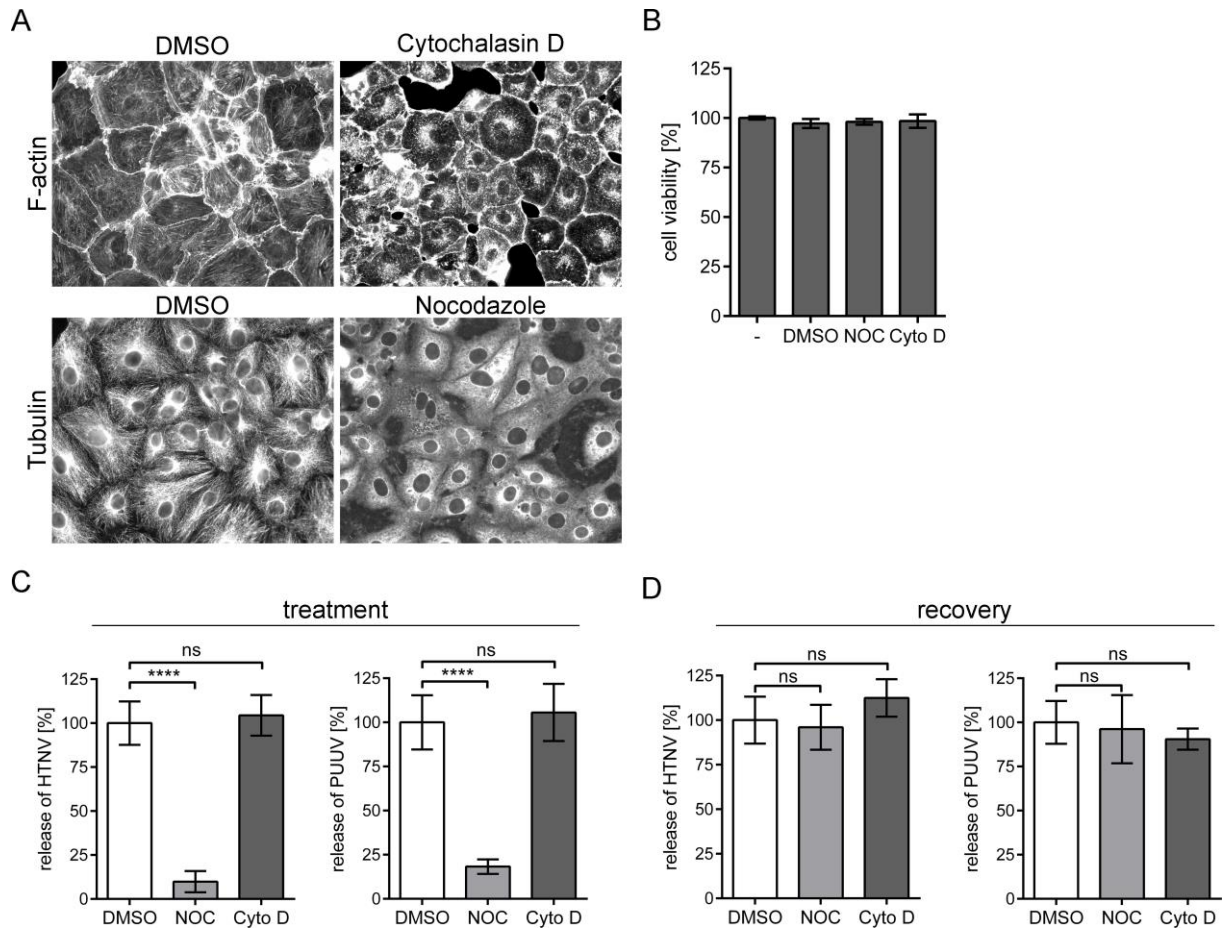


Figure 12 Viral release assay of HTNV- and PUUV-infected Vero E6 cells. (A) Staining of F-actin and microtubules after treatment of uninfected Vero E6 cells with solvent control (DMSO), cytochalasin D (Cyto D), or nocodazole (NOC) for four hours. Representative images are displayed. (B) Viability of uninfected Vero E6 cells after treatment was assessed. The viability of untreated cells was set to 100%. Three independent experiments were performed in triplicates. Shown is mean \pm SD. (C and D) Vero E6 cells were infected with HTNV or PUUV and treated with solvent control (DMSO), cytochalasin D (Cyto D), or nocodazole (NOC) on day six post infection for four hours. (C) Supernatants of treated cells infected with HTNV or PUUV were harvested and the amount of infectious particles was quantified by In-Cell Western. Three independent experiments were performed in triplicates. The viral release of solvent control-treated cells was set to 100%. Shown is mean \pm SD. (D) Cells were washed after treatment and incubated for another four hours in fresh medium. The amount of released viral particles was quantified as described above.

3.1.3.3 Hantaviral effects on the actin cytoskeletal organization of Vero E6 cells

The examined Old World hantaviruses did neither co-localize with F-actin nor depend on its integrity for viral release in Vero E6 cells. To determine if hantaviruses still have an effect on the organization of the actin cytoskeleton, the F-/G-actin ratio was also quantified in HTNV- and PUUV-infected Vero E6 cells (Fig. 13).

Vero E6 cells infected with neither HTNV nor PUUV affected the viability compared to uninfected cells (Fig. 13A and C). Moreover, both virus species did not significantly alter the F-/G-actin ratio in Vero E6 cells (Fig. 13B and D).

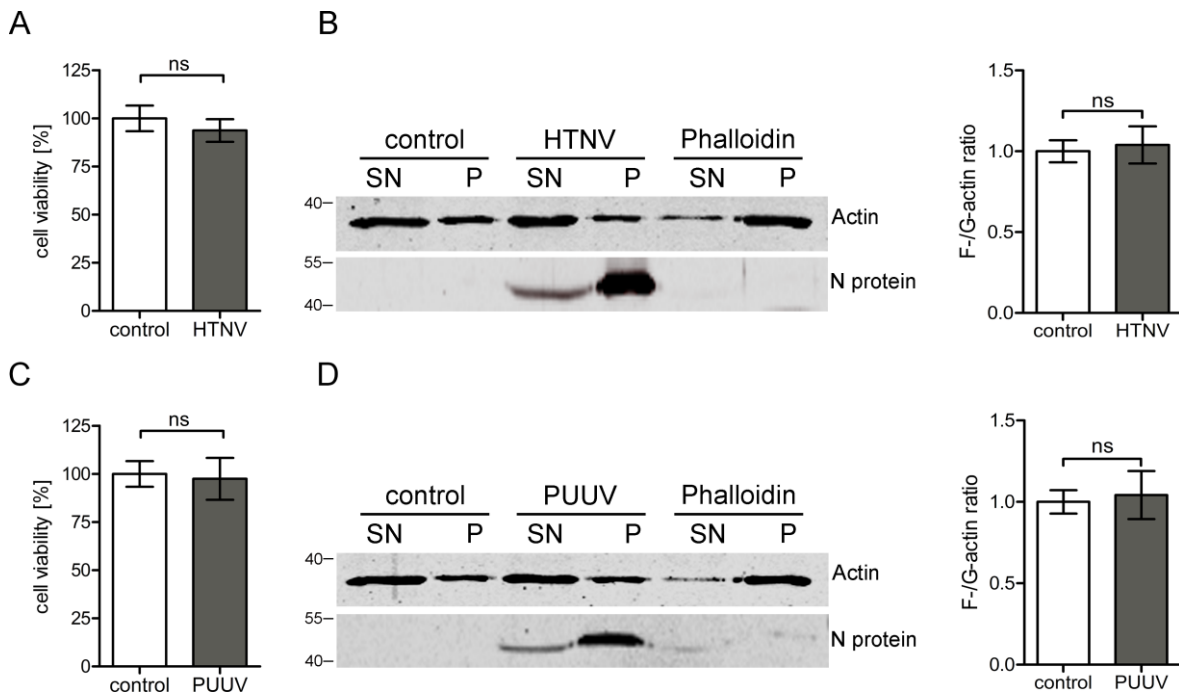


Figure 13 Cytoskeletal organization in HTNV- and PUUV-infected Vero E6 cells. (A and C) Vero E6 cells were infected with HTNV (A) or PUUV (C) and viability was assessed at day six after infection. Control cells remained uninfected and viability was set to 100%. Three independent experiments were performed in triplicates. Shown is mean \pm SD. (B and D) Fractionated cellular lysates (SN: supernatant, P: pellet) of uninfected (control), HTNV- (B) or PUUV (D)-infected, and phalloidin-treated Vero E6 cells were analyzed for actin and N protein by Western blot. One representative Western blot taken out of three independent experiments is displayed. The band intensities from Western blots were quantified to measure the F-/G-actin ratio. The ratio of uninfected Vero E6 cells was set to 1. Shown is mean \pm SD.

3.1.3.4 Functional consequences of hantavirus infection in Vero E6 cells

The localization of hantaviral N protein and the effects of infection on F-actin differed enormously between Vero E6 cells and podocytes. To investigate, if hantaviruses are capable to cause functional consequences without an actin involvement, Vero E6 cells were also analyzed for adhesion and migration to examine cell-specific effects (Fig. 14).

Visualization of N protein during experiments showed that more than 90% of the cells were infected (Fig. 14A-D). The functional assays revealed that neither HTNV nor PUUV were capable to induce impairment of the adhesion or migration of Vero E6 cells compared to control cells.

The different localization of N protein, the absence of actin involvement for viral release and the lack of functional consequences after hantavirus infection in Vero E6 cells demonstrate that the hantaviral replication cycle and subsequent cellular impairments vary tremendously in Vero E6 cells and podocytes.

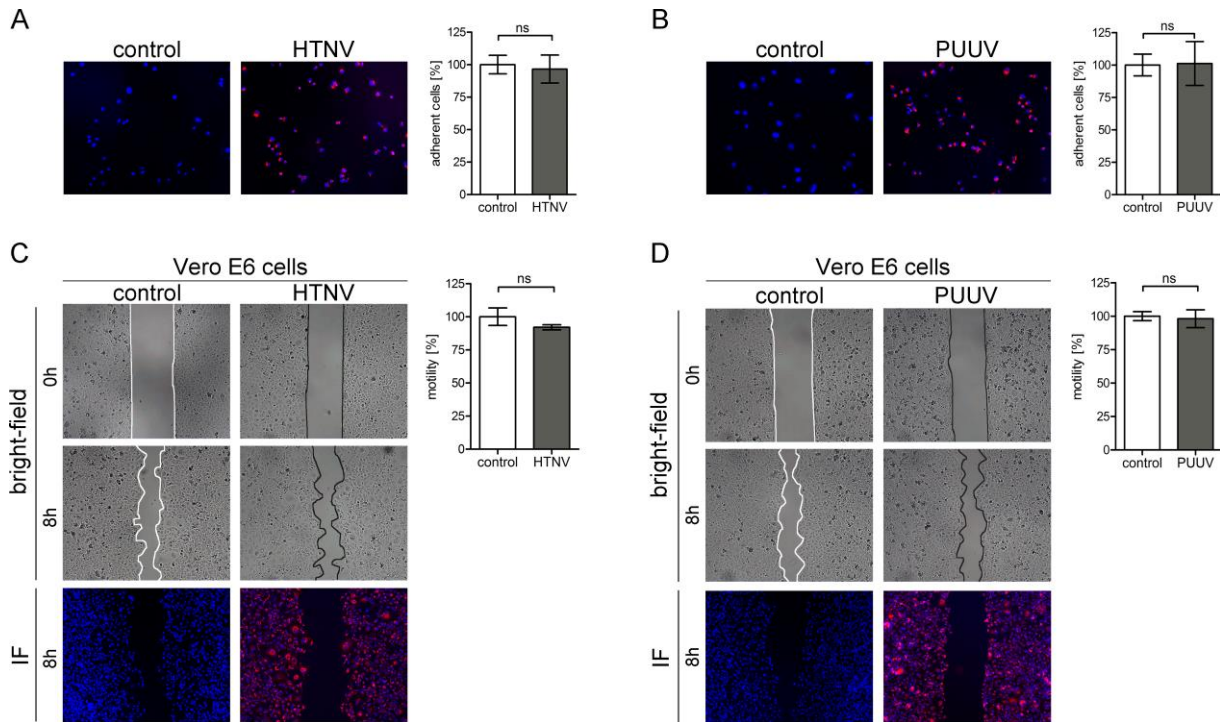


Figure 14 Adhesion and migration capacity of HTNV- and PUUV-infected Vero E6 cells. (A and B) Uninfected and HTNV-(A) or PUUV-infected (B) Vero E6 cells were detached, plated into 96-wells and numbers of attached cells were quantified after one hour by In-Cell Western. Three independent experiments were performed in quadruplicates. N protein was stained in red and cells were imaged at a magnification of $\times 200$. Adhesion of uninfected cells was set to 100%. Shown is mean \pm SD. (C and D) Uninfected or HTNV-(C) or PUUV-infected (D) Vero E6 were seeded confluent into μ -plates. After removal of the insert and after eight hours, cell-free areas were measured and relative migration was calculated. Migration of uninfected Vero E6 cells was set to 100%. N protein was stained in red and cells were imaged at a magnification of $\times 100$. Representative images taken out of three independent experiments are displayed. Shown is mean \pm SD.

3.1.4 Effects of hantaviruses on primary human podocytes

3.1.4.1 Localization of hantaviral N protein in primary podocytes

The observed effects in cell lines caused by hantaviruses were further analyzed focusing on their biological significance by analyzing primary human podocytes as relevant target cells (Fig. 15).

The cells were first analyzed regarding the expression of podocyte-specific synaptopodin (Fig. 15A). Synaptopodin was found in the typical dotted filamentous-like distribution throughout the entirety of the primary podocyte [119].

After HTNV infection, primary podocytes displayed the punctate and filamentous N protein distribution as seen in the cell line (Fig. 15B). The localization of the filamentous pattern revealed that HTNV N protein co-localized in primary cells with F-actin. The number of cells displaying the filamentous pattern increased during infection to $16.74\% \pm 3.71\%$ (Fig. 15C). In contrast, no N protein filamentous distribution was found in PUUV-infected primary podocytes (Fig. 15B and D). The amount of cells infected with HTNV or PUUV differed dramatically. While $77.55\% \pm 3.76\%$ of primary podocytes were infected with PUUV, only $14.48\% \pm 1.33$ showed a HTNV infection.

These results demonstrate that HTNV N protein co-localizes with F-actin and that primary podocytes are more permissive for PUUV than for HTNV infection *in vitro*.

3.1.4.2 Functional consequences of hantavirus-infected primary podocytes

The migration capacity of primary podocytes was also analyzed by the covered distance of single infected cells. Due to a low percentage of HTNV infection, the migration was only determined in PUUV-infected primary podocytes (Fig. 16).

Compared to uninfected control cells, the migration capability of primary podocytes was significantly reduced after infection with PUUV ($62.65\% \pm 6.38$ vs $100\% \pm 6.65\%$, $P = 0.0022$).

In conclusion, filamentous N protein and functional consequences of hantavirus infection are also detected in primary cells. These findings are comparable to the results obtained in the podocyte cell line.

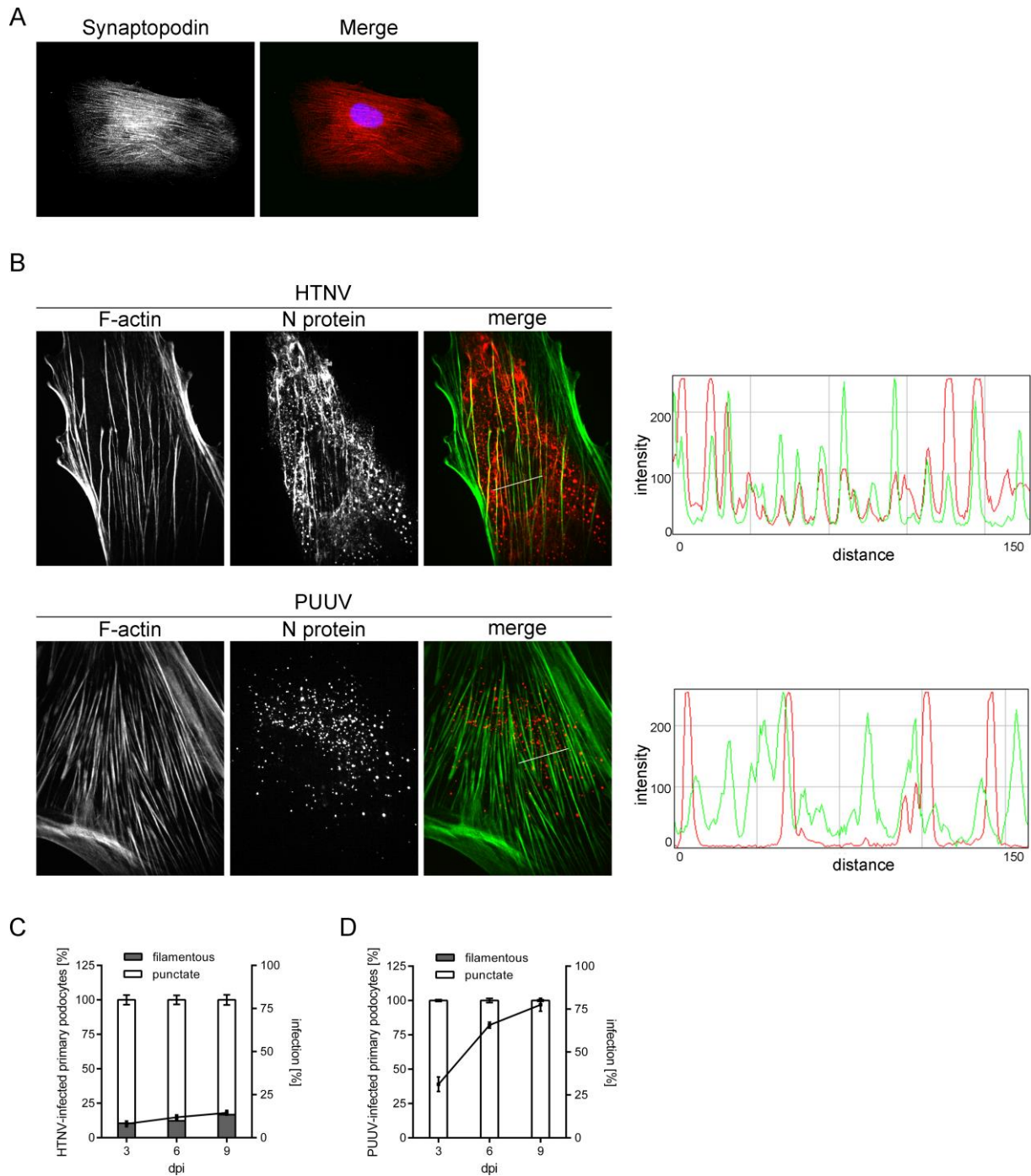


Figure 15 Localization of HTNV and PUUV N protein in primary podocytes. (A) Analysis for the expression of synaptopodin (red) in primary podocytes by immunofluorescence at a magnification of $\times 600$. (B) HTNV- and PUUV-infected cells were analyzed for N protein and F-actin localization by confocal microscopy on day nine after infection. The histogram shows the fluorescence intensity profiles of F-actin (green) and N protein (red) stainings along the indicated lines. Cells were imaged at a magnification of $\times 1000$. (C and D) Primary podocytes were analyzed for the N protein localization pattern (left y-axis) and infection (right y-axis) of HTNV (C) and PUUV (D) at indicated points of time. Data were obtained from three independent experiments. Shown is mean \pm SD.

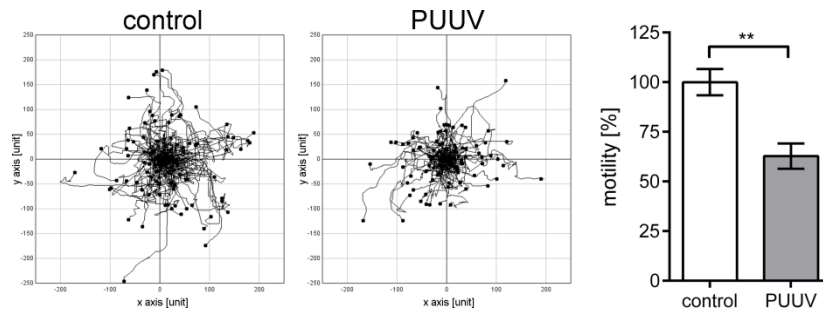


Figure 16 Migration capacity of PUUV-infected primary podocytes. Migration of uninfected and PUUV-infected primary podocytes was examined by live cell imaging. 100 cells per experiment were analyzed by single-cell-tracking. Three independent experiments were performed. Shown is mean \pm SD.

3.2 Analysis of hantaviral infection in renal tubules

3.2.1 Tubular alterations in kidney biopsy specimens of patients with hantavirus disease

Previous studies showed that tubular epithelial cells are infected by hantaviruses *in vivo* and the non-selective proteinuria during hantaviral disease indicates that the function of the tubular apparatus is disturbed.

Renal biopsies of three patients with serologically-confirmed acute hantavirus infection and of one healthy control person were analyzed by electron microscopy for tubular changes between nine and 13 days post onset (Tab. 3, Fig. 17). Compared to the control, biopsies of infected patients showed serious subcellular injuries. Hantavirus disease induced cell swelling and severe cytoplasmic vacuolization of the renal tubular epithelium. Vacuoles are mainly observed beneath the microvilli at the apical surface. Compared to control biopsies, damaged nuclei were found in biopsies of hantavirus-infected patients. The basement membrane and microvilli displayed a normal morphology.

The analysis elucidates that, besides podocytes, tubular cells are also affected by hantaviruses, suggesting that their impairment might play a role during renal disease. The infection of hantaviruses in tubular epithelial cells was further analyzed *in vitro*.

Table 3 Characteristics, peak, and nadir levels of laboratory parameters obtained from three patients with acute PUUV hantavirus disease used for electron microscopy analysis of renal tubules.

| Characteristic | #19 | #36 | #64 | reference |
|---|-------|-------|-------|-----------|
| Age (yr) | 48 | 51 | 37 | - |
| Gender | m | m | m | - |
| Duration of hospitalization (days) | 6 | 11 | 8 | - |
| Max serum creatinine level (mg/dl) | 8.35 | 9.25 | 11.94 | 0.1-1.3 |
| Min serum albumin level (g/liter) | 32.9 | 30.8 | 28 | 30-50 |
| Max leukocyte count (G/liter) | 11.12 | 13.91 | 15.6 | 4-10 |
| Min platelet count (G/liter) | 75 | 33 | 65 | 150-440 |
| Max LDH ^a activity (U/liter) | 335 | 375 | 329 | < 248 |
| Max CRP ^b level (mg/liter) | 51.1 | 85.3 | 94.5 | < 5 |
| Point of renal biopsy (dpo ^c) | 13 | 11 | 9 | - |

^aLDH: lactate dehydrogenase, ^bCRP: C-reactive protein, ^cdpo: days post onset

3.2.2 Effects of hantaviruses on human renal epithelial primary cells (HREPC)

3.2.2.1 Localization of hantaviral N protein in HREPC

Electron microscopy analysis of renal biopsies revealed an alteration of tubular epithelial cell morphology during hantavirus disease. In order to investigate if functional consequences of hantavirus infection exists as in podocytes, the association of the hantaviral N protein to F-actin was analyzed in HREPC (Fig. 18).

As for podocytes, infection of HREPC with HTNV displayed a punctate and filamentous pattern of the HTNV N protein. Analysis of the fluorescence intensities of HTNV N protein and F-actin revealed a co-localization (Fig. 18A). The amount of cells showing filaments increased to a maximum of $42.16\% \pm 1.70\%$ (Fig. 18B). In contrast, the punctate pattern dominated in PUUV-infected HREPC and no filamentous pattern was observed (Fig. 18A and C). Interestingly, as seen in primary podocytes, HREPC were much more permissive for PUUV than for HTNV infection. The amount of PUUV-infected HREPC reached to $79.23\% \pm 6.247\%$ while only $36.33\% \pm 2.10\%$ of cells were infected with HTNV (Fig. 18B and C).

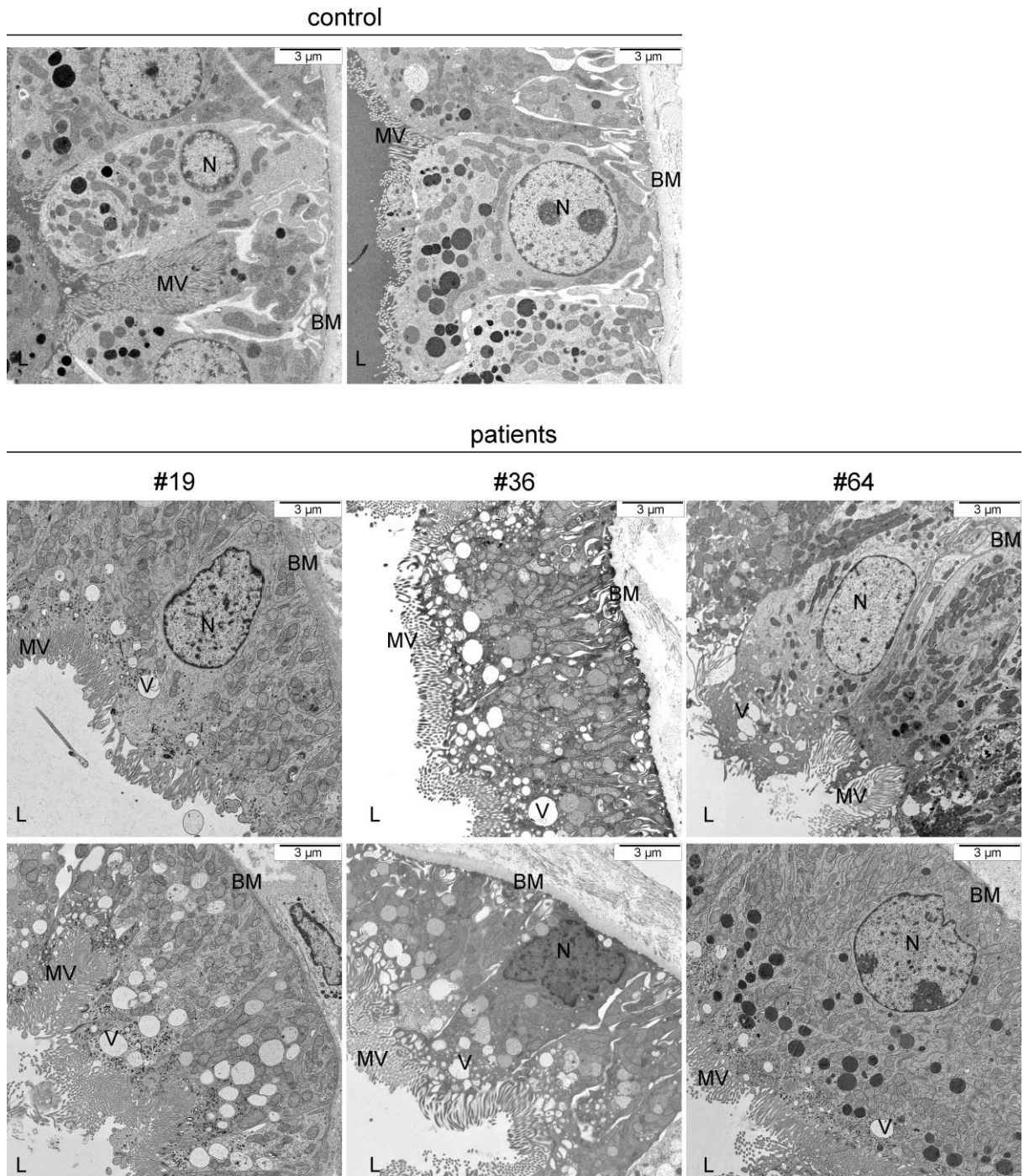
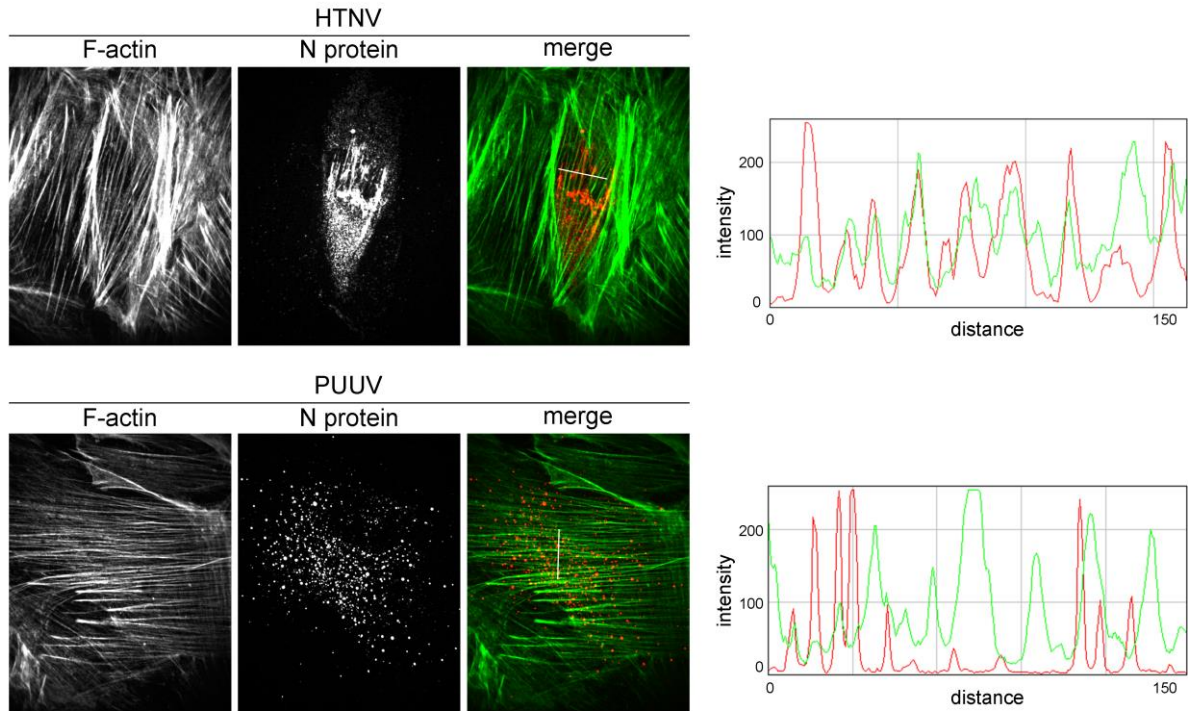
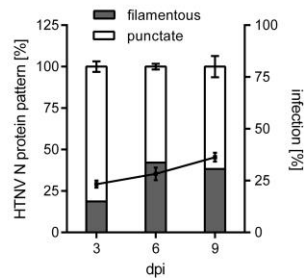


Figure 17 Electron microscopy of human renal tubules. Renal biopsy specimens of three patients with acute hantavirus disease and one of a healthy control kidney were analyzed by transmission electron microscopy. MV: microvilli, BM: basement membrane, L: lumen, V: vacuole, N: nucleus.

A



B



C

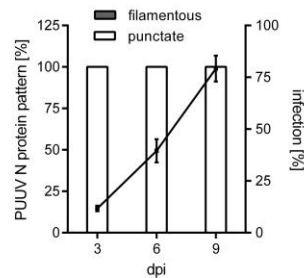


Figure 18 Localization of HTNV and PUUV N protein in HREPC. (A) HREPC infected with HTNV or PUUV were analyzed for N protein and F-actin localization by confocal microscopy on day nine after infection. The histogram shows the fluorescence intensity profiles of F-actin (green) and N protein (red) staining along the indicated lines. Cells were imaged at a magnification of $\times 1000$. (B and C) HREPC were analyzed for the N protein localization pattern (left y-axis) and infection (right y-axis) of HTNV (B) and PUUV (C) at indicated points of time. Data were obtained from three independent experiments. Shown is mean \pm SD.

3.2.2.2 Functional consequences of hantavirus-infected HREPC

Since the adhesion and migration capacity is also of importance for HREPC, functional consequences after infection with HTNV and PUUV were examined (Fig. 19).

In comparison to controls ($100\% \pm 3.35\%$), the adhesion of PUUV- and HTNV-infected cells decreased to $60.83\% \pm 7.74\%$, $P = 0.0097$ and $82.56\% \pm 5.17\%$, $P = 0.0474$, respectively (Fig. 19A). The effect on the migration capacity of HREPC was also more severe after PUUV ($58.63\% \pm 2.87\%$, $P = 0.0006$) than after HTNV infection ($75.57\% \pm 4.94\%$, $P = 0.0136$) compared to uninfected cells (100 ± 3.05) (Fig.

19B). The minor impairment of HTNV infection on the cellular adhesion and migration compared to PUUV was likely to be caused due to low infection efficiencies.

In conclusion, Old World hantavirus infections cause an impairment of the adhesion and migration capacities in primary podocytes and HREPC, which are comparable to the results obtained in the podocyte cell line.

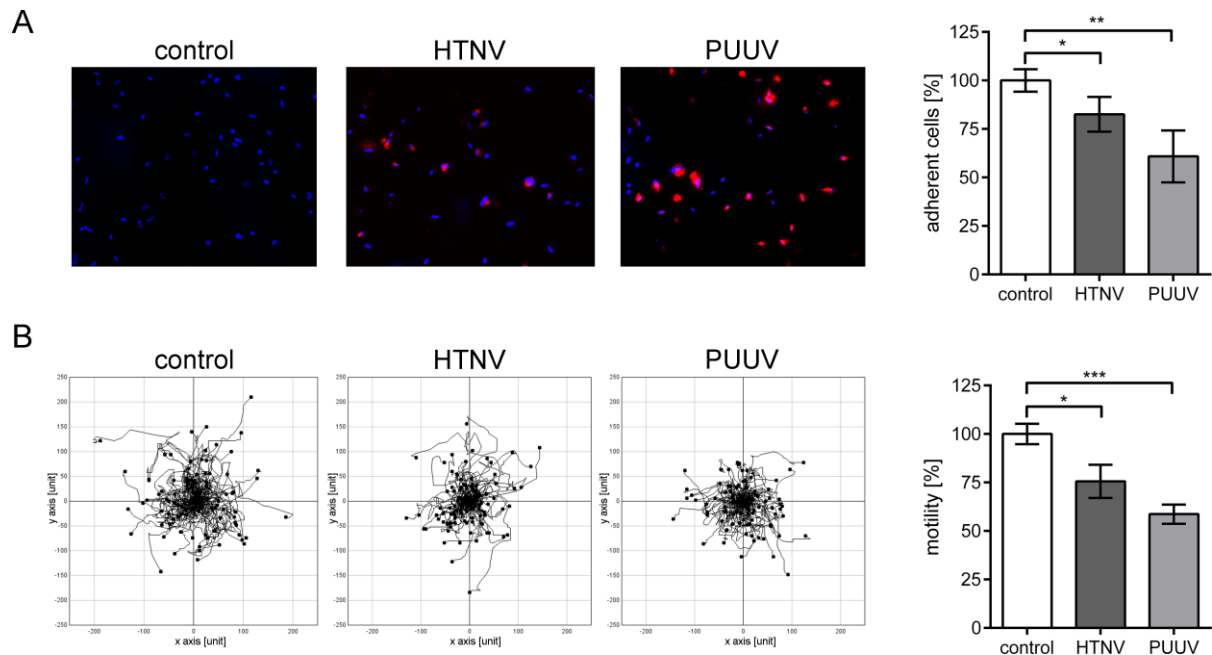


Figure 19 Adhesion and migration capacity of HTNV- and PUUV-infected HREPC. (A) Uninfected and HTNV- or PUUV-infected HREPC were detached on day nine post infection, plated into 96-wells and numbers of attached cells were quantified after one hour by In-Cell Western. Three independent experiments were performed in quadruplicates. N protein was stained in red and cells were imaged at a magnification of $\times 200$. Adhesion of uninfected cells was set to 100%. Shown is mean \pm SD. (B) Migration of uninfected and hantavirus-infected HREPC was analyzed by live cell imaging. 100 cells per experiment were analyzed by single-cell-tracking. Three independent experiments were performed. Shown is mean \pm SD.

3.3 Analysis of underlying hantaviral mechanisms with regards to functional consequences

3.3.1 Soluble factors in supernatant of infected podocytes

The precise mechanism of how Old World hantaviruses induce kidney damage is not completely understood. Analysis of single hantavirus-infected renal cells revealed functional consequences mainly affecting the migration. Therefore, to investigate the underlying mechanism, human

podocytes were further analyzed for direct virus-specific effects. Moreover, it was examined, if soluble factors released by infected cells contributed to the pathogenesis.

In a first step, supernatants of infected podocytes were analyzed for possible soluble factors causing an impairment of motility (Fig. 20). Supernatants were left untreated, UV-treated to inhibit the virus replication cycle, or filtrated to remove viral particles. The efficacy of inactivation and removal of infectious particles was controlled by inoculation of Vero E6 cells and Western blot analysis (Fig. 20A and B). After UV irradiation, the N protein of both virus species was still detectable in the supernatant but no infection was observed in Vero E6 cells. Neither infectious particles nor N proteins were detected after filtration. The supernatants of both virus species were used for subsequent migration assays (Fig. 20C and D). Untreated, UV-treated and filtered supernatants of uninfected podocytes were used as controls. The migration capacity of podocytes in the presence of infectious HTNV particles was reduced compared to control cells ($80.02\% \pm 3.83\%$ vs. $100\% \pm 1.02\%$, $P = 0.0011$) (Fig. 20C). Supernatants with inactivated or removed HTNV particles did not influence the migration of podocytes. In contrast, supernatants derived from PUUV-infected podocytes only caused a slight but not significant impairment of the migration of uninfected podocytes (Fig. 20D). This minor effect was completely abolished by UV treatments or removal of PUUV particles.

These data show that soluble factors released by hantavirus-infected podocytes do not contribute to the reduced migration capacity. Rather, infection itself seems to be responsible for the impaired migration.

3.3.2 Soluble factors in human sera

It might be possible that indirect effects, such as signaling molecules or cytokine production by immune cells or other renal cells during hantavirus disease, contribute to podocyte damage *in vivo*. It is known that several cytokines, chemokines or growth factors are upregulated during hantaviral infection, which might disturb the migration capacity of podocytes.

Therefore, sera samples of three patients with serologically-confirmed acute hantavirus infection were analyzed for the presence of soluble factors causing an effect on podocyte motility (Tab. 4, Fig. 21). The clinical course of each patient is visualized by serum creatinine levels. Sera samples were collected at acute, peak and remission phases of the clinical course and were used for subsequent migration assays with uninfected podocytes *in vitro*. Podocyte medium was supplemented with 50% patient serum simulating the maximum of serum content of regular blood.

Compared to sera of healthy control persons or normal cell culture serum, none of the sera collected at different phases of the clinical course induced an effect on the migration of podocytes. Thus, it seems that possible soluble factors affecting podocyte migration are not present in the sera.

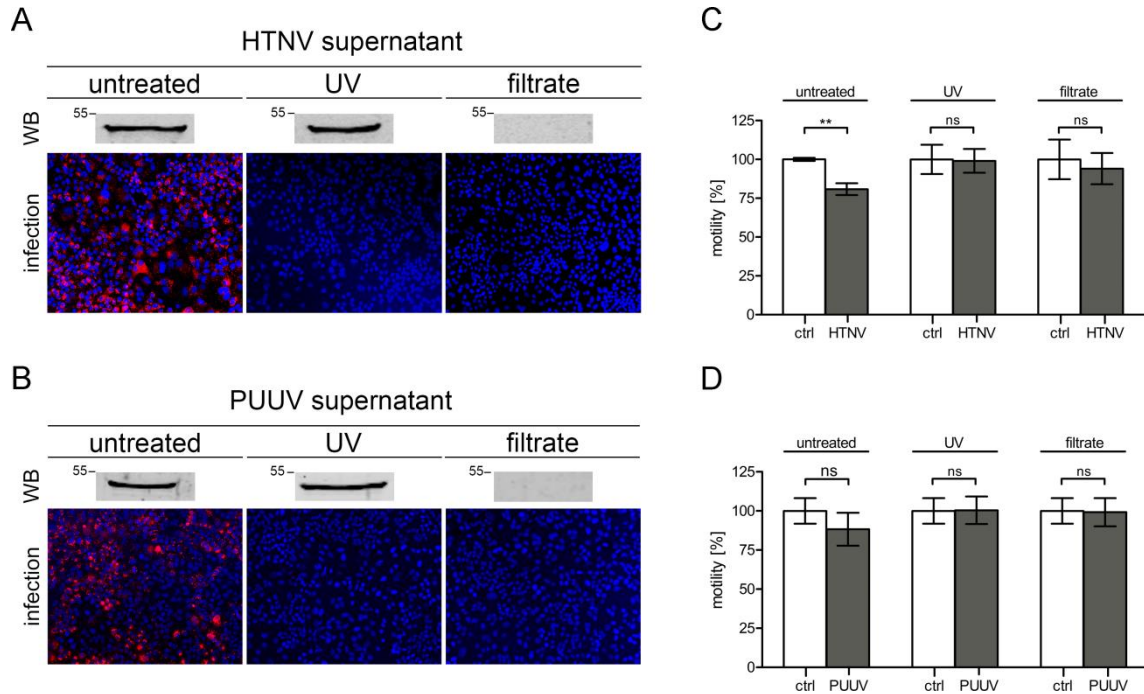


Table 4 Characteristics, peak, and nadir levels of laboratory parameters obtained from three patients with acute PUUV hantavirus disease used for migration assays

| Characteristic | #64 | #176 | #211 | reference |
|---|-------|-------|-------|-----------|
| Age (yr) | 37 | 53 | 25 | - |
| Gender | m | m | m | - |
| Duration of hospitalization (days) | 8 | 15 | 10 | - |
| Max serum creatinine level (mg/dl) | 11.94 | 12.16 | 10.89 | 0.1-1.3 |
| Min serum albumin level (g/liter) | 28 | 31 | 31.1 | 30-50 |
| Max leukocyte count (G/liter) | 15.6 | 15.73 | 7.57 | 4-10 |
| Min platelet count (G/liter) | 65 | 52 | 49 | 150-440 |
| Max LDH ^a activity (U/liter) | 329 | 405 | 422 | < 248 |
| Max CRP ^b level (mg/liter) | 94.5 | 143.7 | 61.2 | < 5 |
| Point of renal biopsy (dpo ^c) | 9 | - | - | - |

^aLDH: lactate dehydrogenase, ^bCRP: C-reactive protein, ^cdpo: days post onset

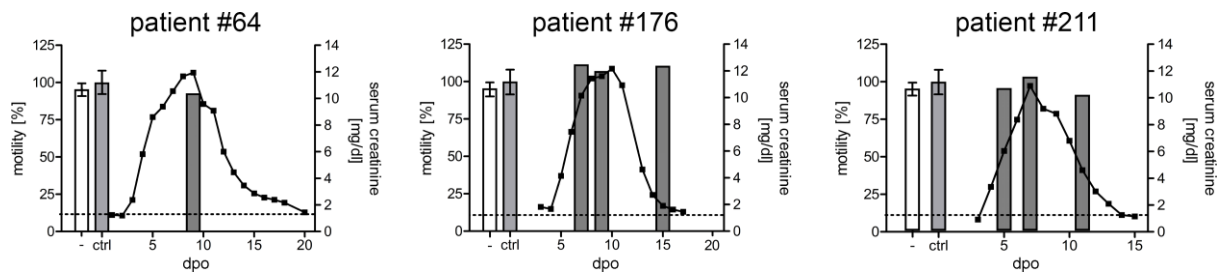


Figure 21 Migration capacity of podocytes after inoculation with sera of PUUV-infected patients. Podocytes were inoculated with normal podocyte medium containing 10% FCS (-), medium containing 50% serum of healthy control persons (ctrl), or with medium containing 50% serum of patients with PUUV infection collected during the clinical course. Uninfected podocytes were seeded confluent into μ -plates. Sera were added 30 minutes before insert removal. After insert removal and after eight hours, cell-free areas were measured and relative migration was calculated and shown on the left y-axis. Migration of podocytes in the presence of sera derived from three healthy donors (ctrl) was set to 100%. Shown is mean \pm SD. Levels of patients' serum creatinine were plotted on the right y-axis. Dashed horizontal line indicates the reference value of serum creatinine for healthy persons (<1.3 mg/dl).

3.3.3 Effects of recombinantly-expressed hantavirus N proteins

3.3.3.1 Localization of recombinant N protein in human podocytes

By investigating supernatants of infected cells or patients' sera, no indirect effects were found contributing to the pathogenesis of podocytes. The absence of soluble factors provides evidence for direct virus-dependent damage in podocytes. To determine a possible role of the N protein during hantavirus disease, human podocytes were transfected with plasmids encoding for HTNV or PUUV N protein. Differentiated podocytes are difficult to transfect with standard methods. Therefore, nucleofection was performed to transfer N protein encoding plasmids by electrical pulse to gain an efficacy of 10-20% transfected cells.

First, the localization of N protein alone was analyzed after transfection (Fig. 22A). Similar to N protein in infection, recombinantly-expressed N proteins showed a similar pattern with punctate and filamentous N protein distribution. The amount of cells showing a filamentous pattern was $23.29\% \pm 2.29$ for HTNV and 4.33 ± 2.31 for PUUV N protein (Fig. 22B). Again, filamentous HTNV N protein partially co-localized with F-actin indicated by the fluorescence intensity profiles. Recombinant PUUV N expression displayed a less pronounced association with the actin cytoskeleton (Fig. 22A).

As seen during infection studies, the filamentous pattern and the association with F-actin are more prominent for recombinantly-expressed HTNV N protein.

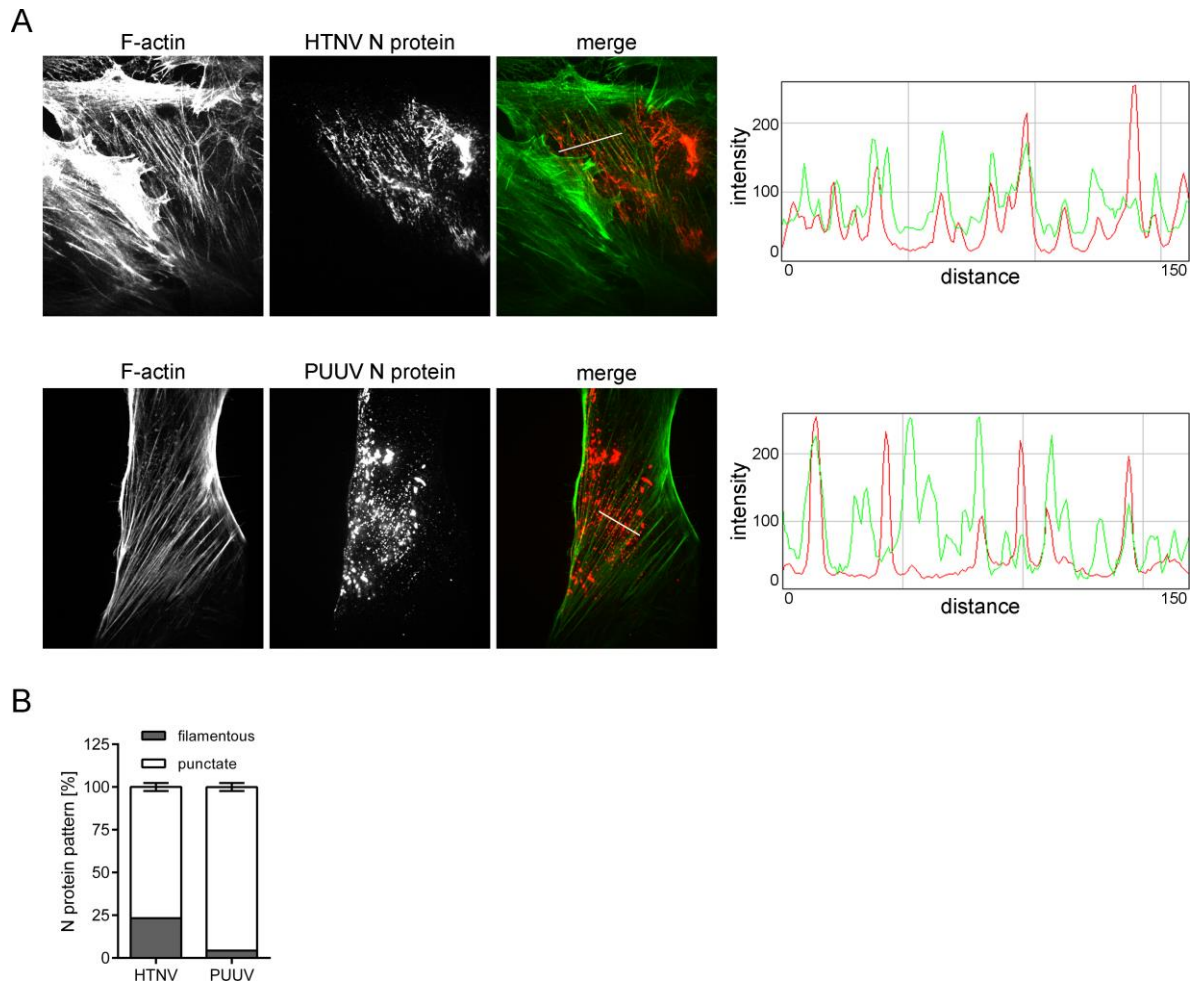


Figure 22 Localization of recombinantly-expressed HTNV and PUUV N protein in podocytes. (A) Podocytes were transfected with plasmids encoding N protein of HTNV or PUUV by nucleofection. Localization of N proteins (red) and F-actin (green) was analyzed 24 hours after transfection by confocal microscopy at a magnification of $\times 1000$. Histograms show fluorescence intensity profiles of F-actin and N protein staining along the indicated lines. (B) Podocytes were analyzed for the N protein localization pattern 24 hours after transfection. Data were obtained from three independent experiments. Shown is mean \pm SD.

3.3.3.2 Effects of recombinant N protein on podocyte migration

To investigate if hantaviral N proteins alone play a role in the impairment of migration, podocytes transfected with plasmids encoding for either HTNV or PUUV N protein were analyzed for their migration capacity by live imaging. Due to a low efficacy of podocyte transfection, the migration assay was inappropriate for analysis. Instead, the motility of individual transfected podocytes was assessed by single-cell-tracking.

To verify that both motility methods provide similar results, HTNV- and PUUV-infected podocytes were also examined by single-cell-tracking (Fig. 23A). By comparison to uninfected cells ($100\% \pm 3.06\%$), the migrated distance was decreased to $40.02\% \pm 1.92\%$, $P < 0.0001$ for HTNV- and to $73.35\% \pm 4.24\%$, $P = 0.0003$ for PUUV-infected podocytes. Stainings of N protein revealed that more than

90% of cells were infected. As already observed in the migration assays, the covered distance of single podocytes was more affected by HTNV than by PUUV infection. The decrease of the motility capacity was comparable to the migration assay and the single-cell-tracking for each virus species, showing that this method is suitable for the analysis of transfected cells (see Fig. 23A and Fig. 10C and D). Next, possible effects on the motility of podocytes by recombinant HTNV or PUUV N proteins were examined (Fig. 23B). Cells were co-transfected with maxGFP to visualize transfected cells during live imaging. Immunofluorescence analysis showed that more than 95% of transfected podocytes were co-expressing N protein and maxGFP. Analysis of the covered distances revealed that the migration of transfected cells was reduced to $46.92\% \pm 8.85\%$, $P = 0.0017$ for HTNV and to $72.90\% \pm 7.22\%$, $P = 0.0134$ for PUUV N protein compared to mock-transfected cells ($100\% \pm 8.45\%$). The impairment of podocyte migration by transfection of HTNV and PUUV N protein alone was comparable to the findings in infected cells.

Infection and transfection studies revealed that HTNV has a greater effect on podocytes than PUUV. To exclude that dissimilar expression levels of both N proteins caused the differences regarding the severity of impaired migration, the fluorescence intensity of N protein-transfected podocytes was determined (Fig. 23C). The analysis showed equal expression levels of HTNV and PUUV N protein indicating that the functional consequences did not depend on the amount, but rather on specific differences of the N proteins, between the two virus species.

Taken together, the transfection experiments demonstrate that the expression of N proteins alone is capable to induce functional consequences of human podocytes.

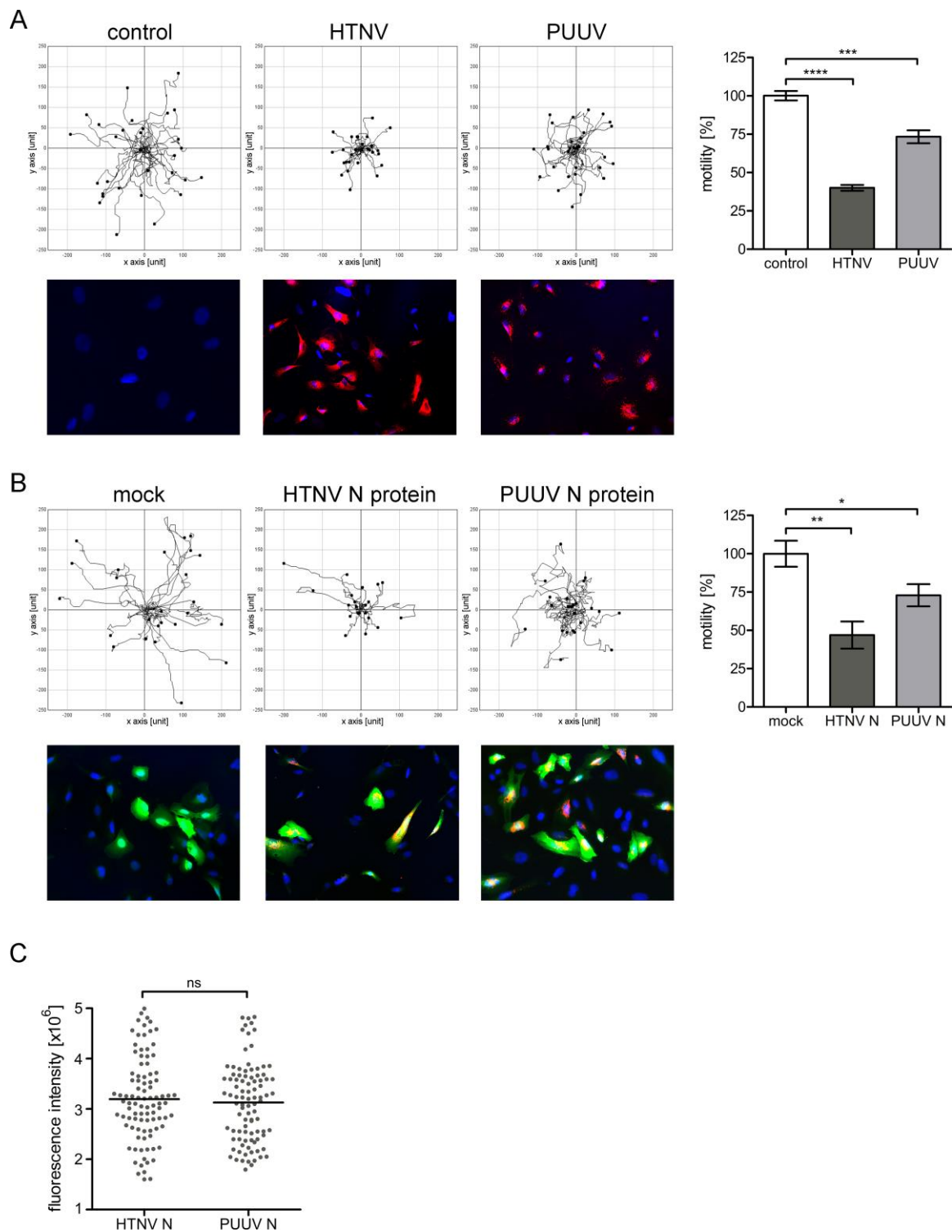


Figure 23 Effect of HTNV and PUUV infection or N protein expression on podocyte migration. (A) Migration of uninfected and PUUV- or HTNV-infected podocytes was analyzed by live cell imaging. Infection was monitored by staining of N proteins (red). 30 cells per experiment were analyzed by single-cell-tracking. Cells were imaged at a magnification of $\times 400$. Three independent experiments were performed. Shown is mean \pm SD. (B) Migration of podocytes transfected with plasmids encoding for maxGFP and N protein of HTNV or PUUV was analyzed by live cell imaging. Cells transfected with pmaxGFP and empty vector served as control (mock). Cells were analyzed as described above. Transfection efficacy of maxGFP and N proteins was visualized by immunostaining of N proteins (red). Cells were imaged at a magnification of $\times 400$. (C) Mean expression levels of N proteins were analyzed by measuring 100 transfected cells for the fluorescence intensity of N protein.

4. Discussion

4.1 Human renal cells as relevant cell culture models to study hantavirus disease

Viruses utilize cellular structures and modulate signaling pathways to successfully enable their replication cycle in target cells. The strategy of Old World hantaviruses results in renal disease in the human host. The infection predominantly manifests in the kidney and leads to acute renal failure with massive proteinuria. The understanding of the viral replication cycle and its effects on host cells after infection is of crucial importance to study hantavirus disease. However, the exact underlying cellular mechanisms responsible for the organ tropism, leading to renal permeability disorders, are unknown. Various factors like immunopathology and direct virus-mediated processes have been reported to be involved in hantaviral pathogenesis. Direct effects are often described to be cell type- and virus-specific. For that reason, choosing a relevant cell culture model is critical in order to study the hantavirus disease.

In previous publications, the hantaviral replication cycle was often examined in Vero E6 cells which are non-human, interferon-deficient and might not portray an ideal cell culture model to analyze hantavirus infection. Moreover, functional consequences of infection have not been investigated in Vero E6 cells so far. Therefore, the aim of this study is to analyze the effects of Old World hantaviruses on a relevant cell culture model. Here, human renal cells, which are important for renal filtration and reabsorption processes, were used and compared to Vero E6 cells.

In the presented work, the hantaviral replication cycle differs enormously between human podocytes and Vero E6 cells regarding the localization of viral antigens and the resulting consequences of infection. In podocytes, the N proteins of Old World hantaviruses display as a filamentous pattern which co-localizes with the actin cytoskeleton and this association increases during infection. Previous studies of Ravkov *et al.* and Ramanathan *et al.* obtained contradictory results concerning the localization of hantaviral N proteins along cytoskeletal components in Vero E6 cells [50, 51, 59]. In the presented study, filamentous N protein and F-actin association were not observed in Vero E6 cells infected either with HTNV or PUUV. The discrepancy of the actin association in Vero E6 cells most likely occurs due to the choosing of varying points of time for the examination after infecting the cells. While Ramanathan *et al.* observed no colocalization in the early stages, Ravkov *et al.* found the N protein association with the actin cytoskeleton late during infection in Vero E6 cells. This effect complies with the findings in human podocytes in which the filamentous N protein pattern and the resulting F-actin association also increase during infection and little N protein localization is seen in

early stages. Nevertheless, the infection kinetics in the presented work demonstrate that an actin localization of N protein is observed in podocytes and not in Vero E6 cells, opposing the study of Ravkov *et al.* [59]. This difference might occur due to the fact that Ravkov *et al.* used New World hantaviruses, while the experiments in the presented work were performed with hantaviruses of the Old World. It might be possible, that hantaviral species utilize cytoskeletal components for their replication cycle differently.

The localization of the Old World hantavirus N proteins in podocytes and in Vero E6 cells might be influenced by cell-specific signaling pathways during infection. Due to their interferon deficiency, Vero E6 cells are not able to induce interferon-stimulated genes (ISG). ISGs, however, are important for the innate immune system and might be involved in the processes leading up to N protein localization and functional disturbances. For example, the myxovirus resistance protein A (MxA) is an ISG protein with known antiviral effects and is highly upregulated in hantavirus-infected human cells [120]. MxA has an actin binding capacity and is able to target the nucleocapsid protein of viruses such as of the influenza virus [121, 122]. Similar interactions by MxA or other ISGs might play a role during the hantaviral replication cycle and contribute to the punctuate or filamentous distribution of N proteins in podocytes.

Both, the actin cytoskeleton and the microtubular network, are important for different steps of various viral replication cycles. Viruses exploit or even rearrange cytoskeletal components for their own purpose during assembly and release of infectious particles, a process that may play a role in the pathogenesis. For Old World hantaviruses, a correlation between the association of N protein to F-actin and its dependence on viral release can be found. HTNV N protein strongly co-localizes with the actin cytoskeleton in podocytes and its integrity is crucial for viral release. In contrast, the N proteins of PUUV associate with F-actin to a lesser extent and its disruption has no effect on the egress of infectious particles. The involvement of the microtubular network differs greatly between podocytes and Vero E6 cells. While hantaviruses only slightly depend on intact microtubules in podocytes, the viral release of HTNV and PUUV was decreased enormously after disruption of this cytoskeletal component in Vero E6 cells. This is, in accordance to previous publications, showing that HTNV strongly depends on microtubules for replication and release of infectious viruses in Vero E6 cells [50, 51].

The results reveal that the utilization of cytoskeletal components for hantaviral release depends on the virus species, but also differs between cell types. Moreover, the fact that the disruption of actin has no effect on PUUV and does not completely decrease the release of HTNV in podocytes, indicates that hantaviruses might use several release pathways. These observations agree with previous studies, indicating, that several sites of hantaviral assembly and budding exist. Old World

hantaviruses have been described to replicate in the ERGIC region and bud either into the Golgi lumen or at the host plasma membrane in Vero E6 cells [55, 56]. However, the sites of assembly and budding of Old World hantaviruses have not been examined in a relevant human renal cell model yet. Different egress pathways might also have an impact on the maturation and morphology of viral particles and can thereby influence the infectivity and the resulting pathogenesis. The hantaviral lipid envelope is derived from host cell membranes of either the Golgi apparatus or the plasma membrane. The molecular composition of membranes differs between organelles and host species and might have an impact on the pathogenicity. For example, variations in the content of certain lipids in the viral envelope are described to influence viral cell attachment or membrane fusion [123]. Old World hantaviruses are transmitted from rodents to humans and do not spread through person-to-person transmission. Moreover, a divergence in the range of viral particle size was already observed in hantaviruses isolated either from humans or rodent hosts [56, 124]. Therefore, in order to display the natural route of transmission, it should be considered to perform infection studies with viruses propagated in rodent cells, for example in the Bank Vole Kidney (BVK) 168 cell line derived from the PUUV host *Myodes glareolus* [125].

Old World hantaviruses differ in utilization of the actin cytoskeleton for egress of infectious particles and N protein localization in human podocytes and monkey Vero E6 cells. Further research will focus on the role of F-actin during hantaviral egress in human renal cells and whether these structures are exploited for assembly and/or as pathways for hantaviral release. The association of F-actin and N protein during the replication cycle might also be a contributing factor to the functional consequences for the target cells since the actin cytoskeleton is responsible for various cellular functions such as cell migration, maintenance of cell shape and transport processes. In fact, a correlation between the localization of N protein to F-actin and the disturbance of cellular functions can be observed. While hantavirus infection decreases the adhesion and migration capacity of podocytes, the observed effects are completely absent in Vero E6 cells. Moreover, the amount of F-actin occurs to be decreased in podocytes and not in Vero E6 cells and indicates that the N protein localization might be a factor in the rearrangement of this cytoskeleton component.

Although podocytes possess properties of primary cells, these cells are still immortalized and act like cell lines. Therefore, the relevance of the results obtained in the podocyte cell line was verified in human primary cells, which resemble the *in vivo* conditions more closely. Analysis of hantavirus infection in primary podocytes and human renal epithelial primary cells (HREPC), which are isolated from the tubules, identifies common characteristics concerning functional consequences and N protein localization in renal cells. An infection with hantaviruses leads to a decrease of cell adhesion and migration in both primary cell types, similar to the observations in the podocyte cell line.

Moreover, the hantaviral N protein displays as filamentous pattern in a comparable amount in primary cells.

Summarized, the localization of hantaviral N protein, modulation of the actin cytoskeleton, release of infectious particles, and the functional consequences after hantavirus infection vary distinctively between human renal cells and Vero E6 cells. Species-specific characteristics might influence the hantaviral replication cycle and can be responsible for a different outcome of infection leading to host cell injury. The results also suggest to further study the underlying pathogenesis mechanism of Old World hantavirus disease in cells, which are rather related to the human renal target organ. Moreover, this study successfully evaluates the podocyte cell line as a new and relevant cell culture model to examine hantavirus infections.

4.2 Old World hantaviruses cause morphological and functional changes in kidney biopsies

The kidney function depends on the intact filtration barrier of the glomerular endothelium and podocytes, as well as on the reabsorption capacity of the tubular epithelium. Dysfunction of these structures during renal disease can result into proteinuria and acute renal failure.

The electron microscopy studies of renal biopsies of hantavirus-infected patients and the cell culture experiments in the presented work show morphological and functional changes in both, podocytes and tubular epithelial cells. The importance of the detected disturbances of podocytes and tubular epithelial cells in biopsies and in *in vitro* experiments, as the underlying cause of disease, is emphasized by the observed non-selective proteinuria during the clinical course indicating that both structures are affected by hantaviruses in humans [94, 95]. After analyzing biopsies of hantavirus-infected patients, morphological alterations with podocyte foot process effacement are revealed. Foot process effacement is typically linked to proteinuric glomerular disease which is driven by a rearrangement of the podocyte actin cytoskeleton leading to a loss of the glomerular slit diaphragm, foot processes and a disturbance of motility dynamics [81]. In fact, rearrangements of the actin cytoskeleton and motility changes can be observed in podocytes after infection *in vitro* in the presented study. The association of foot process effacement and proteinuria *in vivo* and deteriorated podocyte migration capacity *in vitro* has been described in various signaling pathways, controlling the actin cytoskeleton in response to proteinuric stimuli of kidney and model diseases [82, 83, 126]. In combination with the findings of other investigators, these results expand the view of hantavirus-induced renal impairment by adding podocyte injury linked with effacement and proteinuria as a

hantaviral target structure [91, 127]. An intact actin cytoskeleton is crucial for the integrity of cell-to-cell contacts due to its connection to tight and adherens junctions and furthermore the cell motility is also important for the tubular epithelium during repair processes after kidney injury [89, 128]. The remodeling and/or hijacking of actin for the viral replication cycle might lead to a change in the cytoskeleton and subsequent breakdown of cell-to-cell contacts contributing to the enhanced permeability during hantavirus disease [65, 129].

In summary, podocytes and tubular epithelial cells represent substantial cell types to study the pathogenesis pathway of Old World hantaviruses. It would be of interest to examine glomerular endothelial cells for similar morphological and functional changes during hantavirus disease. These cells have already been shown to be permissive for hantaviruses and display cellular damage after infection [65]. It might be possible that a general mechanism of direct viral effects on human cells exists contributing to the pathogenesis.

However, the mechanism causing actin remodeling, disruption of cell-to-cell contacts, and functional consequences of these cells, leading to the enhanced cellular permeability, is not well understood yet. There has been the assumption that the clinical picture of hantavirus infection is caused by an interplay of direct cellular viral effects and indirect immunopathological mechanisms due to activation of the immune system.

In the presented study, non-infectious supernatants derived from infected podocytes and sera from hantavirus-infected patients did not have any effect on podocytes *in vitro*. This result matches the observation of Krautkrämer *et al.* in renal biopsies of hantavirus-infected patients. The analysis of renal tubules revealed an association between cell-to-cell contact disruption and expression of hantaviral antigens, whereas neighboring uninfected tubules showed no cellular damage [65]. Together, these results indicate the absence of systemic soluble factors during hantavirus disease leading to the observed functional impairments and suggest that cellular changes during hantaviral infection are crucial for causing permeability. This would also explain the organ-specific localization of kidney damage for Old World hantaviruses. The connection of cellular damage and N protein expression has also been described in tubules of patients with acute hantavirus disease and in a macaque model of hantavirus infection [62, 65]. Nevertheless, it is possible that local effects of cytokines released by immune or renal cells contribute to hantaviral pathogenesis *in vivo*, in addition to the direct hantaviral effects on functional consequences observed in cell culture. This assumption is, at least, demonstrated for endothelial cells. Particular cytokines, which are increased during hantavirus infection *in vivo*, do not only enhance the permeability of HUVEC, but together with HTNV infection, induce a hyper responsive cellular permeability *in vitro* [104, 105].

These results of cell culture experiments and biopsies indicate that, besides immunopathological effects, virus-direct properties also play a role in causing hantaviral disease. Hantavirus species might have acquired virulence determinants leading to cellular alterations and/or manipulation of the immune system and thereby determining the severity of the hantaviral clinical picture.

4.3 Determinants of hantavirus virulence

The severity, as well as, the organ involvement of hantavirus disease differ enormously between Old and New World hantaviruses. Moreover, symptoms can vary from a mild form to fatal outcome even within the species of Old World hantavirus. The reason for the renal-specific involvement and, in addition, the question why the clinical picture varies considerably between hantaviral species, is to this day poorly understood.

In this study, the hantaviruses HTNV and PUUV with diverse seriousness of the clinical symptoms are compared in renal cells *in vitro*. The two species differ in the cellular actin localization and their potential to cause functional consequences. The impairment of renal cells after infection is more pronounced for HTNV than for PUUV. These observations from cell culture experiments are compliant with the hantaviral clinical picture of both species with HTNV having the more pathogenic potential [46].

Various factors have been discussed as the possible underlying cause leading to the disease severity of hantavirus species. A correlation between high viral plasma RNA levels at early stages of disease and a severe clinical picture was found in Old World hantavirus-infected patients [130-132]. Interestingly, the viral load of the more pathogenic hantaviruses HTNV and DOBV was higher than the viral load of PUUV indicating a replication advantage of distinct hantavirus species, that might contribute to disease severity. It is unknown if a high viral titer at the onset of disease is important for a viral spread in humans causing initial effects and a stronger renal manifestation. The viral RNA levels decrease during later stages of disease and are comparable among hantavirus species, which indicates that other mechanisms play an important role in the pathogenesis. Moreover, analysis of the cellular functional consequences in the presented study demonstrate that even single cells are disturbed in their function and the severity varies between HTNV and PUUV. Therefore, it can be concluded that hantavirus species have a different potential to cause cellular damage in target cells *in vitro*.

By now, little is known about hantavirus-induced deterioration of signaling pathways and processes that alter the host cell machinery to facilitate the replication cycle and/or circumvent defense

mechanisms that might have an impact on hantavirus pathogenicity. Both, pathogenic and nonpathogenic hantaviruses are able to infect the same cell types, suggesting that specific virus-cell interactions contribute to the disease severity [47, 120].

The entry pathway of hantaviruses is discussed to be directly involved in the pathogenesis since pathogenic hantaviruses use integrin $\alpha_v\beta_3$ in contrast to nonpathogenic species, which enter cells by utilizing integrin $\alpha_5\beta_1$ [47]. This might have functional consequences due to activation of cellular signaling pathways since integrin $\alpha_v\beta_3$ is involved in migration and tissue organization [133]. Gavrilovskaya *et al.* already demonstrated that pathogenic hantaviruses inhibit the integrin β_3 -migration of HUVEC [134]. Interestingly, integrin $\alpha_v\beta_3$ has been reported to form signaling complexes with uPAR which is elevated in the plasma of hantavirus infected patients [103]. The induction of uPAR has been reported to control cellular migration and was described to cause proteinuria and FP effacement during kidney disease via a mechanistic link with integrin $\alpha_v\beta_3$ [83, 135, 136]. The activation of uPAR and the involvement of integrin $\alpha_v\beta_3$ during hantavirus disease might display a possible mechanism contributing to the clinical picture of pathogenic hantaviruses. It would be of interest to study uPAR in more detail in order to analyze if the observed elevated levels contribute to local effects of hantavirus disease. However, the usage of integrin $\alpha_v\beta_3$ does neither explain the spectrum of the severity between pathogenic hantaviruses, nor the organ-specific manifestation since integrin $\alpha_v\beta_3$ is an abundant surface protein.

Viruses evolved strategies to manipulate the gene expression of host cells in order to facilitate the viral replication cycle, shut down the antiviral response, or inhibit the expression of specific proteins which enable the dissemination of infectious particles. Analysis of mRNA levels in infected epithelial and endothelial cells demonstrated that cellular genes are specifically regulated by different hantaviruses. Alterations in the cellular gene expression pattern were found between pathogenic and nonpathogenic hantaviruses, as well as, between HFRS- and HCPS-causing species which might contribute to the distinct clinical pictures [120]. Interestingly, the cellular expression profiles after infection also vary between various DOBV genotypes, indicating differences even in between highly-related hantaviruses [137].

However, species-specific factors and genetic alterations responsible for the different hantaviral virulence still remain to be determined. First evidence that specific viral genomic sequences might be involved in the mechanism of disease was obtained by the work of Kirsanovs *et al.* with genotypes of DOBV, which have different pathogenic potentials [138]. The authors performed DOBV reassortment experiments *in vitro* regarding the induction of the innate immune response with the highly virulent subtype DOBV-Dobrava and the weakly pathogenic subtype DOBV-Kurkino (see Tab. 1). It was

demonstrated that the virulence was determined by the L segment and S segment encoding for RdRP and N protein, respectively.

4.4 Hantaviral N protein as virulence factor

Hantaviral N proteins have been reported to coordinate the viral replication cycle by multiple functions and binding partners. However, little is known about the pathogenesis role of Old World hantavirus N proteins in interfering with cellular signaling pathways or host structures which might contribute to the clinical picture of enhanced permeability.

Here, in the presented study, it is demonstrated that the expression of recombinant hantaviral N protein alone is able to partly co-localize with F-actin and is sufficient to cause functional consequences in podocytes. The effect of recombinantly-expressed HTNV N protein on the motility of podocytes is more prominent than for PUUV N which corresponds to the clinical severity and the results obtained during infection experiments. Since the expression levels of HTNV and PUUV N protein are comparable in transfected cells, the severity of impaired function is not caused by a varying cellular amount of N proteins but rather by species-specific N protein differences. Previous publications analyzed the role of New World hantaviral N proteins and demonstrated pathogenesis properties by interfering with host cell signaling pathways. Cimica *et al.* showed in transfection experiments of human embryonic kidney 293T (HEK293T) cells that the ANDV N protein carries an immune-regulating determinant that interferes with signaling pathways of the innate immune response [112]. Interestingly, the effect was completely absent after transfection of the N proteins of the other HCPS-causing hantavirus Sin Nombre (SNV) and New York-1 (NY-1) virus, indicating virulence-determining differences even in highly homolog species. The work of Gorbunova *et al.* revealed that the expression of ANDV N protein in pulmonary endothelial cells activates signaling pathways leading to the activation of the small GTPase RhoA which resulted in an enhanced permeability [113].

The data gathered in this work and by other investigators demonstrate that N proteins of New and Old World hantaviruses act as a virulence factor interfering with cellular signaling and structures, which leads to the clinical picture of hantavirus disease. Nevertheless, further research is required to identify virulence elements within the N protein sequence.

The observations in the presented study show that the N protein of Old World hantaviruses during infection and by recombinantly expression is associated with F-actin. Thereby, this interaction might have an impact on the cytoskeleton organization responsible for the breakdown of proper cell-to-cell

contacts and permeability disorders during infection [65]. Hijacking or reorganization of cellular actin through different viral strategies play a crucial role during the replication cycles of many viruses. The modification of actin structures is often caused by viral proteins interfering with cell signaling pathways or in recruitment of actin-remodeling proteins.

Podocytes also represent target cells during HIV infection resulting in the clinical picture of HIV-associated nephropathy (HIVAN) which is characterized by foot process effacement and proteinuria [139]. The HIV accessory protein *Nef* has been identified to play an important role in the development of HIVAN. As observed during hantavirus infection for N protein, *Nef* colocalized with F-actin, altered the actin cytoskeleton and caused functional consequences in podocytes [140]. The morphological changes are mediated by the association of *Nef* with the diaphanous interacting protein which is a regulator of small GTPases leading to actin changes [141]. Moreover, treatment of epithelial monolayers with *Nef* resulted in loss of cell-to-cell contact proteins and enhanced permeability [142]. HIV *Nef* and hantaviral N protein might share similarities in causing podocyte damage. Enzymatic activities have not been described for both proteins and cellular changes are most likely mediated due to interaction with host proteins. Similar to hantaviral N protein, *Nef* is a small protein, which has various functions during the viral replication cycle leading to manipulations of the host cell machinery. For *Nef*, several sequence motifs have already been identified interacting with host proteins involved in pathogenesis due to changes in cellular trafficking or signaling [143].

Until now, specific binding and interaction motifs in N proteins of hantavirus species contributing to the pathogenesis have not yet been identified. Analysis of the N protein sequence in the eukaryotic linear motif (ELM) resource database reveal seminal functional motifs as identified in *Nef*, which, however, have to be experimentally verified [144]. Hantaviral N proteins might also be capable of interacting with specific proteins in human renal cells and it would be of great interest to identify cellular interaction partners involved in pathogenesis. Old World hantaviruses differ enormously in their severity *in vivo* and effects on cells *in vitro* even between highly related species. Therefore, future research will also have to focus on the analysis of N proteins of different hantavirus species. The identification of virulence domains within the protein sequence that are responsible for the cellular localization and functional damage might help to understand the pathogenesis mechanism of hantavirus disease. Analysis of the HTNV and PUUV N protein sequences in the ELM resource database indicate a theoretical PDZ (abbreviation of post synaptic density protein, *Drosophila* disc large tumor suppressor, and zonula occludens-1 protein) binding domain for both species. PDZ domains can be found in many scaffolding proteins which maintain the formation of signaling pathways, cell-to-cell contact complexes, and its anchoring to the cytoskeleton. Many viral proteins such as of coronaviruses or human papilloma viruses interfere with the assembly of cell-to-cell

contact complexes via PDZ binding motives, leading to a breakdown of the cell barrier [145, 146]. Similar mechanisms are conceivable for N proteins since a breakdown and redistribution of the tight junction protein ZO-1 was detected during hantavirus infection [65]. Furthermore, a possible actin binding domain is found in the N protein sequence of HTNV but is absent in PUUV. This finding might explain why the N protein of HTNV is frequently more often associated with the actin cytoskeleton. It is possible that N proteins of hantavirus species contain a variable amount of virulence-determining domains and are able to differentially interact with host structures which might explain the varying severity of the clinical course. However, the putative PDZ and actin binding domains have to be experimentally proven.

In summary, the presented study demonstrates that hantavirus infection causes morphological and functional changes of podocytes and the tubular epithelium in cell culture experiments and renal human biopsies that play a key role in kidney function. Moreover, the cellular alterations by hantaviruses are species-specific and suggest the study of the pathogenesis mechanisms in relevant human cell models. The results also reveal an important role of Old World hantaviral N proteins as virulence factor. The severity of HTNV and PUUV N protein concerning the impairment of podocytes suggest alterations within the N protein sequence that are crucial for interaction with host proteins. These findings provide useful insight into the clinical picture of Old World hantaviruses leading to the clinical picture of HFRS.

5. References

1. Jha, V., et al., *Chronic kidney disease: global dimension and perspectives*. Lancet, 2013. **382**(9888): p. 260-72.
2. Brennan, D.C., *Cytomegalovirus in renal transplantation*. J Am Soc Nephrol, 2001. **12**(4): p. 848-55.
3. Hariharan, S., *BK virus nephritis after renal transplantation*. Kidney Int, 2006. **69**(4): p. 655-62.
4. Ross, M.J. and P.E. Klotman, *Recent progress in HIV-associated nephropathy*. J Am Soc Nephrol, 2002. **13**(12): p. 2997-3004.
5. Ladino, M., F. Pedraza, and D. Roth, *Hepatitis C Virus Infection in Chronic Kidney Disease*. J Am Soc Nephrol, 2016. **27**(8): p. 2238-46.
6. Beeching, N.J., M. Fenech, and C.F. Houlihan, *Ebola virus disease*. BMJ, 2014. **349**: p. g7348.
7. Oliveira, J.F. and E.A. Burdmann, *Dengue-associated acute kidney injury*. Clin Kidney J, 2015. **8**(6): p. 681-5.
8. Lee, H.W., P.W. Lee, and K.M. Johnson, *Isolation of the etiologic agent of Korean Hemorrhagic fever*. J Infect Dis, 1978. **137**(3): p. 298-308.
9. International Committee on Taxonomy of Viruses (ICTV), *Virus Taxonomy: 2016*. [12/11/2017]: Budapest, Hungary Available from: <https://talk.ictvonline.org/taxonomy/>
10. Meyer, B.J. and C.S. Schmaljohn, *Persistent hantavirus infections: characteristics and mechanisms*. Trends Microbiol, 2000. **8**(2): p. 61-7.
11. Hardestam, J., et al., *Puumala hantavirus excretion kinetics in bank voles (*Myodes glareolus*)*. Emerg Infect Dis, 2008. **14**(8): p. 1209-15.
12. Padula, P.J., et al., *Hantavirus pulmonary syndrome outbreak in Argentina: molecular evidence for person-to-person transmission of Andes virus*. Virology, 1998. **241**(2): p. 323-30.
13. Martinez, V.P., et al., *Person-to-person transmission of Andes virus*. Emerg Infect Dis, 2005. **11**(12): p. 1848-53.
14. Van Loock, F., et al., *A case-control study after a hantavirus infection outbreak in the south of Belgium: who is at risk?* Clin Infect Dis, 1999. **28**(4): p. 834-9.
15. Mustonen, J., et al., *Genetic susceptibility to severe course of nephropathia epidemica caused by Puumala hantavirus*. Kidney Int, 1996. **49**(1): p. 217-21.
16. Vapalahti, K., et al., *Case-control study on Puumala virus infection: smoking is a risk factor*. Epidemiol Infect, 2010. **138**(4): p. 576-84.
17. Maes, P., et al., *Tumor necrosis factor-alpha genetic predisposing factors can influence clinical severity in nephropathia epidemica*. Viral Immunol, 2006. **19**(3): p. 558-64.
18. Brummer-Korvenkontio, M., et al., *Epidemiological study of nephropathia epidemica in Finland 1989-96*. Scand J Infect Dis, 1999. **31**(5): p. 427-35.
19. Klein, S.L., et al., *Sex differences in the incidence and case fatality rates from hemorrhagic fever with renal syndrome in China, 2004-2008*. Clin Infect Dis, 2011. **52**(12): p. 1414-21.
20. Krautkramer, E., et al., *No gender-related differences in the severity of nephropathia epidemica, Germany*. BMC Infect Dis, 2013. **13**: p. 457.
21. Klingstrom, J., T. Lindgren, and C. Ahlm, *Sex-dependent differences in plasma cytokine responses to hantavirus infection*. Clin Vaccine Immunol, 2008. **15**(5): p. 885-7.
22. Brummer-Korvenkontio, M., et al., *Nephropathia epidemica: detection of antigen in bank voles and serologic diagnosis of human infection*. J Infect Dis, 1980. **141**(2): p. 131-4.
23. Zeier, M., et al., *[Acute kidney failure caused by Hantaan virus. Case report from the West Germany]*. Dtsch Med Wochenschr, 1986. **111**(6): p. 207-10.
24. Balabanova, Y., et al., *Communicable diseases prioritized for surveillance and epidemiological research: results of a standardized prioritization procedure in Germany, 2011*. PLoS One, 2011. **6**(10): p. e25691.
25. European Centre for Disease Prevention and Control. *Annual Epidemiological Report 2016 – Hantavirus infection*. 2016 [10/07/2017]; Available from: <https://ecdc.europa.eu>.

26. Reil, D., et al., *Beech Fructification and Bank Vole Population Dynamics--Combined Analyses of Promoters of Human Puumala Virus Infections in Germany*. PLoS One, 2015. **10**(7): p. e0134124.
27. Robert-Koch-Institute. *SurvStat@RKI 2.0*. 2017 [12/09/2017]; Available from: <https://survstat.rki.de>.
28. Jonsson, C.B., L.T. Figueiredo, and O. Vapalahti, *A global perspective on hantavirus ecology, epidemiology, and disease*. Clin Microbiol Rev, 2010. **23**(2): p. 412-41.
29. Pan American Health Organization. *Epidemiological Alert. Hantavirus Pulmonary Syndrome 2013*; [10/07/2017] Available from: <http://paho.org/hq/>.
30. Braun, N., et al., *Characterization and outcome following Puumala virus infection: a retrospective analysis of 75 cases*. Nephrol Dial Transplant, 2010. **25**(9): p. 2997-3003.
31. Schmaljohn, C. and B. Hjelle, *Hantaviruses: a global disease problem*. Emerg Infect Dis, 1997. **3**(2): p. 95-104.
32. Duchin, J.S., et al., *Hantavirus pulmonary syndrome: a clinical description of 17 patients with a newly recognized disease*. The Hantavirus Study Group. N Engl J Med, 1994. **330**(14): p. 949-55.
33. Zaki, S.R., et al., *Hantavirus pulmonary syndrome. Pathogenesis of an emerging infectious disease*. Am J Pathol, 1995. **146**(3): p. 552-79.
34. Rasmuson, J., et al., *Time to revise the paradigm of hantavirus syndromes? Hantavirus pulmonary syndrome caused by European hantavirus*. Eur J Clin Microbiol Infect Dis, 2011. **30**(5): p. 685-90.
35. Vaheri, A., et al., *Hantavirus infections in Europe and their impact on public health*. Rev Med Virol, 2013. **23**(1): p. 35-49.
36. Hjertqvist, M., et al., *Mortality rate patterns for hemorrhagic fever with renal syndrome caused by Puumala virus*. Emerg Infect Dis, 2010. **16**(10): p. 1584-6.
37. Avsic-Zupanc, T., et al., *Hemorrhagic fever with renal syndrome in the Dolenjska region of Slovenia--a 10-year survey*. Clin Infect Dis, 1999. **28**(4): p. 860-5.
38. Klempa, B., et al., *Hemorrhagic fever with renal syndrome caused by 2 lineages of Dobrava hantavirus, Russia*. Emerg Infect Dis, 2008. **14**(4): p. 617-25.
39. Dzagurova, T.K., et al., *Molecular diagnostics of hemorrhagic fever with renal syndrome during a Dobrava virus infection outbreak in the European part of Russia*. J Clin Microbiol, 2009. **47**(12): p. 4029-36.
40. Klempa, B., et al., *Complex evolution and epidemiology of Dobrava-Belgrade hantavirus: definition of genotypes and their characteristics*. Arch Virol, 2013. **158**(3): p. 521-9.
41. Falzarano, D. and H. Feldmann, *Vaccines for viral hemorrhagic fevers--progress and shortcomings*. Curr Opin Virol, 2013. **3**(3): p. 343-51.
42. Huggins, J.W., et al., *Prospective, double-blind, concurrent, placebo-controlled clinical trial of intravenous ribavirin therapy of hemorrhagic fever with renal syndrome*. J Infect Dis, 1991. **164**(6): p. 1119-27.
43. Malinin, O.V. and A.E. Platonov, *Insufficient efficacy and safety of intravenous ribavirin in treatment of haemorrhagic fever with renal syndrome caused by Puumala virus*. Infect Dis (Lond), 2017. **49**(7): p. 514-520.
44. Plyusnin, A., O. Vapalahti, and A. Vaheri, *Hantaviruses: genome structure, expression and evolution*. J Gen Virol, 1996. **77** (Pt 11): p. 2677-87.
45. Jaaskelainen, K.M., et al., *Tula and Puumala hantavirus NSs ORFs are functional and the products inhibit activation of the interferon-beta promoter*. J Med Virol, 2007. **79**(10): p. 1527-36.
46. Vaheri, A., et al., *Uncovering the mysteries of hantavirus infections*. Nat Rev Microbiol, 2013. **11**(8): p. 539-50.
47. Gavrilovskaya, I.N., et al., *Cellular entry of hantaviruses which cause hemorrhagic fever with renal syndrome is mediated by beta3 integrins*. J Virol, 1999. **73**(5): p. 3951-9.

48. Krautkramer, E. and M. Zeier, *Hantavirus causing hemorrhagic fever with renal syndrome enters from the apical surface and requires decay-accelerating factor (DAF/CD55)*. J Virol, 2008. **82**(9): p. 4257-64.
49. Choi, Y., et al., *A hantavirus causing hemorrhagic fever with renal syndrome requires gC1qR/p32 for efficient cell binding and infection*. Virology, 2008. **381**(2): p. 178-83.
50. Ramanathan, H.N., et al., *Dynein-dependent transport of the hantaan virus nucleocapsid protein to the endoplasmic reticulum-Golgi intermediate compartment*. J Virol, 2007. **81**(16): p. 8634-47.
51. Ramanathan, H.N. and C.B. Jonsson, *New and Old World hantaviruses differentially utilize host cytoskeletal components during their life cycles*. Virology, 2008. **374**(1): p. 138-50.
52. Ogino, M., et al., *Cell fusion activities of Hantaan virus envelope glycoproteins*. J Virol, 2004. **78**(19): p. 10776-82.
53. Hong, L., et al., *Characterization of a Cdc42 protein inhibitor and its use as a molecular probe*. J Biol Chem, 2013. **288**(12): p. 8531-43.
54. Mir, M.A., et al., *Storage of cellular 5' mRNA caps in P bodies for viral cap-snatching*. Proc Natl Acad Sci U S A, 2008. **105**(49): p. 19294-9.
55. Shi, X. and R.M. Elliott, *Golgi localization of Hantaan virus glycoproteins requires coexpression of G1 and G2*. Virology, 2002. **300**(1): p. 31-8.
56. Xu, F., et al., *Morphological characterization of hantavirus HV114 by electron microscopy*. Intervirology, 2007. **50**(3): p. 166-72.
57. Goldsmith, C.S., et al., *Ultrastructural characteristics of Sin Nombre virus, causative agent of hantavirus pulmonary syndrome*. Arch Virol, 1995. **140**(12): p. 2107-22.
58. Ravkov, E.V., S.T. Nichol, and R.W. Compans, *Polarized entry and release in epithelial cells of Black Creek Canal virus, a New World hantavirus*. J Virol, 1997. **71**(2): p. 1147-54.
59. Ravkov, E.V., et al., *Role of actin microfilaments in Black Creek Canal virus morphogenesis*. J Virol, 1998. **72**(4): p. 2865-70.
60. Ravkov, E.V. and R.W. Compans, *Hantavirus nucleocapsid protein is expressed as a membrane-associated protein in the perinuclear region*. J Virol, 2001. **75**(4): p. 1808-15.
61. Golden, J.W., et al., *Animal Models for the Study of Rodent-Borne Hemorrhagic Fever Viruses: Arenaviruses and Hantaviruses*. Biomed Res Int, 2015. **2015**: p. 793257.
62. Sironen, T., et al., *Pathology of Puumala hantavirus infection in macaques*. PLoS One, 2008. **3**(8): p. e3035.
63. Groen, J., et al., *A macaque model for hantavirus infection*. J Infect Dis, 1995. **172**(1): p. 38-44.
64. Klingstrom, J., et al., *Wild-type Puumala hantavirus infection induces cytokines, C-reactive protein, creatinine, and nitric oxide in cynomolgus macaques*. J Virol, 2002. **76**(1): p. 444-9.
65. Krautkramer, E., et al., *Pathogenic old world hantaviruses infect renal glomerular and tubular cells and induce disassembling of cell-to-cell contacts*. J Virol, 2011. **85**(19): p. 9811-23.
66. Guhl, S., et al., *Infection of in vivo differentiated human mast cells with hantaviruses*. J Gen Virol, 2010. **91**(Pt 5): p. 1256-61.
67. Raftery, M.J., et al., *Hantavirus infection of dendritic cells*. J Virol, 2002. **76**(21): p. 10724-33.
68. Temonen, M., et al., *Susceptibility of human cells to Puumala virus infection*. J Gen Virol, 1993. **74** (Pt 3): p. 515-8.
69. Hung, T., et al., *Identification of Hantaan virus-related structures in kidneys of cadavers with haemorrhagic fever with renal syndrome*. Arch Virol, 1992. **122**(1-2): p. 187-99.
70. Groen, J., et al., *Hantavirus antigen detection in kidney biopsies from patients with nephropathia epidemica*. Clin Nephrol, 1996. **46**(6): p. 379-83.
71. Kim, S., et al., *Localization of Hantaan viral envelope glycoproteins by monoclonal antibodies in renal tissues from patients with Korean hemorrhagic fever H*. Am J Clin Pathol, 1993. **100**(4): p. 398-403.
72. Latus, J., et al., *Detection of Puumala hantavirus antigen in human intestine during acute hantavirus infection*. PLoS One, 2014. **9**(5): p. e98397.

73. Hautala, T., et al., *Hypophyseal hemorrhage and panhypopituitarism during Puumala Virus Infection: Magnetic Resonance Imaging and detection of viral antigen in the hypophysis*. Clin Infect Dis, 2002. **35**(1): p. 96-101.
74. Hautala, T., et al., *Young male patients are at elevated risk of developing serious central nervous system complications during acute Puumala hantavirus infection*. BMC Infect Dis, 2011. **11**: p. 217.
75. Kurts, C., et al., *The immune system and kidney disease: basic concepts and clinical implications*. Nat Rev Immunol, 2013. **13**(10): p. 738-53.
76. Arif, E. and D. Nihalani, *Glomerular Filtration Barrier Assembly: An insight*. Postdoc J, 2013. **1**(4): p. 33-45.
77. Fukasawa, H., et al., *Slit diaphragms contain tight junction proteins*. J Am Soc Nephrol, 2009. **20**(7): p. 1491-503.
78. Reiser, J., et al., *The glomerular slit diaphragm is a modified adherens junction*. J Am Soc Nephrol, 2000. **11**(1): p. 1-8.
79. Drenckhahn, D. and R.P. Franke, *Ultrastructural organization of contractile and cytoskeletal proteins in glomerular podocytes of chicken, rat, and man*. Lab Invest, 1988. **59**(5): p. 673-82.
80. Faul, C., et al., *Actin up: regulation of podocyte structure and function by components of the actin cytoskeleton*. Trends Cell Biol, 2007. **17**(9): p. 428-37.
81. Mundel, P. and J. Reiser, *Proteinuria: an enzymatic disease of the podocyte?* Kidney Int, 2010. **77**(7): p. 571-80.
82. Kistler, A.D., M.M. Altintas, and J. Reiser, *Podocyte GTPases regulate kidney filter dynamics*. Kidney Int, 2012. **81**(11): p. 1053-5.
83. Wei, C., et al., *Modification of kidney barrier function by the urokinase receptor*. Nat Med, 2008. **14**(1): p. 55-63.
84. Chugh, S.S., L.C. Clement, and C. Mace, *New insights into human minimal change disease: lessons from animal models*. Am J Kidney Dis, 2012. **59**(2): p. 284-92.
85. D'Amico, G. and C. Bazzi, *Pathophysiology of proteinuria*. Kidney Int, 2003. **63**(3): p. 809-25.
86. Christensen, E.I., et al., *Endocytic receptors in the renal proximal tubule*. Physiology (Bethesda), 2012. **27**(4): p. 223-36.
87. Sakhrani, L.M., et al., *Transport and metabolism of glucose by renal proximal tubular cells in primary culture*. Am J Physiol, 1984. **246**(6 Pt 2): p. F757-64.
88. Lang, F. and W. Rehwald, *Potassium channels in renal epithelial transport regulation*. Physiol Rev, 1992. **72**(1): p. 1-32.
89. Bonventre, J.V., *Dedifferentiation and proliferation of surviving epithelial cells in acute renal failure*. J Am Soc Nephrol, 2003. **14** Suppl 1: p. S55-61.
90. Mustonen, J., et al., *Renal biopsy findings and clinicopathologic correlations in nephropathia epidemica*. Clin Nephrol, 1994. **41**(3): p. 121-6.
91. Boehlke, C., et al., *Hantavirus infection with severe proteinuria and podocyte foot-process effacement*. Am J Kidney Dis, 2014. **64**(3): p. 452-6.
92. Temonen, M., et al., *Cytokines, adhesion molecules, and cellular infiltration in nephropathia epidemica kidneys: an immunohistochemical study*. Clin Immunol Immunopathol, 1996. **78**(1): p. 47-55.
93. Mustonen, J., et al., *Nephropathia epidemica in Finland: a retrospective study of 126 cases*. Scand J Infect Dis, 1994. **26**(1): p. 7-13.
94. Ala-Houhala, I., et al., *Increased glomerular permeability in patients with nephropathia epidemica caused by Puumala hantavirus*. Nephrol Dial Transplant, 2002. **17**(2): p. 246-52.
95. Mantula, P.S., et al., *Glomerular Proteinuria Predicts the Severity of Acute Kidney Injury in Puumala Hantavirus-Induced Tubulointerstitial Nephritis*. Nephron, 2017. **136**(3): p. 193-201.
96. Markotic, A., et al., *Role of peripheral blood mononuclear cell (PBMC) phenotype changes in the pathogenesis of haemorrhagic fever with renal syndrome (HFRS)*. Clin Exp Immunol, 1999. **115**(2): p. 329-34.
97. Hartsock, A. and W.J. Nelson, *Adherens and tight junctions: structure, function and connections to the actin cytoskeleton*. Biochim Biophys Acta, 2008. **1778**(3): p. 660-9.

98. Kawachi, H., et al., *Role of podocyte slit diaphragm as a filtration barrier*. Nephrology (Carlton), 2006. **11**(4): p. 274-81.
99. Fromm, M., et al., *Tight junctions of the proximal tubule and their channel proteins*. Pflugers Arch, 2017. **469**(7-8): p. 877-887.
100. Mehta, D. and A.B. Malik, *Signaling mechanisms regulating endothelial permeability*. Physiol Rev, 2006. **86**(1): p. 279-367.
101. Sadeghi, M., et al., *Cytokine expression during early and late phase of acute Puumala hantavirus infection*. BMC Immunol, 2011. **12**: p. 65.
102. Nusshag, C., et al., *Deregulation of levels of angiopoietin-1 and angiopoietin-2 is associated with severe courses of hantavirus infection*. J Clin Virol, 2017. **94**: p. 33-36.
103. Outinen, T.K., et al., *Plasma levels of soluble urokinase-type plasminogen activator receptor associate with the clinical severity of acute Puumala hantavirus infection*. PLoS One, 2013. **8**(8): p. e71335.
104. Li, Y., et al., *Elevated vascular endothelial growth factor levels induce hyperpermeability of endothelial cells in hantavirus infection*. J Int Med Res, 2012. **40**(5): p. 1812-21.
105. Niikura, M., et al., *Modification of endothelial cell functions by Hantaan virus infection: prolonged hyper-permeability induced by TNF-alpha of hantaan virus-infected endothelial cell monolayers*. Arch Virol, 2004. **149**(7): p. 1279-92.
106. Fanning, A.S., et al., *The tight junction protein ZO-1 establishes a link between the transmembrane protein occludin and the actin cytoskeleton*. J Biol Chem, 1998. **273**(45): p. 29745-53.
107. Mir, M.A. and A.T. Panganiban, *Trimeric hantavirus nucleocapsid protein binds specifically to the viral RNA panhandle*. J Virol, 2004. **78**(15): p. 8281-8.
108. Cheng, E., Z. Wang, and M.A. Mir, *Interaction between hantavirus nucleocapsid protein (N) and RNA-dependent RNA polymerase (RdRp) mutants reveals the requirement of an N-RdRp interaction for viral RNA synthesis*. J Virol, 2014. **88**(15): p. 8706-12.
109. Lee, B.H., et al., *Association of the nucleocapsid protein of the Seoul and Hantaan hantaviruses with small ubiquitin-like modifier-1-related molecules*. Virus Res, 2003. **98**(1): p. 83-91.
110. Li, X.D., et al., *Hantavirus nucleocapsid protein interacts with the Fas-mediated apoptosis enhancer Daxx*. J Gen Virol, 2002. **83**(Pt 4): p. 759-66.
111. Taylor, S.L., et al., *Hantaan virus nucleocapsid protein binds to importin alpha proteins and inhibits tumor necrosis factor alpha-induced activation of nuclear factor kappa B*. J Virol, 2009. **83**(3): p. 1271-9.
112. Cimica, V., et al., *An innate immunity-regulating virulence determinant is uniquely encoded by the Andes virus nucleocapsid protein*. MBio, 2014. **5**(1).
113. Gorbunova, E.E., et al., *The Andes Virus Nucleocapsid Protein Directs Basal Endothelial Cell Permeability by Activating RhoA*. MBio, 2016. **7**(5).
114. Welzel, T.M., et al., *Stable expression of nucleocapsid proteins of Puumala and Hantaan virus in mammalian cells*. Virus Genes, 1998. **17**(2): p. 185-98.
115. Saleem, M.A., et al., *A conditionally immortalized human podocyte cell line demonstrating nephrin and podocin expression*. J Am Soc Nephrol, 2002. **13**(3): p. 630-8.
116. Gligic, A., et al., *Hemorrhagic fever with renal syndrome in Yugoslavia: antigenic characterization of hantaviruses isolated from Apodemus flavicollis and Clethrionomys glareolus*. Am J Trop Med Hyg, 1989. **41**(1): p. 109-15.
117. Burgess, A., et al., *Loss of human Greatwall results in G2 arrest and multiple mitotic defects due to deregulation of the cyclin B-Cdc2/PP2A balance*. Proc Natl Acad Sci U S A, 2010. **107**(28): p. 12564-9.
118. McCloy, R.A., et al., *Partial inhibition of Cdk1 in G 2 phase overrides the SAC and decouples mitotic events*. Cell Cycle, 2014. **13**(9): p. 1400-12.
119. Mundel, P., et al., *Synaptopodin: an actin-associated protein in telencephalic dendrites and renal podocytes*. J Cell Biol, 1997. **139**(1): p. 193-204.

120. Geimonen, E., et al., *Pathogenic and nonpathogenic hantaviruses differentially regulate endothelial cell responses*. Proc Natl Acad Sci U S A, 2002. **99**(21): p. 13837-42.
121. Horisberger, M.A., *Interferon-induced human protein MxA is a GTPase which binds transiently to cellular proteins*. J Virol, 1992. **66**(8): p. 4705-9.
122. Verhelst, J., et al., *Interferon-inducible protein Mx1 inhibits influenza virus by interfering with functional viral ribonucleoprotein complex assembly*. J Virol, 2012. **86**(24): p. 13445-55.
123. Lorizate, M. and H.G. Krausslich, *Role of lipids in virus replication*. Cold Spring Harb Perspect Biol, 2011. **3**(10): p. a004820.
124. Hung, T., et al., *Morphology and morphogenesis of viruses of hemorrhagic fever with renal syndrome (HFRS). I. Some peculiar aspects of the morphogenesis of various strains of HFRS virus*. Intervirology, 1985. **23**(2): p. 97-108.
125. Essbauer, S.S., et al., *A new permanent cell line derived from the bank vole (Myodes glareolus) as cell culture model for zoonotic viruses*. Virol J, 2011. **8**: p. 339.
126. Reiser, J., et al., *Podocyte migration during nephrotic syndrome requires a coordinated interplay between cathepsin L and alpha3 integrin*. J Biol Chem, 2004. **279**(33): p. 34827-32.
127. Gnemmi, V., et al., *Microvascular inflammation and acute tubular necrosis are major histologic features of hantavirus nephropathy*. Hum Pathol, 2015. **46**(6): p. 827-35.
128. Forster, C., *Tight junctions and the modulation of barrier function in disease*. Histochem Cell Biol, 2008. **130**(1): p. 55-70.
129. Witkowski, P.T., et al., *Gastrointestinal Tract As Entry Route for Hantavirus Infection*. Front Microbiol, 2017. **8**: p. 1721.
130. Saksida, A., et al., *Dobrava virus RNA load in patients who have hemorrhagic fever with renal syndrome*. J Infect Dis, 2008. **197**(5): p. 681-5.
131. Pettersson, L., et al., *Viral load and humoral immune response in association with disease severity in Puumala hantavirus-infected patients--implications for treatment*. Clin Microbiol Infect, 2014. **20**(3): p. 235-41.
132. Yi, J., et al., *Hantaan virus RNA load in patients having hemorrhagic fever with renal syndrome: correlation with disease severity*. J Infect Dis, 2013. **207**(9): p. 1457-61.
133. Brooks, P.C., R.A. Clark, and D.A. Cheresh, *Requirement of vascular integrin alpha v beta 3 for angiogenesis*. Science, 1994. **264**(5158): p. 569-71.
134. Gavrillovskaya, I.N., et al., *Pathogenic hantaviruses selectively inhibit beta3 integrin directed endothelial cell migration*. Arch Virol, 2002. **147**(10): p. 1913-31.
135. Blasi, F. and P. Carmeliet, *uPAR: a versatile signalling orchestrator*. Nat Rev Mol Cell Biol, 2002. **3**(12): p. 932-43.
136. Wei, C., et al., *Circulating urokinase receptor as a cause of focal segmental glomerulosclerosis*. Nat Med, 2011. **17**(8): p. 952-60.
137. Witkowski, P.T., et al., *Infection of human airway epithelial cells by different subtypes of Dobrava-Belgrade virus reveals gene expression patterns corresponding to their virulence potential*. Virology, 2016. **493**: p. 189-201.
138. Kirsanovs, S., et al., *Genetic reassortment between high-virulent and low-virulent Dobrava-Belgrade virus strains*. Virus Genes, 2010. **41**(3): p. 319-28.
139. Barisoni, L., et al., *The dysregulated podocyte phenotype: a novel concept in the pathogenesis of collapsing idiopathic focal segmental glomerulosclerosis and HIV-associated nephropathy*. J Am Soc Nephrol, 1999. **10**(1): p. 51-61.
140. Tan, R., et al., *Nef interaction with actin compromises human podocyte actin cytoskeletal integrity*. Exp Mol Pathol, 2013. **94**(1): p. 51-7.
141. Lu, T.C., et al., *HIV-1 Nef disrupts the podocyte actin cytoskeleton by interacting with diaphanous interacting protein*. J Biol Chem, 2008. **283**(13): p. 8173-82.
142. Quaranta, M.G., et al., *Exogenous HIV-1 Nef upsets the IFN-gamma-induced impairment of human intestinal epithelial integrity*. PLoS One, 2011. **6**(8): p. e23442.
143. Pereira, E.A. and L.L. daSilva, *HIV-1 Nef: Taking Control of Protein Trafficking*. Traffic, 2016. **17**(9): p. 976-96.

-
144. Dinkel, H., et al., *ELM--the database of eukaryotic linear motifs*. Nucleic Acids Res, 2012. **40**(Database issue): p. D242-51.
 145. Teoh, K.T., et al., *The SARS coronavirus E protein interacts with PALS1 and alters tight junction formation and epithelial morphogenesis*. Mol Biol Cell, 2010. **21**(22): p. 3838-52.
 146. Kranjec, C. and L. Banks, *A systematic analysis of human papillomavirus (HPV) E6 PDZ substrates identifies MAGI-1 as a major target of HPV type 16 (HPV-16) and HPV-18 whose loss accompanies disruption of tight junctions*. J Virol, 2011. **85**(4): p. 1757-64.

6. Acknowledgment

First of all, I would like to thank my supervisors Prof. Dr. Stephan Frings and Prof. Dr. Martin Zeier for giving me the opportunity to perform my PhD studies here in Heidelberg.

Foremost, I would like to express my gratitude to Dr. Ellen Krautkrämer for her support during my PhD program, for helping me in designing the experiments, for her knowledge, as well as the possibility to profit from her experience. Her guidance helped me to accomplish my research project and to write this thesis.

I would like to thank all my labmates for the enjoyable working atmosphere, the discussions, and all the fun we have had together in the last four years. In particular, I am grateful for Vanessa Bollinger, Alexandra Baumann, and Alexander Müller.

I would like to thank Christian Ackermann (Nikon Imaging Center, Heidelberg) for his guidance regarding the confocal microscopy and Friedrich Frischknecht (Parasitology, Heidelberg) for giving me the opportunity to use the Amaxa nucleofector. I would also like to thank Ingrid Haußer-Siller and her lab-team (Pathology, Heidelberg) for helping me with their skills in performing the electron microscopy studies.

Lastly, I would like to thank my parents who raised me with endurance and encouragement, and for their support in all my pursuits and my girlfriend Christina for her motivation and patience during my PhD years.